MODELING OF SELF-ASSEMBLY OF CHARGED POLYMERS

Beibei Huang

Dipòsit Legal: T 1350-2015

MODELING OF SELF-ASSEMBLY OF CHARGED POLYMERS

Beibei Huang

Dipòsit Legal: T 1350-2015

DOCTORAL THESIS

Modeling of Self-assembly of Charged Polymers

Beibei Huang

Universitat Rovira i Virgili
Departament d'Enginyería Química

empty.pdf

UNIVERSITAT ROVIRA I VIRGILI
MODELING OF SELF-ASSEMBLY OF CHARGED POLYMERS
Beibei Huang
Dipòsit Legal: T 1350-2015

Beibei Huang

MODELING OF Self-Assembly of Charged Polymers

DOCTORAL THESIS

Supervised by Dr. Vladimir Baulin

UNIVERSITAT ROVIRA I VIRGILI

Departament d'Enginyería Química

Tarragona

2015

Acknowledgments

First, I would like to thank my PhD supervisor Dr. Vladimir Baulin for the oportunity to do this PhD project, for many provided opportunities during doing this project, for support during the work and for helpful advices. I am very grateful to him for his kindness and guidance. Second, I would like to thank Dr. Josep Bonet i Avalos, Dr. Allan D. Mackie and Dr. Fabian Garcia for their support and helpfulness.

I would also like to specially thank Nuria Juanpere for her priceless aid in solving administrative issues. I would also like to thank my group colleagues (Adrien, Berardo, Yachong) and ex-group colleague (Olena) for the useful discussion or debate, and collaborative working atmosphere.

Many thanks to all my Chinese-speaking friends here in Spain for sharing their spare time and priceless support.

Last, but not least, I would like to express my deep gratefulness to my mother H. Tang, and my wife Apple. Especially this work is dedicated to the memory of my father Z.Y. Huang.

Tarragona, May 2015.

UNIVERSITAT ROVIRA I VIRGILI
MODELING OF SELF-ASSEMBLY OF CHARGED POLYMERS
Beibei Huang
Dipòsit Legal: T 1350-2015

UNIVERSITAT ROVIRA I VIRGILI

Departament d'Enginyeria Química

Av Països Catalans, 26
43007 Tarragona
Tel. 977 558675
Fax. 977 559621

I STATE that the present study, entitled "Modeling OF Self-Assembly of Charged Polymers", presented by Beibei Huang for the award of the degree of Doctor, has been carried out under my supervision at the Department of Chemical Engineering of this university, and that it fulfils all the requirements for the Doctoral Degree.

Tarragona, 26 May 2015
Doctoral Thesis Supervisor

Dr. Vladimir Baulin

Acknowledgments

Abstract

Self-assembly is a spontaneous and reversible organization of molecular units into ordered structures. The self-assembly process plays an important role in materials science and life science, for example it includes the formation of molecular crystals, colloids, lipid bilayers, phase-separated polymers, and self-assembled monolayers. Since the 1950s, scientists have built self-assembly systems exhibiting centimeter-sized components ranging from passive mechanical parts to mobile robots, and present work is devoted to development and usage in practical applications of the computer simulation of the nanometer-sized components such as surfactants. When these amphiphilic molecules are dispersed in a single solvent likes water, the hydrophobic interactions of the hydrocarbon chains drive the molecules to self-assemble into microstructures called micelles, where the hydrophobic tails are shielded from unfavorable interactions with the polar solvent by the hydrophilic, polar head groups. Two principle factors in the self-assembly process are considered in this work. First is the Hydrophobic Effect, which leads to the spontaneous self-assembly of the molecules into micelles, and second is the Electrostatic Interactions. The surfactant with charged polar head group is considered in our model, and the electrostatic interaction originates from two sources. One is the charge-charge repulsions between the charged head groups which limit the number of surfactant monomers aggregated, another source comes from the interaction between the charged head groups and free ions in the solution, which affects the size of the aggregated complex usually.

Self-assembly by linear oppositely charged polyelectrolytes is studied through Poisson-Boltzmann (PB) theory and implemented into software IPEC, which can be used to analyze the stability of core–shell inter-polyelectrolyte complexes formed by complexation of oppositely charged block copolymers. Secondly, combined with single chain mean field (SCMF) theory, we adopt coarse grained model to simulate chemical structures of ionic surfactants and their micellization process. In this simulation not only the charge-charge repulsions between charged surfactant are considered, but also the electrostatic screening effects by free salt ions are taken into account. By selecting the surfactant chain with certain quantity of charge on the hydrophilic groups, we can predict the micellization properties of surfactants, structures and thermodynamics of micelles, such as the critical micelle concentration as well as the aggregation number and the size distributions of micelles. Besides, by tuning the density of free salt ions we can obtain the corresponding micelles as predicted in the computer simulation, and it can be used for the structural modeling in experimental techniques that require the specific molecular structure. Furthermore, the 2D SCMF theory is incorporated with PB theory to explore the electrostatic

effect in the shape transition behavior of the micelles composed by ionic surfactant molecules, and similarly it can be used for the structural modeling in experimental techniques that require the specific molecular structure.

Contents

Contents

1. Introduction

1.1. Background

Long range electrostatic interactions are instrumental in determining the structure and function of living organisms, biopolymers and drug delivery systems. Charged macromolecules can self-assemble and aggregate into compact intermolecular complexes. The oppositely charged polymers can form finite size complexes whose structure determines their biological function, likes gene transfection and compactization of DNA, that provide promising alternatives in gene delivery is based on the use of soluble interpolyelectrolyte complexes (IPEC) formed between nucleic acids and linear polycations. For example, first studies on the utilization of IPEC for DNA delivery were reported in [71]. Subsequently, this field has been intensively developed by many laboratories worldwide. These complexes self-assemble owing to formation of a cooperative system of interchain electrostatic bonds [39]. The charge, dimensions and other properties of these complexes can be varied by altering the DNA/polycation ratio and the molecular parameters of the polycation [37]. In such macromolecular system, the electrostatic forces is usually stronger than van der Waals or hydrogen bonds, hence determine rich behavior and structural variability. The structures formed by opposite charges are usually more stable than neutral block copolymers micelles dissociating upon dilution or slight change in the external conditions[7]. Due to this high stability, interpolyelectrolyte or polyion complexes (PIC) and polyion complex micelles (PIC micelles) can be used as functional devices whose responsiveness to external stimuli will be utilized to realize certain function[7] (Fig. 1.1). For example recognition at the molecular level [28] and pH-sensitive switching devices [24]. Another important function of PIC is it can be applied as drug delivery carriers. Since the structure of polyion complexes change subject to external conditions, artificially tuning the molecular architecture and global properties of PICs would allow for precise control of their delivery proper-

ties. For example [75] demonstrated the great potential of the pH-sensitive micelles as an effective multifunctional nanomedician platform for cancer therapy due to their active tumor targeting, pH-triggered drug release and ultrasensitive MRI responsiveness, as shown in Fig. 1.2. Besides the response in change of temperature and solvent quality[74], the structure of the some charged complexes can be very sensitive to changes in salt concentration[11, 21, 65, 38], pH[45, 24, 38, 69], charge ratio[67, 19], addition of ions[19], or mixing ratio[28]. All these properties supply us possibility to realize accurate control of drug delivery system, although combining these comprehensive effect into a general model seems impossble, we could consider one or several aspects from them to build up a simplified model.

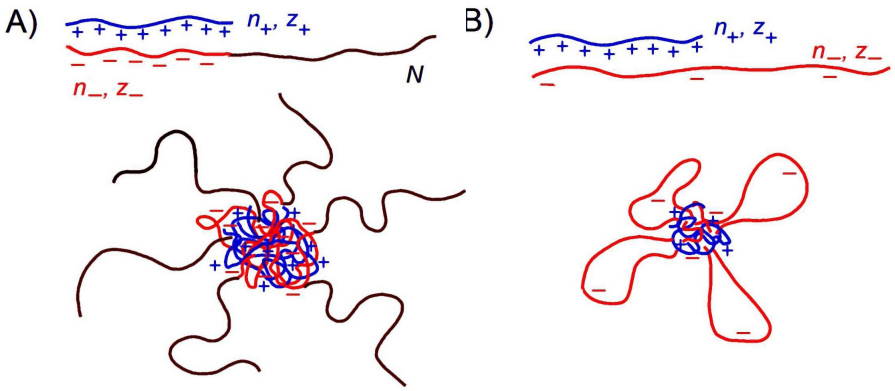

Figure 1.1.: 1 Interpolyelectrolyte complexes formed by A) a linear polyelectrolyte (blue) and a diblock copolymer composed of an oppositely charged block (red) and a neutral block (black); B) two linear oppositely charged polyelectrolytes (blue and red) with large asymmetry in the distances between charges (n_+ and n_-). The segments with noncompensated charges form a charged corona of loops.

On the other side, the surfactants which composed of polar hydrophilic (attracting water) and non polar hydrophobic (repelling water) parts, have a peculiar and important property, under certain conditions likes in low concentrations, with low concentrations of salt, at room temperature, the surfactants form a dilute homogeneous solution of individual amphiphilic molecules. However once change one of some of the conditions over a threshold, the amphiphilic molecules, spontaneously self-assemble into aggregates or microstructures known as micelles, with their hydrophilic groups exposed to solvent, forming corona of the micelle, and their hydrophobic groups shielded in the micellar interior. And such a self-assembly phenomenon of surfactant solutions plays an important role in biological, pharmaceutical and industrial processes such as in drug loading and delivery[44, 43, 52][44, 43, 52], catalysis,

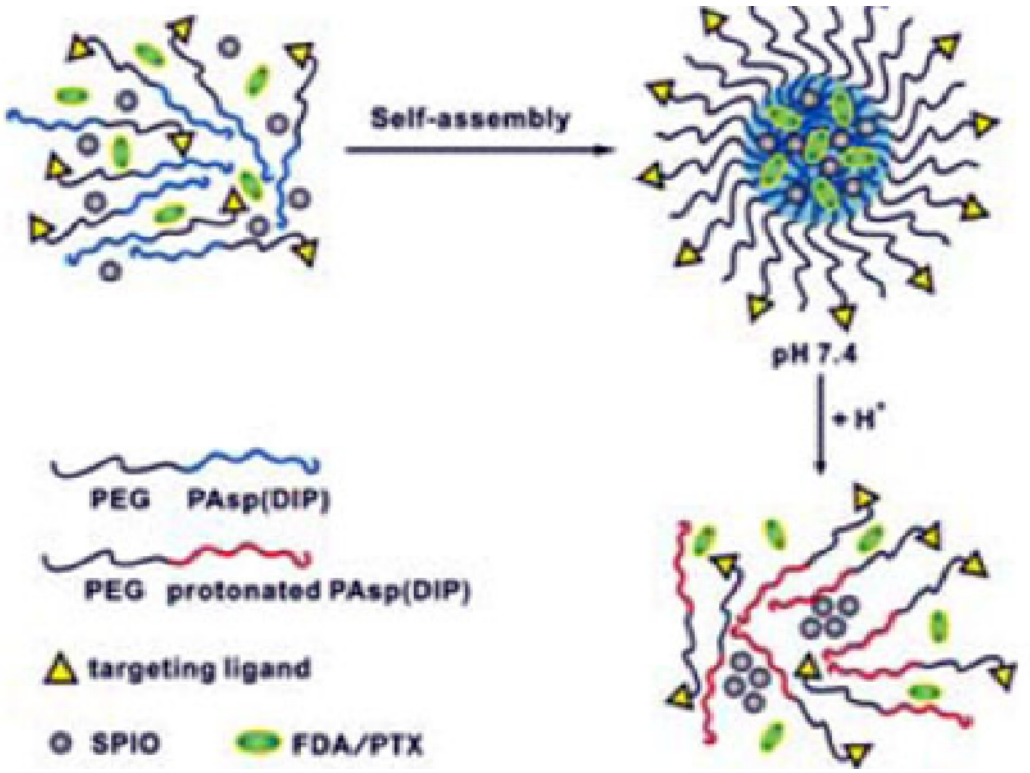

Figure 1.2.: The copolymers can self-assemble into nanoscaled micelles encapsulated with hydrophobic model drug Fluorescein Diacetate (FDA) and MRI diagnostic agents superparamagnetic iron oxide nanoparticles (SPIONs) in aqueous solution of a neutral pH resembling physiological environment, whereas disassemble in acidic endosomal/lysosomal compartments of tumor cells to achieve rapid drug release. In vitro drug release study showed that FDA release from the pH-sensitive micelles was much faster at pH 5.0 than at pH 7.4.

cosmetics, separation processes in engineering and environmental science and technology because of their unique solution properties. Large amount of experiments, and theoretical simulations have been done, to investigate the mechanism of the micellization, and these profoundly enhanced our understanding of surfactant self-assembly in complex solutions, growing research suggests that besides surfactant concentration, other factors like salt concentration, charge density will not only effect the Critical Micelle Concentration, CMC, but also related to the micellar shape, and the micellar size. [9, 10, 11, 27, 28]. Further more, recent researches has focused on the electrostatic interaction influence on the aggregation of surfactant. [29] investigated the interaction between conjugated polyelectrolytes and surfactants in solution and solid phases, it identified multiple modes of interaction and propose a model that accounts for their interplay and pronounced variation in photophysics

over a wide range of conditions, as shown in Fig. 1.3. With these challenges and opportunities, this thesis focuses on the influence of electrostatic interaction on the micellization.

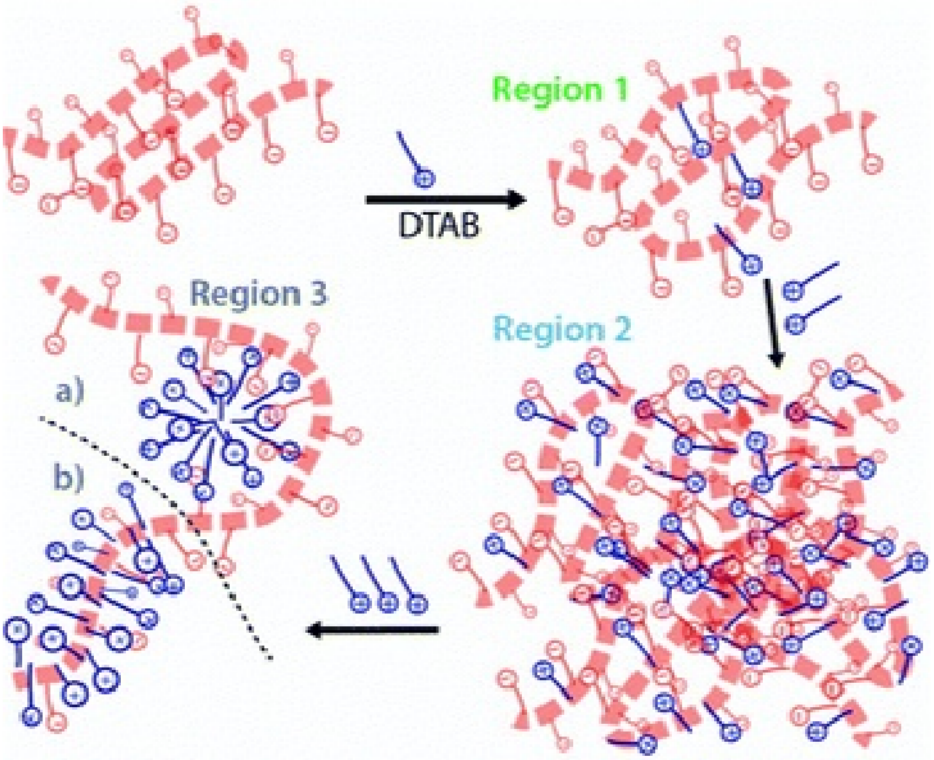

Figure 1.3.: Different CPE–surfactant interaction modes with increasing surfactant concentration; (i) electrostatically induced steric disruption of interchain states, (ii) surfactant cross-linked aggregation, and (iii) CPE templated spherical (a) and cylindrical (b) micelle complexes.

1.2. Objectives

1. To develop software package inter-polyelectrolyte complexes (IPEC) solver to analyze the stability of core–shell inter-polyelectrolyte complexes formed by complexation of oppositely charged block copolymers. To develop fast, efficient, stable solver for solving the corresponding Poisson-Boltzmann equations in IPEC. Through IPEC studying the salt effects, charge distribution and distributions of labile cations and anions around the complexes are calculated numerically as a function of chain composition and solvent properties.

2. To study the influence of electrostatic effect in the micellization process and stability analysis for spherical micelles of model surfactants. Surfactants model H_xT_y is adopted in our simulation. We combine the Single Chain Mean Field Theory and Poisson Boltzmann Theory to create a new model, and based on this model our simulation explore the relation between the size of the spherical micelles and the charge of the surfactants carried, and how the concentration of free ions in the solution effect the micelles.

2. Simulations of spherical interpolyelectrolyte complexes formed by oppositely charged polymers

2.1. Introduction

Dilute solutions of oppositely charged block-polymers can form thermodynamically stable finite size inter-polyelectrolyte complexes (IPEC) [27, 19, 20, 76, 59, 21] or polyion micelles [13, 54]. The stability of finite size aggregates results from the balance of the electrostatic attraction between opposite charges in the core of the complexes and the steric repulsion of backbone segments forming a corona around the core[7]. Adjusting the structure of the polymer chain as well as the solution properties allows one to control the composition and structure of the resulting IPECs.

The Poisson–Boltzmann (PB) equation describes electrostatic interactions and distribution of ions around charged objects in equilibrium at a mean field level. Numerical approaches to solve the PB equation [68, 5, 33] in different practical situations and different geometries are widely available[33]. The common methods to solve the PB equation include finite difference methods and finite element methods[5], where the space is discretized in grids and elements; boundary element[48] and boundary integral equation methods[47], where only the surface of a big molecule is discretized while the surrounding distribution of labile ions is treated as a continuous field. Most of these methods are more suitable for 3D geometry models describing a big molecule of arbitrary shape in the electrostatic field. In contrast, IPEC complexes usually have symmetrical shapes with uniform distribution of charges. In [7], block copolymers of opposite charge aggregate into a spherical complex comprised of m_+ polycations and m_- polyanions. The total free energy of the solution of IPECs of different compositions (m_+, m_-) is written as

$$\frac{F}{VkT} = \sum_{m_+,m_-=0}^{\infty} c_{m_+,m_-} \left\{ \ln(c_{m_+,m_-}) - 1 + F_{m_+,m_-} \right\}$$

where V is the volume of the system, v is the molecular volume associated with the de Broglie length, and c_{m_+,m_-} is the concentration of the complexes of a given

composition (m_+, m_-). And the free energy of the complex F_{m_+,m_-} consists of an electrostatic contribution Ω_{el}, and a term accounting for the steric repulsion of chains forming a corona around the complex F_{corona}. Then the electrostatic contribution is given by[7]

$$\Omega_{el} = \int dr \left\{ \frac{\rho(r)\phi(r)}{2} + kT \sum_{\alpha} \rho_\alpha(r) \ln \frac{\rho_\alpha(r)}{c_\infty} - kT \sum_{\alpha} \rho_\alpha(r) + 2c_\infty \right\}$$

where r is the distance from the center of the complex, $\phi(r)$ is the electrostatic potential at a distance r, and $\rho(r)$ is the charge density, $\alpha = \pm$. c_∞ is the bulk salt concentration. The electrostatic contributions to the free energy from the isolated copolymers is given by [7]

$$\frac{\Omega_{el}}{kTN_\pm} = \frac{u(0)\xi}{2} + \frac{1}{4} \int_{\kappa a}^{\infty} \tilde{r} d\tilde{r} u(\tilde{r}) \sinh(u(\tilde{r})) - \frac{1}{2} \int_{\kappa a}^{\infty} \tilde{r} d\tilde{r} u(\tilde{r}) \Big[\cosh(u(\tilde{r})) - 1 \Big]$$

where $\tilde{r} = \kappa r$ is a dimensionless distance. The chain lengths $N_\pm$ are expressed in units of l_B and ξ is the Manning parameter. Now tuning the chain composition, charge and lengths of the blocks, and solvent properties one can obtain the regions of stability of IPEC complexes, the size of the complexes and their size distribution.

2.2. Theoretical model and method

2.2.1. Poisson–Boltzmann equation in spherical geometry

[7] considers a complex that is formed by m_+ positively charged linear polyelectrolytes and m_- negatively charged block copolymer chains, and each diblock copolymer contains neutral block with length N. Then we assume the core of the complex as a sphere with radius R_c, and the charge is uniformly spread over the core(Fig. 2.1), hence the PB equation is defined

$$\nabla^2 \phi(r) = \frac{4\pi q}{\epsilon} \left\{ \frac{3Z_1 H(R_c - r)}{4\pi R_c^3} - 2c_\infty sinh(\beta q \phi(r)) \right\} \tag{2.1}$$

where $\phi(r)$ is the potential at a distance r, q is the elementary charge, $\beta = 1/kT$. And $H(R_c - r)$ is a Heaviside step function, c_∞ is the bulk density of labile cations and anions. $Z_1 = z_+ m_+ - z_- m_-$ is the bare charge of the core (due to polymers and not screened by labile cations and anions). We assume the potential is a constant at two boundaries. After Introducing the dimensionless electrostatic potential $u(r) = \beta q \phi(r)$ and the dimensionless distance $x = r/R_c$, R_c denotes the radius of the

charged sphere. Then Eq.2.1 can be written into

$$\begin{cases} u''(x) + \frac{2}{x}u'(x) = -3\tilde{Z}H(1-x) + (\kappa R_c)^2 sinh(u(x)) \\ u'(0) = 0 \\ u'(\infty) = 0 \end{cases} \tag{2.2}$$

where $\tilde{Z} = \frac{Z_1 l_B}{R_c}$ is the dimensionless bare charge of the sphere. $l_B = \frac{\beta q^2}{\epsilon}$ is the Bjerrum length and $\kappa^2 = 8\pi l_B c_\infty$is a rescaled labile cations and anions concentration.

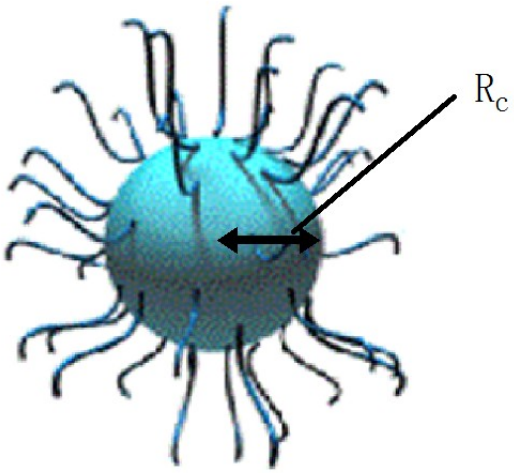

Figure 2.1.: The core of the complex is assumed as a sphere with radius R_c, and the charge is uniformly spread over the core, with charge density $\frac{3(z_+m_+ - z_-m_-)q}{4\pi R_c^3}$. The bulk density of labile cations and anions outside the core is c_∞. The coronas are treated neutral.

2.2.2. Poisson–Boltzmann equation in cylindrical geometry

Spherical IPECs coexist in the solution with isolated chains of both signs. To calculate the electrostatic contribution to the free energy of an isolated chain, one can approximate a polymer chain with a linear charge $\lambda_\pm$ with an infinite cylinder surrounded by counterions and salt molecules. Then the PB equation can be written into

$$\begin{cases} \frac{1}{\tilde{r}}\frac{d}{d\tilde{r}}\left(\tilde{r}\frac{d}{\tilde{r}}\right)u = sinh(u) \\ \left.\frac{du}{d\tilde{r}}\right|_{\tilde{r}=\kappa a} = \pm\frac{2\xi}{\kappa a} \\ u(\tilde{r}\to\infty) = 0 \end{cases} \tag{2.3}$$

where $\xi = l_B\lambda_\pm$ is the so called Manning parameter, and $\tilde{r} = \kappa r$ is a dimensionless

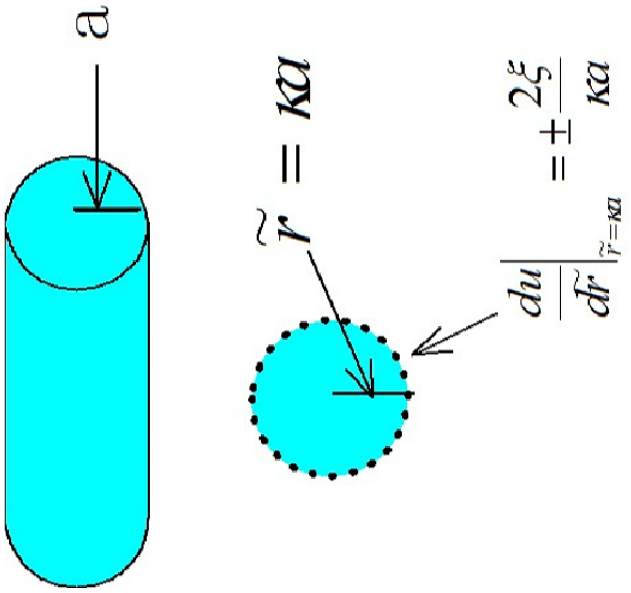

Figure 2.2.: The dimensionless boundary lies in a sphere with radius κa, which is determined by the charge density of copolymer chains $\lambda_{\pm}$ and the concentration of salt c_{∞} in solution.

distance. a is the radius of the cylinder, and $\kappa^2 = 8\pi l_B c_{\infty}$ is a rescaled labile cations and anions concentration (Fig. 2.2).

2.2.3. Simulation Method

In the nonlinear Eq.2.2, the term $\sinh(u)$ may lead to overflow for large values of $u(x)$ and the same question happen when solving Eq.2.3. Thus, for convenience we set $w = e^u$, $y = w\prime$ and get an equivalent system

$$\begin{cases} y' = \dfrac{y^2}{w} - \dfrac{2y}{x} - 3\tilde{Z}_1 w + \dfrac{w^2-1}{2}(kR_c)^2 \\ w' = y \\ y(0) = 0 \\ y(\infty) = 0 \end{cases} \tag{2.4}$$

where $\tilde{Z}_1$ and kR_c are two control parameters. The solution of this equation can be obtained by the conventional approach based on the finite difference method and the Newton–Raphson method[41, 72, 18]. Similar to the spherical case, the Eq.2.3

can be written into

$$\begin{cases} y' = \dfrac{y^2}{w} - \dfrac{y}{x} + \dfrac{w^2-1}{2} \\ w' = y \\ \dfrac{y}{w}\Big|_{\tilde{r}=\kappa a} = \pm\beta \\ w(\infty) = 1 \end{cases} \tag{2.5}$$

where $\beta = \dfrac{2\xi}{\kappa a}$, hereinafter for short.

For Eq.2.4, we found standard approach may not be stable for all sets of parameters, and later the stability of such a nonlinear system will be analyzed. Eq.2.5 is even worse. For this boundary value problem (BVP), the commonly used method is the 4th- Order-Runge–Kutta iteration technique[41], combined with the shooting method[57] we found Eq.2.5 is very sensitive to the parameter β. It is quite difficult to choose an appropriate initial estimate for the shooting method. In addition, slight variations in the boundary values may lead to great fluctuation in the solution, thus it is not possible to use a previous solution as an initial guess for the next solution. Such a method can be used to solve the equation only for small values of β.

In order to overcome this problem, we use the finite difference method[53] to discretize the differential equations into a set of nonlinear equations. There are two sources of error in this method: one is the rounding error which may accumulate in a sequence of calculations and another is the discretization error or truncation error, which comes from the difference between the exact solution and the solution of the finite difference equation. Substitution of $y = w'$ into Eq.2.5 leads to

$$\begin{cases} w" = \dfrac{w'^2}{w} - \dfrac{w'}{x} + \dfrac{w^2-1}{2} \\ \dfrac{w'}{w}\Big|_{\tilde{r}=\kappa a} = \pm\beta \\ w(\infty) = 1 \end{cases} \tag{2.6}$$

The first and second order derivatives are discretized into finite differences approximations

$$\begin{aligned} w_i &= w(x_i) \\ w_i' &= -\frac{w_{i-1}}{3h} - \frac{w_i}{2h} + \frac{w_{i+1}}{h} - \frac{w_{i+1}}{6h} \\ w_i" &= \frac{w_{i-1}}{h^2} - \frac{2w_i}{h^2} + \frac{w_{i+1}}{h^2} \end{aligned}$$

For the first grid point, we adopt the first order approximation

$$w_i' = \frac{-3w_i + 4w_{i+1} - w_{i+2}}{2h}$$

The truncation errors for the above three differences expressions are of order $O(h^2)$.

This method effectively decreases the discretization error and accelerates the convergence speed. For weakly charged chains or large salt concentrations, i.e. when $\beta \ll 1$, the potential $u < 1$ and the DH equation is close to the exact solution of PB. Thus, using its solution as an initial guess provides a good convergence of the PB equation. When $\beta > 1$, the solution of the PB equation can be obtained in the iterative process by a gradual increase of β, when the solution of the PB equation with smaller β is used as the initial guess for larger β.

However, a gradual increase of β slows down the calculation. Thus, we use the adaptive method to approach larger β, starting with the DH solution as the initial guess for small β and using it as an initial guess for larger β. Using an adaptive step in β values, we can approach the solution faster. Such a "relay race strategy" is summarized in Algorithm 2.1 with grid vector x, step size h, boundary condition value β and relative iteration convergence tolerance *tol* as input parameters, and the vector w_0 as the output solution.

Solution of these equations provides an equilibrium distribution of counterions and salt ions in the solution, distribution of charges, free energy of the chains in the solution and in the self-assembled complexes and thus allows us to determine the range of stability of IPEC micelles in terms of the numbers of polyanions and polycations in the complex.

2.3. Analysis and numerical tests results

In order to evaluate the stability of Eqs.2.4 and 2.6, we rely on the stiffness ratio of the solutions of equation. First Eq.2.4 is written in a general form

$$\frac{d\mathbf{y}}{dx} = f(x, \mathbf{y}) \tag{2.7}$$

now if $\tilde{y}(x)$ is the solution of the equation that satisfies the corresponding boundary condition, we can write a linear approximation function

$$\frac{dZ}{dx} = J(x)(Z - \tilde{y}(x)) + f(x, \tilde{y}(x))$$

or

$$\frac{dZ}{dx} = J(x)Z + F(x)$$

hence

$$F(x) = f(x, \tilde{y}(x)) - J(x)\tilde{y}(x)$$

where $J(x)$ is the Jacobian matrix. Substituting $\tilde{y}$ by the vector $[w, y]^T$ in Eq.2.4 one obtains the corresponding Jacobian matrix

$$J = \begin{bmatrix} 0 & 1 \\ (\kappa R_c)^2 w - \frac{y^2}{w^2} - 3\tilde{Z}_1 & \frac{2y}{w} - \frac{2}{x} \end{bmatrix} \tag{2.8}$$

According to Ref.[22], if the eigenvalues of Jacobian matrix J of dimension k, $\lambda_j = \lambda_j(x)$, $j = 1, 2...k$ satisfy

1 . $Re(\lambda_j) < 0, \quad j = 1, 2....k$

2 . $s(x) = \dfrac{\max_{1\le i\le k}(Re(\lambda_i))}{\min_{1\le j\le k}(Re(\lambda_j))} \gg 1$

the nonlinear system is considered to be stiff on x, and $s(x)$ is the stiffness ratio at x. This signifies the instability of the solution of the equation. The stiffness ratio $s(x)$ of the finite-difference method combined with the Newton–Raphson method to solve Eq.2.4 with values of x in the range from 0.02 to 0.8, and the eigenvalues of the matrix J, Eq.2.8, is given in Tab. 2.1. All the values in the table are smaller

x	$\tilde{Z}_1 = 42$	$\tilde{Z}_1 = 60$	$\tilde{Z}_1 = 138$	$\tilde{Z}_1 = 216$	$\tilde{Z}_1 = 294$
0.02	0.01	0.02	0.04	0.07	0.11
0.04	0.06	0.08	0.26	1.00	1.00
0.06	0.15	0.25	1.00	1.00	1.00
0.08	0.38	1.00	1.00	1.00	1.00
0.10	1.00	1.00	1.00	1.00	1.00
0.12	1.00	1.00	1.00	1.00	1.00
0.14	1.00	1.00	1.00	1.00	1.00
0.16	1.00	1.00	1.00	1.00	1.00
0.18	1.00	1.00	1.00	1.00	1.00

Table 2.1.: Stiffness ratio $s(x)$ of Eq.2.4

than or equal to 1, thus the system is not stiff for most $\tilde{Z}_1$ and the solution is stable. However, we obtain the corresponding Jacobian matrix J arising from Eq.2.6

$$J = \begin{bmatrix} 0 & 1 \\ w - \frac{y^2}{w^2} & \frac{2y}{w} - \frac{1}{x} \end{bmatrix} \tag{2.9}$$

and the stiffness ratios $s(x)$ are given in Tab. 2.2. The values of the stiffness ratios$(x) > 1$ for certain sets of parameters in this table may indicate that commonly used methods to solve differential equations could be unstable, and no general strategy guarantees [41] the existence or uniqueness of a solution of such nonlinear second-order equations.

Hence we adopt the method described in Algorithm 2.1, which provides a stable solution of the PB equation in cylindrical geometry, Eq.2.6 for a large range of

x	$\xi = 1.0$				$\xi = 2.0$			
	$\beta = 1.0$	$\beta = 2.0$	$\beta = 10.0$	$\beta = 20.0$	$\beta = 2.0$	$\beta = 4.0$	$\beta = 20.0$	$\beta = 40.0$
0.02	1.0e+004	1.0e+003	48.22	18.51	1.0e+003	228.85	18.51	17.43
0.04	2.91	1.04	40.92	16.26	1.04	220.85	16.26	15.41
0.06	0.09	4.80	40.94	15.87	4.80	311.77	15.87	15.04
0.08	0.03	0.67	43.52	16.05	0.67	970.65	16.05	15.19
0.10	0.02	0.25	48.3	16.53	0.25	548.75	16.53	15.62
0.12	0.01	0.14	56.07	17.23	0.14	189.83	17.24	16.24
0.14	0.00	0.09	69.02	18.15	0.09	108.06	18.15	17.04
0.16	0.00	0.07	93.2	19.30	0.07	72.78	19.30	18.04
0.18	0.00	0.05	151.38	20.73	0.05	53.5	20.73	19.27
0.20	0.00	0.04	464.77	22.50	0.04	41.55	22.50	20.78

Table 2.2.: Stiffness ratio $s(x)$ of nonlinear equations 2.6.

parameters, although it takes more time than the solution of the PB equation in spherical geometry, Eq.2.4. Solution of these equations provides an equilibrium distribution of counterions and salt ions in the solution, distribution of charges, free energy of the chains in the solution and in the self-assembled complexes and thus allows us to determine the range of stability of IPEC micelles in terms of the numbers of polyanions and polycations in the complex. The performance of this algorithm is shown in Tab. 2.3.

β	$\kappa a = 0.5$		$\kappa a = 1.0$		$\kappa a = 2.0$		$\kappa a = 10.0$	
	β steps	Iter num	β steps	Iter num	β steps	Iter num	β steps	Iter num
0.4	2	6	2	7	2	8	2	8
2.0	2	10	2	10	2	10	2	10
4.0	2	12	2	12	2	12	2	12
8.0	7	35	7	36	7	41	7	34
16.0	7	50	7	42	7	62	7	55
32.0	7	53	7	69	7	71	7	54
64.0	12	88	12	63	12	72	12	134
128.0	12	79	12	76	12	91	12	92
256.0	12	103	12	78	12	84	12	88
512.0	17	11	17	88	17	105	17	90

Table 2.3.: The number of steps in β and the number of iterations of Newton-Raphson method.

The first step in calculation of the size distributions of complexes is the solution of PB equations for linear chains, Eq.2.6. This time consuming step can be optimized by using the interpolation of the stored results. Indeed, Eq.2.6 depends only on two parameters, κa and ξ, thus solving the equation for different combinations of

κa and ξ in advance and storing the result in a table may save time. We compute the value of the free energy for given κa and ξ for each intersection point and store it in the table. The dependence of electrostatic energy of a cylinder on κa and ξ becomes linear [7] when κa and ξ are sufficiently large. Thus, the interpolation table is divided into two regions: region I with step 0.1 and region II with step 0.2. The electrostatic energy between the table values is obtained using Eq.2.10 . Here v denotes the required value of the energy, κa_1 , κa_2, ξ_1 and ξ_2 are the values in the table with the corresponding values a, b, c, d, as shown in Fig. 2.3:

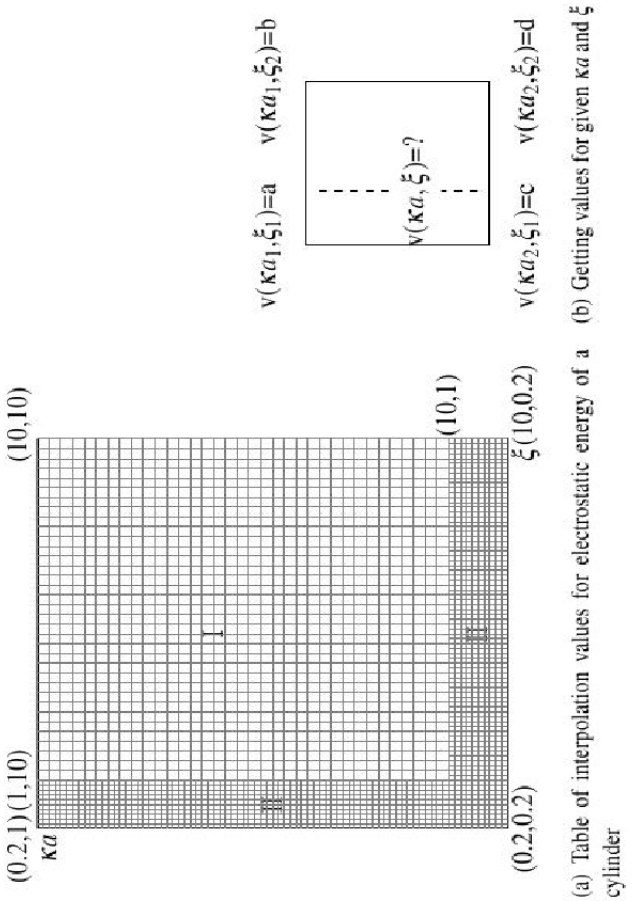

Figure 2.3.: Interpolation of electrostatic energy of a cylinder

$$\begin{cases} v = v2 + (v1 - v2) * (\kappa a - \kappa a_1)/(\kappa a_2 - \kappa a_1) \\ v_1 = b - (b - a) * \frac{\xi_2 - \xi}{\xi_2 - \xi_1} \\ v_2 = d - (d - c) * \frac{\xi_2 - \xi}{\xi_2 - \xi_1} \end{cases} \tag{2.10}$$

Algorithm 2.1 Adaptive "relay race" algorithm using combination of finite difference and Newton–Raphson methods.

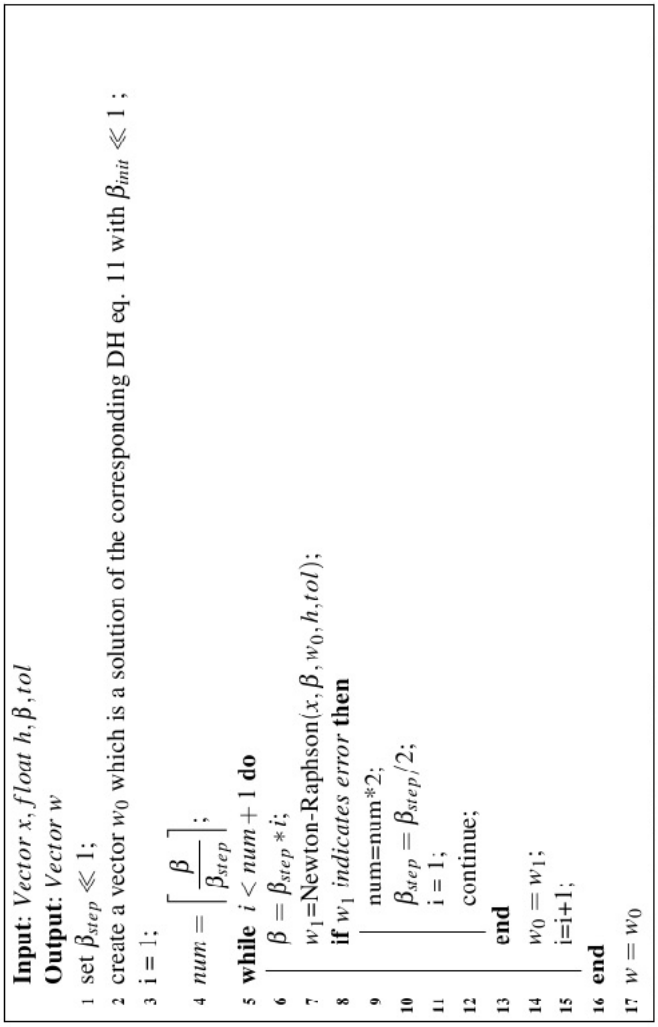

3. Efficient and stable method to solve Poisson-Boltzmann equation with steep gradients

3.1. Introduction

Poisson-Boltzmann Equation (PBE) describes equilibrium distribution of charged objects surrounded by counterions and salt molecules in a mean field approximation, which neglects fluctuations and correlations. Popular methods to solve PBE include Newton methods, finite difference methods, adaptive methods [68, 5]. These methods can successfully solve nonlinear PBE in different geometries and shapes of charged objects such that universal solvers can be used for different practical applications. For example, a package DelPhi [42, 25, 55] is a 3D nonlinear solver of PBE. It is successfully used for modeling of electrostatic interactions of biomolecules. However, universal solvers may not always converge or be always efficient, especially if the solution exhibits abrupt changes. This is the case, for example, for electrostatic potential around highly charged objects in low salt solutions. Thus, such particular cases need a special treatment, that may improve the convergence of the approximation scheme to the exact solution of the nonlinear system.

In this work we show that a method using adaptive step in the region of abrupt change of the solution may greatly improve the convergence and the stability of the approximation scheme. This method uses invertible mapping algorithm to transform PBE into a form with a smooth profile. This is similar in spirit to successive relaxation strategy described in Ref. [55] or similar invertible mappings strategies used for accurate description of the solution close to boundaries [63], solution of Burgers' equation with high Reynolds numbers [40]. Such a strategy applied to solution of different equations [73, 70, 31, 30] electively reduce the number of grid points and thus decreasing the degrees of freedom of the corresponding matrices in the computation process.

The method is implemented for solution of PBE in cylindrical geometry of infinite charged rod with large charge fixed in the boundary condition. Although the method is implemented in 1D, it can be generalized, in principle, for other dimensions.

3.2. Poisson-Boltzmann Equation

Poisson-Boltzmann equation describes electrostatic potential of charged objects in implicit ionic solutions, and its general form is written as

$$\nabla \cdot \Big[\epsilon(\vec{r})\nabla\psi(\vec{r})\Big] = -4\pi\rho^f(\vec{r}) - 4\pi\sum_i c_i^\infty z_i q \exp\Big[\frac{-z_i q\psi(\vec{r})}{\kappa_B T}\Big] \tag{3.1}$$

where $\epsilon(\vec{r})$ is the position dependent dielectric constant, $\Psi(\vec{r})$ is the electrostatic potential, $\rho^f(\vec{r})$ is the charge density of fixed charges, c_i^∞ represents the concentration of the ion i in the bulk, z_i is the charge of the ion i, q is the elementary charge, k_B is the Boltzmann constant and T is the temperature.

We solve this equation in cylindrical geometry for infinitely long rod with arbitrary charge and surrounded by small ions and counterions providing electroneutrality of the system. Charged rod is represented by a cylinder with homogeneously distributed linear charge λ.

Aqueous solution outside the rod is homogeneous and thus $\epsilon(\vec{r})$ can be treated as a constant ϵ. For simplicity we consider monovalent ions only. Since we calculate the electrostatic potential outside the rod, all fixed charges are on the rod, and thus $\rho^f = 0$. Using $\nabla^2 = \frac{1}{r}\frac{\partial}{\partial r}\Big(r\frac{\partial}{\partial r}\Big)$ in cylindrical coordinates and introducing dimensionless distance $\widetilde{r} = \kappa r$, where $\kappa^2 = 8\pi l_B c_\infty$ is a rescaled ion concentration, PBE of infinitely charged rod takes the form [34, 7]

$$\begin{cases} \frac{1}{\widetilde{r}}\frac{d}{d\widetilde{r}}\left(\widetilde{r}\frac{d}{d\widetilde{r}}\right)u = \sinh u \\ \left.\frac{du}{d\widetilde{r}}\right|_{\widetilde{r}=\kappa a} = -\frac{2\xi}{\kappa a} \\ u(\widetilde{r}\longrightarrow\infty) = 0 \end{cases} \tag{3.2}$$

where $\xi = l_B\lambda$ is a dimensionless linear charge, the so-called Manning parameter [64], a is the radius of the cylinder. This equation is controlled by two parameters: κa related to salt concentration, and a dimensionless parameter $\beta = 2\xi/\kappa a$ which reflects the effective charge of a cylinder screened by salt solution.

The difficulty in solving this equation may arise from two terms: (i) $\sinh(u)$ may lead to overflow for large values of $u(\widetilde{r})$, and (ii) high charges and low ion concentration, i.e. when $\beta \gg 1$, produce steep gradients in the potential. To overcome first problem we set $w = e^u$, $y = w'$ and get an equivalent system

$$\begin{cases} y' = \frac{y^2}{w} - \frac{y}{\widetilde{r}} + \frac{w^2-1}{2} \\ w' = y \\ \frac{y}{w}\big|_{\widetilde{r}=\kappa a} = -\beta \\ w(\infty) = 1 \end{cases} \tag{3.3}$$

To analyze the stability of the equation for different sets of parameters, we use the same procedure as in [34] and derive the corresponding Jacobian matrix arising from the above Eq. (3.3)

$$J(\widetilde{r}) = \begin{bmatrix} 0 & 1 \\ w - \frac{y^2}{w^2} & \frac{2y}{w} - \frac{1}{\widetilde{r}} \end{bmatrix} \tag{3.4}$$

According to [22], if the eigenvalues λ_i of Jacobian matrix J satisfy

- $Re(\lambda_i) < 0$, $i = 1, 2, 3 \ldots k$
- $S(\widetilde{r}) = \frac{\max_{1 \le i \le k}(Re(\lambda_i))}{\min_{1 \le i \le k}(Re(\lambda_i))} \gg 1$

the nonlinear system is considered to be stiff on $\widetilde{r}$, and $S(\widetilde{r})$ is the stiffness ratio at $\widetilde{r}$. The stiffness ratios $S(\widetilde{r})$ arising from Eq. (3.4) are given in [34], and they indicate that commonly used methods to solve differential equations could be unstable, and no general methods guarantee the existence or uniqueness of a solution of such nonlinear second-order equations [41]. Furthermore, the 4th-Order-Runge-Kutta iteration technique was used and incorporated it with shooting method [57]. It turns out that the solution is very sensitive to the initial guess when the boundary value β is large. Thus, to address this issue [34], we adopted a method that successively increases β from small values, using previous solution in each iteration as the initial guess for solving the PBE with larger β. As a result, the number of iterations greatly increases making this method slow and unstable for $\beta \gg 1$. Thus a more efficient method is required to solve PBE for $\beta \gg 1$.

3.3. Invertible Mappings for PBE

The idea behind invertible mappings methods [70] is to replace a uniform discretization of space in a common finite-difference technique by adaptive discretization resulting in sufficiently higher density of points in the region of large variations of the solution and lower density outside this range.

To implement this strategy for Eq. (3.2) we introduce mapping of the coordinate $\widetilde{r}$ with the function f to a new coordinate $t = f(\widetilde{r})$, or $\widetilde{r} = f^{-1}(t)$. Function f should satisfy the condition that large but finite gradient of the solution in the large variation region is effectively reduced in t-space. The inverse function

$$f(\widetilde{r}) = \frac{\arctan\left[\widetilde{r}\tan(A)\right]}{A} \tag{3.5}$$

satisfies these conditions. Here a smoothing parameter A is used to adjust the number of grid points in the large variation region. With the help of such function f, one can find a uniform distribution of grid points in coordinates t that map non-uniform distribution in original coordinates $\widetilde{r}$, as shown in Ref. [70]. Thus, we

substitute first and second derivatives

$$\frac{dw}{d\widetilde{r}} = \frac{dw}{dt} f(t) \tag{3.6}$$

$$\frac{d^2w}{d\widetilde{r}^2} = \frac{d^2w}{dt^2} f^2(t) + \frac{dw}{dt} f(t) f'(t) \tag{3.7}$$

into Eq. (3.3), and obtain PBE in coordinates t

$$\frac{d^2w}{dt^2} f^2(t) - \left(\frac{dw}{dt}\right)^2 \frac{f^2(t)}{w} + \frac{dw}{dt}\left\{\frac{1}{\tan(At)} - \sin(2At)\right\} \tan(A) f(t) = \frac{w^2-1}{2} \tag{3.8}$$

where $f(t) = \frac{\tan(A)\cos^2(At)}{A}$ and $f'(t) = \frac{\tan(At)}{A}$. Substituting Eq. (3.6) into Eq. (3.3), we get the first boundary condition in the form

$$\frac{\tan(A)\cos^2(At)}{wA} \frac{dw}{dt}\bigg|_{t=(\arctan[\kappa a \tan(A)])/A} = -\beta \tag{3.9}$$

To obtin the second boundary condition, we cut off ∞ up to a constant r_{cut}, and get $t = \frac{\tan(r_{cut}A)}{\tan A}$, hence

$$w\left(\frac{\arctan\left[r_{cut}\tan(A)\right]}{A}\right) = 1 \tag{3.10}$$

To evaluate the stability of Eq. (3.8), we transform it into equations

$$\begin{cases} W' = \frac{W^2}{w} - \frac{W}{f(t)}\left\{\frac{\tan(A)}{\tan(At)} - \tan(A)\sin(2At)\right\} + \frac{\left(w^2-1\right)}{2f^2(t)} \\ w' = W \\ w'\Big|_{t=(\arctan[\kappa a \tan(A)])/A} = -\frac{\beta w A}{\tan(A)\cos^2(At)} \end{cases} \tag{3.11}$$

and the corresponding Jacobian matrix reads

$$J(t) = \begin{bmatrix} \frac{2W}{w} - \frac{1}{f(t)}\left\{\frac{\tan(A)}{\tan(At)} - \tan(A)\sin(2At)\right\} & -\frac{W^2}{w^2} + \frac{w}{f^2(t)} \\ M & N \end{bmatrix} \tag{3.12}$$

where $M = 1$, $N = 0$ when $t \neq \frac{\arctan[\kappa a \tan(A)]}{A}$, $M = 0$, $N = -\frac{\beta A}{\tan(A)\cos^2(At)}$ when $t = \frac{\arctan[\kappa a \tan(A)]}{A}$.

The best convergence of the equation is obtained for $A = 1.45$. The corresponding stiffness ratios for $A = 1.45$ are shown in Tab. 3.1. Comparing the stability of the two equations, we consider the stiffness ratios of the grid points in the same interval through mapping $t = \frac{\arctan[\widetilde{r}\tan(A)]}{A}$, but reduce the number of grid points to 100.

Table 3.1.: Stiffness ratios S($\widetilde{r}$) of nonlinear PBE, Eq. (3.8)

	$\xi = 0.02$				$\xi = 0.2$			
$\widetilde{r}(t)$	$\beta = 1.0$	$\beta = 2.0$	$\beta = 10.0$	$\beta = 20.0$	$\beta = 10.0$	$\beta = 20.0$	$\beta = 30.0$	$\beta = 60.0$
0.04	22.10	2180.64	6230.57	1603.52	4.01	14.23	14.27	13.88
0.06	183.20	198.54	185.68	277.00	10.98	11.12	10.73	10.70
0.08	39.46	40.53	44.18	46.96	7.64	7.68	7.53	7.49
0.10	9.37	9.51	8.78	11.12	4.96	4.98	4.74	4.69
0.12	2.01	2.06	2.05	2.01	2.71	2.74	2.76	2.69
0.14	1.50	1.59	1.47	1.24	1.00	1.00	1.00	1.00
0.16	3.00	3.11	2.75	2.79	1.00	1.00	1.00	1.00
0.18	4.50	4.66	4.14	4.16	1.00	1.00	1.00	1.00
0.20	5.53	5.43	5.55	5.29	1.00	1.00	1.00	1.00

The values of S in Tab. 3.1 suggest that the solver may be unstable in some isolated grid points, that does not affect the overall stability, while in most cases it is stable in all grid points. Further more, it reduces the number of grid points and hence greatly speeding up the solving process. The value of A in Eq. (3.5) can be used to tune the distribution of the grid points. If we set A close to 0, the grid points are distributed more or less evenly both in $\widetilde{r}$- and t-spaces. When A is close to $\pi/2$ the grid points are densely distributed in the vicinity of κa in $\widetilde{r}$-space. Such high distribution density leads to high values of derivatives close to 0 (Figure Fig. 3.1). This situation corresponds to Eq. (3.9) when value of β in boundary condition is large.

Note that when A is close to $\pi/2$, the convergence may decrease as shown in Figure Fig. 3.2. This can be attributed to the fact that fixed number of grid points crowd around limited area in the vicinity of κa, which prevents the convergence. To overcome it, we can treat A as adaptive variable, i.e. gradually increasing A from an initial value $S(A_0)$ (for example $A_0 = 1.0$) until $S(A_0 + h)$ such that $\|S(A_0) - S(A_0 + h)\| < C$, where C is a certain threshold.

3.4. Numerical Test

We ran a series of tests to check the performance of the method using invertible mapping and solving Eq. (3.8) in t-space compared to the solver of PBE with fixed step and solving directly Eq. (3.3) in $\widetilde{r}$-space. Such solver was implemented in IPEC-solver for electrostatic potential of a linear chain in salt solution, which serves

as a reference state for equilibrium structures of self-assembled inter-polyelectrolyte complexes [7, 34]. The solver corresponding to Eq. (3.3) corresponds to the version IPEC V1.0, while the solver corresponding to Eq. (3.8) corresponds to IPEC V1.2.

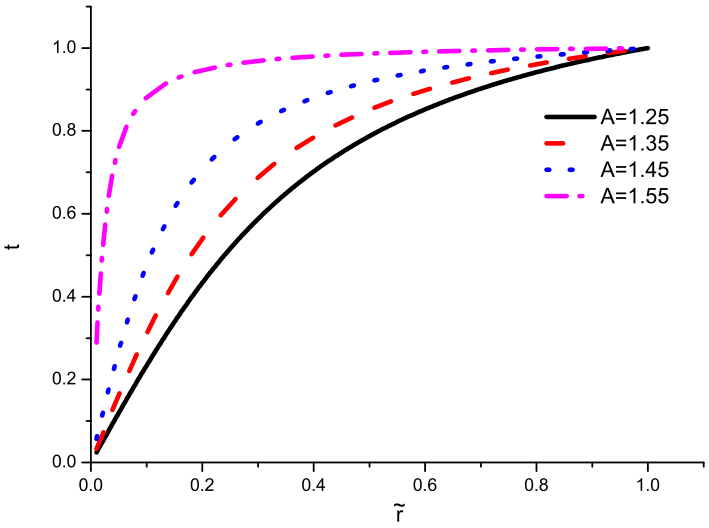

Figure 3.1.: Distribution of grid points in t- and $\tilde{r}$- spaces with different values of tuning parameter A.

The performance of two methods is illustrated in Figure Fig. 3.3 for large β. It allows to conclude that (i) invertible mappings method implemented in IPEC V1.2 can converge to the solution with the same precision with smaller number of grid points; (ii) for sufficiently high values of β invertible mappings method converge to a solution when the direct method fails (blue dashed line for $\beta = 300$). However, invertible mappings method slightly decrease the accuracy of the solution, since the inverse function transmits the original error $O(h_{\tilde{r}})$ to the solver with the error $O(h_t)$ when the number of grid points is fixed. Here $h_{\tilde{r}}$ and h_t are two steps in corresponding solvers respectively and satisfy $h_t = \frac{\arctan[h_{\tilde{r}}\tan(A)]}{A}$.

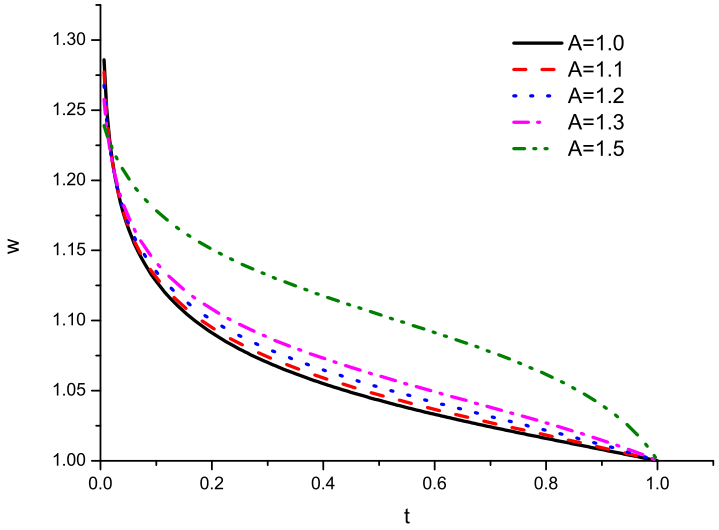

Figure 3.2.: The solution of Eq. (3.3), $w = \exp(u)$ for different values of A obtained with 200 grid points, and$\beta = 10$, $\xi = 0.02$. The curve $A = 1.5$ is distorted due to lack of gird points in numerical test interval $(0.0, 1.0)$.

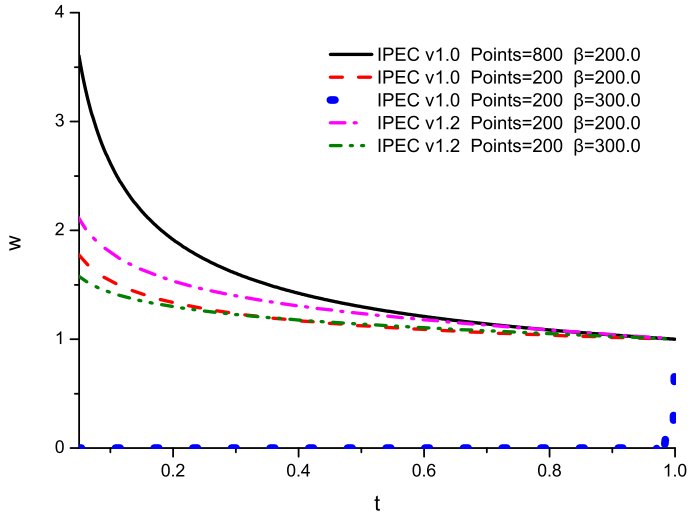

Figure 3.3.: The solution of Eq. (3.3), $w = \exp(u)$ for large values of β and fixed $A = 1.05$. The value of A is obtained by starting from an initial value $A_0 = 1.0$, and set $S(A)$ denote the corresponding solution, $h = 0.05$,$C = 0.1$ then $\|S(A_0 + h) - S(A_0)\| < C$. Invertible mapping method (IPEC V1.2) needs less grid points and converges readily when the direct method (IPEC V1.0) fails (blue dashed line).

4. Electrostatic Effect in the Self Assembly of Charged Surfactants

4.1. Introduction

Electrostatic interactions are instrumental in the self-assemble process of short amphiphilic molecules. At low concentrations the amphiphilic molecules form a dilute homogeneous solution of individual molecules, while at high concentrations the amphiphilic molecules aggregate as micelles with their hydrophilic groups exposed to solvent and their hydrophobic groups shielded in the micellar interior [32, 2, 26]. Among amphiphilic molecules, surfactants are an important class of chemicals consisting of two moieties that interact very dfferently with a solvent [35, 32, 2, 26], in which the hydrophobic tail, interacts unfavorably with the solvent while the hydrophilic group interacts favorably with the solvent. In everyday life, the surfactants molecules are playing a crucial role in many areas including such diverse fields as detergency, food, paint, pharmaceutical products, cosmetics and industrial as well as biological processes [35, 6, 69, 49, 50]. The critical micelle concentration, (CMC) and critical aggregate concentration (CAC) designate the onset of aggregation of free surfactants into micelles in the spontaneous micellization process[36, 14]. [15, 14, 16] report the electrostatic interaction between the polyelectrolyte and the surfactant lead to a red shift compared to absorption spectra in aqueous Poly(methacrylic acid) solution and in water. [1] describes the effect of increasing salt concentration in the solution near the CMC, and it gives the relation between the surface charge adaptation and the change of salt concentration.

The Poisson-Boltzmann equation (PBE) describes electrostatic interactions between molecules in ionic solutions, and it can be used in modeling implicit solvation, an approximation of the effects of solvent on the structures and interactions of amphiphilic molecules and the corresponding micelles or aggregates[7, 5]. Although the generalized PBE has been modified to adapt to many different applications[42], it is still a powerful tool to study the effect on the aggregation into micelles or aggregates.

The Single Chain Mean Field (SCMF) theory is another tool to explore the self-assembly of a mixture of an arbitrary number of types of molecules of an arbitrary structure interacting with each other through mean fields[61, 62, 8], and this method is quite universal that can be applied to solutions of linear or branched polymers,

solutions of low-molecular weight surfactants and various additives, mixtures of various components and structural and shape transitions. Specifically, recent years SCMF theory has been used to simulate the self-assembly process of surfactants into micelles, and even the equilibrium structure of phospholipid membranes at the molecular level [23, 56]. This method enable us to calculate the equilibrium properties for models of surfactant systems at a coarse grained level which does not include fluctuations and inter-particle correlations, however it can be compensated by the combination of the SCMF with MD simulations. Although SCMF theory can be used for modeling the surfactant or polymer systems in both a lattice and continuous space [4, 3], considering Poisson-Boltzmann theory that is combined with SCMF is applied in implicit solvation, we choose the continuous model for SCMF[12, 46].

4.2. Single Chain Mean Field Theory

In continuous space, SCMF calculation is built on coarse-grained model in which amphiphile molecules are treated as coarse grained beads. The amphiphile configurations are obtained using the Rosenbluth and Rosenbluth chain growth self-avoiding random walk algorithm[51] and periodic boundary conditions are used.

First we consider the free energy F of the system in a simulation box volume, V , containing N linear polyelectrolytes

$$\begin{aligned}\frac{F}{VkT} &= \int c(\Gamma)\ln\frac{c(\Gamma)}{e}\Lambda^3 d\Gamma + \int\frac{d\mathbf{r}}{V}c_s(\mathbf{r})\ln\frac{c_s(\mathbf{r})}{e}\Lambda_s^3 + \int c(\Gamma)u_{total}(\Gamma)d\Gamma \\ &\quad + \frac{1}{V}\int d\mathbf{r}\frac{\rho(\mathbf{r})u(\mathbf{r})}{2} + \frac{1}{V}\int d\mathbf{r}\Big\{\sum_{\varpi=\pm}\rho_\varpi(r)\Big(\ln\Big[\rho_\varpi(r)\Big]-1\Big)\Big\} \qquad (4.1)\end{aligned}$$

where $c(\Gamma) = \frac{NP(\Gamma)}{V}$ is the distribution function that related to the probability of a single surfactant of conformation $P(\Gamma)$, and $c_s(\mathbf{r})$ is the concentration of solvent molecules. Λ and Λ_s are the de Broglie lengths of the beads and solvent respectively. The last term is the entropy of free ions in the solution, and $\rho_\varpi(r)$ denotes the positive and negative free ions which satisfy the equality $\ln[\rho_\varpi(r)/c_\infty] = -\varpi u(r)$, and $u(r)$ is the electrostatic potential at r. Function $u_{total}(\Gamma)$ represents the interaction potential of the conformation Γ within the Fields, and it can be written

$$\begin{aligned}u_{total}(\Gamma) &= u_{intro}(\Gamma) + \frac{N-1}{2}\int dr\Big\{\varepsilon_{HH}\phi_{int}^H(\Gamma,\mathbf{r})\langle c_H(\mathbf{r})\rangle \\ &\quad + \varepsilon_{TT}\phi_{int}^T(\Gamma,\mathbf{r})\langle c_T(\mathbf{r})\rangle\Big\} + \varepsilon_{TW}\int dr\phi_{int}^T(\Gamma,\mathbf{r})c_s(r) \\ &\quad + \varepsilon_{HW}\int dr\phi_{int}^H(\Gamma,\mathbf{r})c_s(r) \qquad (4.2)\end{aligned}$$

where $u_{intro}(\Gamma)$ denotes interactions of the beads inside a given conformation, the second term denotes the interactions with beads in another conformation. The factor $\frac{1}{2}$ is to avoid double counting and $(N-1)$ is to delete the intra-molecular devotion $u_{intro}(\Gamma)$. The last two terms involve the electrostatic interaction and corresponding entropy. $u(\mathbf{r}) = \beta q\varphi(\mathbf{r})$ describes the electrostatic potential at $\mathbf{r}$, and q denotes the elementary charge, $\beta = \frac{1}{kT}$, and

$$\rho(\mathbf{r}) \;=\; N\int P(\Gamma)d\Gamma\left\{c_H(\Gamma,\mathbf{r})\lambda_H + c_T(\Gamma,\mathbf{r})\lambda_T\right\} + c_\infty\left[e^{-u(\mathbf{r})} - e^{u(\mathbf{r})}\right] \tag{4.3}$$

is the charge density stems from the surfactants and the free ions, and N is the number of the surfactants of conformation Γ. The first term in Eq.4.3 denotes the so called fixed charge density which is assumed in proportion to the concentration of H and T beads, while the second term $\rho_\varpi = c_\infty e^{\mp u(r)}$ denotes the density of free ions arising from the electrostatic potential.

As our surfactants are composed by only two types of beads: hydrophilic, H and hydrophobic, T, we introduce interaction parameter ε_{TT} which denotes the contact energy between hydrophobic beads and parameter ε_{HH} between hydrophilic beads. Likewise, ε_{TW} and ε_{HW} denote interaction parameters between hydrophobic beads and solvent, and hydrophilic beads and solvent respectively. Then the average concentrations of beads T and H are

$$\langle c_T(\mathbf{r})\rangle = \int P(\Gamma)c_T(\Gamma,\mathbf{r})d\Gamma \tag{4.4}$$

$$\langle c_H(\mathbf{r})\rangle = \int P(\Gamma)c_H(\Gamma,\mathbf{r})d\Gamma \tag{4.5}$$

And the average volume fraction

$$\langle \phi(\mathbf{r})\rangle = \int P(\Gamma)\phi_{ex}(\Gamma,\mathbf{r})d\Gamma \tag{4.6}$$

where $\phi_{ex}(\Gamma,\mathbf{r})$ is the excluded volume of the conformation Γ, and it is obtained after all conformations are generated. Then incompressibility condition is

$$\phi_s(\mathbf{r}) + N\langle\phi(\mathbf{r})\rangle = 1 \tag{4.7}$$

where $\phi_s(\mathbf{r}) = c_s(\mathbf{r})v_s$ is the solvent volume fraction. Hence the augmented free

energy F_{aug} can be written into

$$\begin{aligned}\frac{F_{aug}}{VkT} &= \int c(\Gamma)\ln\frac{c(\Gamma)}{e}\Lambda^3 d\Gamma + \int\frac{dr}{V}c_s(\mathbf{r})\ln\frac{c_s(\mathbf{r})}{e}\Lambda_s^3 + \int c(\Gamma)u_{total}(\Gamma)d\Gamma \\ &+\frac{1}{V}\int d\mathbf{r}\frac{\rho(\mathbf{r})u(\mathbf{r})}{2} + \int d\mathbf{r}\frac{\pi(\mathbf{r})}{V}\Big\{\phi_s(\mathbf{r}) + N\left\langle\phi(\mathbf{r})\right\rangle - 1\Big\} \\ &+\frac{1}{V}\int d\mathbf{r}\Big\{\sum_{\varpi=\pm}\rho_\varpi(r)\Big(\ln\Big[\rho_\varpi(r)\Big] - 1\Big)\Big\} \end{aligned} \tag{4.8}$$

We minimize F_{aug} with respect to the concentration of the solvent $c_s(r)$ to get the approximate expression for the Lagrange multiplier $\pi(\mathbf{r})$.

$$\pi(\mathbf{r}) \approx -\frac{\ln\phi_s(\mathbf{r})}{v_s} \tag{4.9}$$

Finally, Eq.4.9 is inserted into Eq.4.8 and it is minimized in terms of $P(\Gamma)$, then it gives

$$P(\Gamma) = \frac{\exp\left(-H_N(\Gamma)\right)}{Q} \tag{4.10}$$

where Q is the normalization factor such that

$$\int P(\Gamma)d\Gamma = 1 \tag{4.11}$$

As term $\frac{N}{V}\int d\Gamma\ln c(\Gamma)$ is a constant and can be eliminated after normalization, the effective Hamiltonian $H_N(\Gamma)$ expressed in units kT is given by Eq.4.12

$$\begin{aligned}H_N(\Gamma) &= -\frac{\ln\phi_s(\mathbf{r})}{v_s}\phi_{ex}(\Gamma,\mathbf{r}) + u_{intro}(\Gamma) + (N-1)\Big[\varepsilon_{HH}\phi_{int}^H(\Gamma,\mathbf{r})\left\langle c_H(\mathbf{r})\right\rangle \\ &+\varepsilon_{TT}\phi_{int}^T(\Gamma,\mathbf{r})\left\langle c_T(\mathbf{r})\right\rangle\Big] + \varepsilon_{TW}\int dr\phi_{int}^T(\Gamma,\mathbf{r})c_s(r) + \varepsilon_{HW}\int dr\phi_{int}^H(\Gamma,\mathbf{r})c_s(r) \\ &+2\pi N\int r^2 dr u(r)\int d\Gamma\left\{c_H(\Gamma,r)\lambda_H + c_T(\Gamma,r)\lambda_T\right\} \end{aligned} \tag{4.12}$$

Finally, we take the obtained values of $P(\Gamma)$ back to the total free energy Eq.4.1. It is noted that the free energy F contains the fixed number of surfactants N, and the distribution between micelles of different sizes can be described by the minimum of free energy per surfactant. Furthermore the semi-grand potential of the system can be written as 4.13[60]

$$\Omega = \sum_{N=1}^{\infty} c_N\Big[\log\Big(c_N/e\Big) + F_N - F_{ref}\Big] \tag{4.13}$$

whereF_N and c_N are respectively the free energy and concentration of micelles with N surfactants. The free energies are measured in units kT and the interactions between micelles are ignoringed. F_{ref} is the free energy per surfactant in a reference state, defined as

$$F_{ref} = \int dr \frac{1}{v_s} \ln \frac{\Lambda_s^3}{v_s e} - 2c_\infty \int dr \tag{4.14}$$

Under the constraint of conservation of the total chain concentration c_t

$$c_1 + \sum_{N=2}^{\infty} N c_N = c_t \tag{4.15}$$

and

$$c_N = c_1^N \exp\left[N(F_1 - F_{ref}) - (F_N - F_{ref}) \right] \tag{4.16}$$

then substitute Eq.4.16 into Eq.4.15, we obtain the total concentration of micelles in terms of free energy F_N and F_1 by

$$c_1 + \sum_{N=2}^{\infty} N c_1^N \exp\left[N(F_1 - F_{ref}) - (F_N - F_{ref}) \right] = c_t \tag{4.17}$$

through Eq.4.17 we can obtain the distribution of micelles composed by N surfactants in the solution with dierent salt density.

4.3. Poisson Boltzmann Theory For The Charged Complex

We consider the Coulombic contribution F_{el} of the aggregated complex, and the corresponding entropy F_{idea} arising from free ions is also taken into account. The simulation box is discretized into concentric spherical shells, hence we only need to consider its equilibrium properties in this one dimensional system with the radius r of the shells as the coordinate. Firstly, Poisson Equation is one of the fundamental equations of classical electrostatics, which relates the variation of the potential $\varphi(r)$ within the dielectric variable $\varepsilon(r)$ to the total charge density $\rho_{total}(\Gamma, r)$. If in a medium of uniform dielectric constant ε, the Poisson equation adopts the following form:

$$\nabla^2 \varphi(r) = -\frac{4\pi q}{\varepsilon} \rho_{total}(r) \tag{4.18}$$

In this homogeneous solution, the total charge density $\rho_{total}(r)$ reads

$$\begin{aligned}\rho_{total}(r) &= N\int P(\Gamma)d\Gamma\left\{c_H(\Gamma,r)\lambda_H + c_T(\Gamma,r)\lambda_T\right\} \\ &\quad +c_\infty\left(e^{-\beta q\varphi(r)} - e^{\beta q\varphi(r)}\right)\end{aligned} \tag{4.19}$$

where the first term is the density of fixed charge which is in proportion to the linear combination of the concentrations of polymers, and λ_H and λ_T denotes the charge ratio which is a scale coefficient in proportion to the corresponding beads concentration. It is noted that Eq.4.18 connects the microscopic properties of individual surfactant ($(\Gamma,r)\lambda_H$ and $c_T(\Gamma,r)\lambda_T$) to the macroscopic charge density $\rho_{total}(r)$. The second term is the charge density of the free ions in the solution, c_∞ the bulk concentration of ions. In our model, we divided the space of the box into nested spherical cells, and denote δ as the thinkness of each cell, and substitute $x = \frac{r}{l_B}$, hence the total charge density $\rho_{total}(\Gamma, x)$ can be written into a dimensionless form

$$\begin{aligned}\rho_{total}(x) &= N\int P(\Gamma)d\Gamma\left\{c_H(\Gamma,x)\lambda_H + c_T(\Gamma,x)\lambda_T\right\} \\ &\quad +c_\infty(e^{-\beta q\varphi(x)} - e^{\beta q\varphi(x)})\end{aligned} \tag{4.20}$$

Then we substitute Eq.4.20 into Eq.4.18. As it can be approximated in symmetrical spherical coordinates, we obtain the differencial Poisson-Boltzmann equation in the spherical coordinates. For brevity we set $u(x) = \beta q\varphi(x)$, and we define the Debye length $\frac{1}{\kappa}$ by $\kappa^2 = 8\pi l_B c_\infty \Rightarrow \frac{\kappa^2}{8\pi} = l_B c_\infty$, where $l_B = \frac{\beta q^2}{\varepsilon}$ is the Bjerrum length and ε is the solvent dielectric constant.

$$\begin{aligned}\frac{d^2u(x)}{dx^2} + \frac{2}{x}\cdot\frac{du(x)}{dx} &= -4\pi N l_B^3\int P(\Gamma)d\Gamma\left\{c_H(\Gamma,x)\lambda_H + c_T(\Gamma,x)\lambda_T\right\} \\ &\quad +(\kappa l_B)^2\sinh u(x)\end{aligned} \tag{4.21}$$

where $(\kappa l_B)^2$ is a parameter which is proportional to the salt density. It is noted $c_H(\Gamma,x)$ and $c_T(\Gamma,x)$ are in units of Bjerrum length l_B , and for compatible with the dividing space of the box we need to convert units in l_B to the thickness of the cell δ when solving the equation. Finally, discretisation of the boundary Γ with the Dirichlet boundary condition is

$$u(x)|_{x\to\infty} = 0 \tag{4.22}$$

For solving this differencial equation we add in an extra boundary condition

$$u'(x)|_{x=0} = 0 \tag{4.23}$$

The electrostatic free energy functional F_{el} in terms of the local co- and counterion

densities ρ_{total} which include Coulombic contribution F_{el}, and the ions detached from the polymers consist of the usual ideal F_{id}

$$\frac{F_{el}}{VkT} = \frac{4\pi}{V}\int_V r^2 dr \frac{\rho_{total}(r)u(r)}{2} \tag{4.24}$$

and from Eq.4.24 we can obtain the corresponding contribution F_{el-eff} in the effective Hamiltonian

$$\frac{F_{el-eff}}{kT} = 2\pi N \int r^2 dr u(r)\left\{c_H(\Gamma,r)\lambda_H + c_T(\Gamma,r)\lambda_T\right\} \tag{4.25}$$

Then the contribution to the free energy due to the entropy of free ions can be written as

$$\begin{aligned}\frac{F_{idea}}{VkT} &= \frac{4\pi}{V}\int_V r^2 dr\Big\{\sum_{\varpi=\pm}\rho_\varpi(r)\left(\ln\left[\frac{\rho_\varpi(r)}{c_\infty}\right]-1\right)\Big\} \\ &= \frac{8c_\infty\pi}{V}\int_V r^2 dr\Big\{u(r)\sinh u(r)-\cosh u(r)\Big\}\end{aligned}$$

where $\rho_\pm(r) = c_\infty e^{\mp u(r)}$, as $u(r)$ is independent of $P(\Gamma)$, hence the entropy of free ions $F_{idea-eff}$ makes no effective contribution to the final Hamiltonian

$$\frac{F_{idea-eff}}{kT} = 0$$

Finally, combined with the contribution of the entropy of free ions

$$\frac{F_{el-eff}+F_{idea-eff}}{kT} = \frac{1}{2}\int_V 4\pi r^2 N dr\Big\{u(r)c_H(\Gamma,r)\lambda_H + u(r)c_T(\Gamma,r)\lambda_T\Big\}$$

then substitute $x = \frac{r}{l_B}$,

$$\frac{F_{el-eff}+F_{idea-eff}}{kT} \approx \sum_k l_B^3 V_k(l_B) N\left\{\frac{u(k)c_H(\Gamma,k)\lambda_H}{2}+\frac{u(k)c_T(\Gamma,k)\lambda_T}{2}\right\}$$

where k denotes the number of kth layer, and $u(k)$ is the electrostatic potential at the kth layer. $V_k(l_B)$ denotes the volume of the kth layer in units of l_B, and similarly in calculation we substitute $l_B^3 V_k(l_B) = \delta^3(\frac{l_B}{\delta})^3 V_k(\delta)$ into Eq.4.12, where δ is the thickness of the cell, and $V_k(\delta)$ denotes the volume of the kth layer in units of δ, and $\frac{l_B}{\delta}$ is the ratio of the Bjerrum length to the thickness of the cell.

Furthermore, Eq.4.21 can be solved analytically in the DH approximation when the electrostatic potential is small, $u(x) \ll 1$. In this case, the charge density can be

linearized, $\sinh u(x) \approx u(x)$, and the solution can be written in the form

$$u(x) = \frac{\mathrm{M}_1 \mathrm{e}^{\sqrt{b}x}}{x} - \frac{M_2\sqrt{b}}{2bx\mathrm{e}^{\sqrt{b}x}} - \frac{a(x)}{b} \tag{4.26}$$

where $a(x) = -4\pi N\delta^3/(\frac{\delta}{l_B})\int P(\Gamma)d\Gamma\left\{c_H(\Gamma,x)\lambda_H + c_T(\Gamma,x)\lambda_T\right\}$, $b = (\kappa l_B)^2(\frac{\delta}{l_B})^2$, and M_1, M_2 are two coefficients determined by boundary conditions Eqs.4.23,4.22. Furthermore, from Eq.4.23 we derive $M_2 = 2\sqrt{b}M_1$, hence

$$u(x) = \frac{\mathrm{M}_1 \mathrm{e}^{\sqrt{b}x}}{x} - \frac{M_1\mathrm{e}^{-\sqrt{b}x}}{x} - \frac{a(x)}{b} \tag{4.27}$$

where $\mathrm{M}_1 = \lim\limits_{x\to\infty} \frac{a(x)}{2b}\frac{x}{\sinh\left(\sqrt{b}x\right)}$ which is determined by the boundary condition Eq.4.22.

4.4. Numerical test and disscussion

We develop the programm in C++ for the simulation. For brevity and clarity, the numerical tests are organized into 2 groups according to the parameters, in the first group we fix the charge density of free ions, and tune the fixed charge density by changing the values of coefficients related to the linear combination of the concentrations of polymers $\rho^f(\Gamma,r) = c_H(\Gamma,r)q\lambda_H + c_T(\Gamma,r)q\lambda_T$, while in the second group the charge ratio on beads H of the polymers (λ_H) are fixed to study the variation of the size of the aggregated complex in different salt density of the solution.

In numerical tests, all the surfactants consist of 6 beads in type H and 6 beads in type T, and the size of the box is $24 \times 24 \times 24$ (in units of kuhn length). 1 million of conformations is adopted in the sampling simulation, and the configuration parameters are summarized in Tab. 4.1.

	Configuration Parameters
Units radius (In units of Kuhn length)	1.0
Interaction range (In units of Kuhn length)	1.61
Bond length (In units of Kuhn length)	1.47
T-T contact energy	-7.0
H-H contact energy	-1.0
T-S contact energy	0.5
H-S contact energy	2.0

Table 4.1.: Configuration parameters in numerical test for simulation of electrostatic effect in the self assembly of charged surfactants

In the first group, the charge density of free ions is fixed and Fig. 4.1 shows the free energy of the spherical complex per surfactant, and the complex are aggregated by

different charged surfactants in the solution with fixed dimensionless density of salt ions.

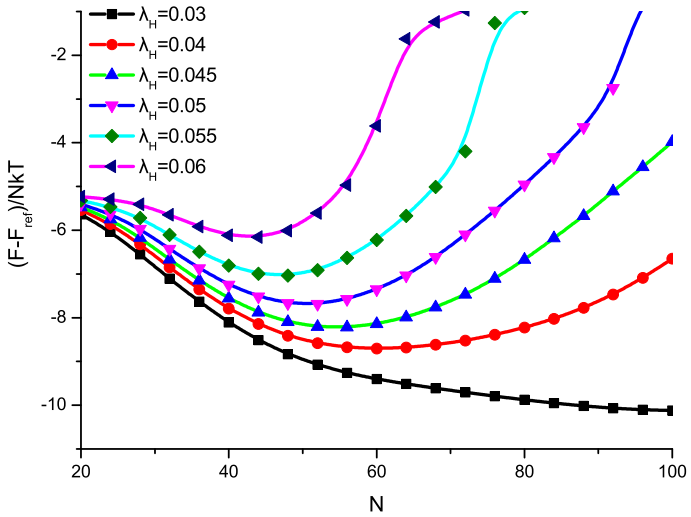

Figure 4.1.: Free energy per surfactant of H_6T_6 in solution with dimensionless salt density $\kappa l_B = 0.001$, increase the charge on H beads by different values of λ_H, the numbers of aggregating polymers according to the minimum free energy per surfactant decrease.

Fig. 4.2 illustrates the self-assembly behaviors of H_6T_6, and radial variation of volume fraction profile of all parts of the complex, in which beads H carry different quantities of electric charge. In particular, the volume fraction of ϕ_H decreases prominently.

Rather than the distribution c_p, we adopt the more convenient function $\Omega_p = \ln \frac{c_1}{c_p}$ to consider the variation of distribution of the ionic micelles composed by different charged surfactants with different charge ratio. The values of Ω_p are shown in Fig. 4.3, and it illustrates the more charge the surfactants carry, the less aggregate and the lower concentration of corresponding micelles in the solution. The influence of charge ratio on critical micelle concentration (CMC) are listed in Fig. 4.4.

Reversely, in the second group we fixed the charge ratio on beads H of the polymers (λ_H) to study the variation of the size of the aggregated complex in different salt density of the solution. We fix λ_H, and gradually increase the salt density of the solution κl_B. Fig. 4.5 presents the free energy of the complex aggregated by the charged surfactants with the fixed charge ratio $\lambda_H = 0.07$, and it indicates more charged surfactants aggregating into the complexes with the salt density κl_B increasing. Fig. 4.6 illustrates the radial variation of volume fraction profile of the spherical micelle in the solution with different salt density κl_B. It demonstrates that it will swell as salt density of the solution increases, and the corresponding electrostatic

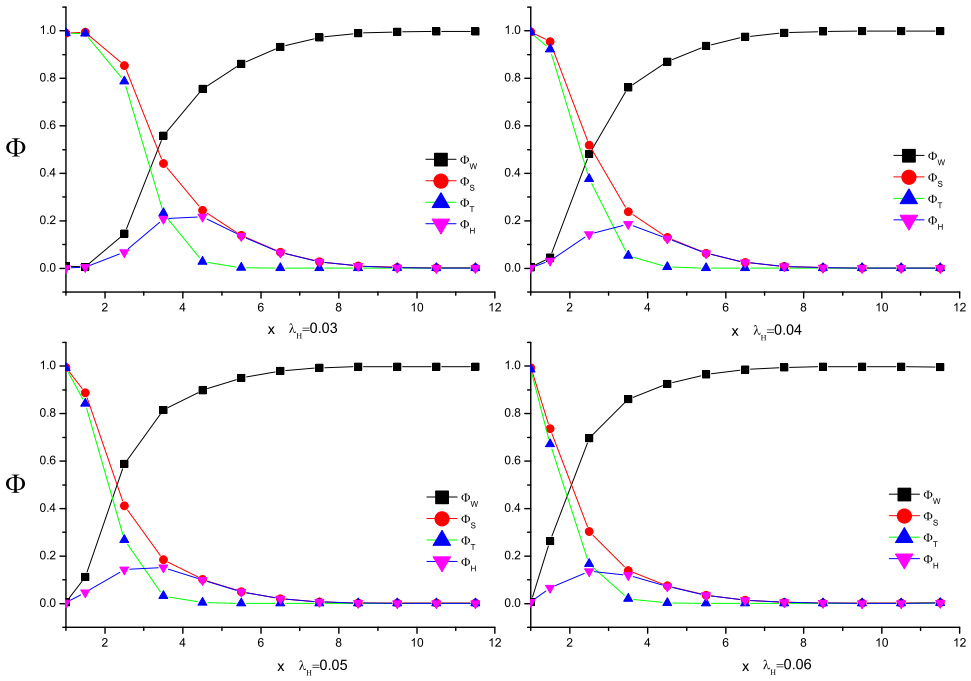

Figure 4.2.: Radial variation of volume fraction profile of tail $\phi_T(x)$, head$\phi_H(x)$, solvent $\phi_W(x)$ and solute$\phi_S(x)$ of the spherical micelle, which are aggregated by the charged surfactants with different charge ratio λ_H on beads H, and the salt density in the solution is fixed by $\kappa l_B = 0.001$.

potentials are shown in Fig. 4.7. Analogously we calculate the distribution of the ionic micelles in solution with different salt density and the corresponding CMC, as shown in Fig. 4.8 and Fig. 4.9.

4.5. Conclusions

In this chapter we incorporate the single chain mean field (SCMF) theory with Poisson Boltzmann theory to explore the electrostatic effect in the aggregation behavior of ionic surfactant molecules. We adopt coarse grained model to simulate chemical structures of ionic surfactants and their micellization process. Combined with the Poisson Boltzmann theory, the charge-charge repulsions between charged surfactant, and the electrostatic screening effects by free salt ions are both taken into account. By selecting the surfactant chain with certain quantity of charge on the hydrophilic groups, we can predict the micellization properties of surfactants, structures and

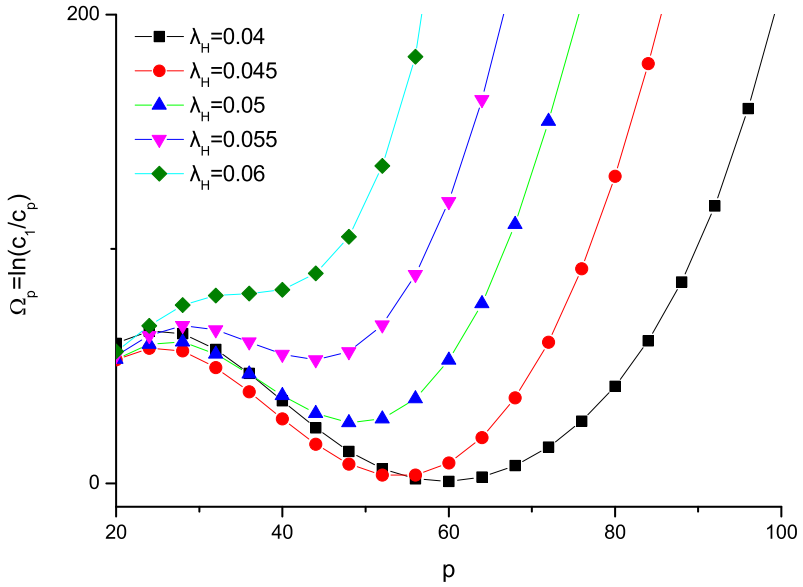

Figure 4.3.: Potential Ω_p as a function of the aggregation number p for inoic micelles composed by charged surfactants with different charge ratio λ_H. The valley value of Ω_p increase and correspondingly p decrease with the charge ratio λ_H increases. The salt density in the solution is fixed by $\kappa l_B = 0.001$.

thermodynamics of micelles, such as the critical micelle concentration as well as the aggregation number and the size distributions of micelles. Besides, by tuning the density of free salt ions we can obtain the corresponding micelles as predicted in the computer simulation, and it can be used for the structural modeling in experimental techniques that require the specific molecular structure.

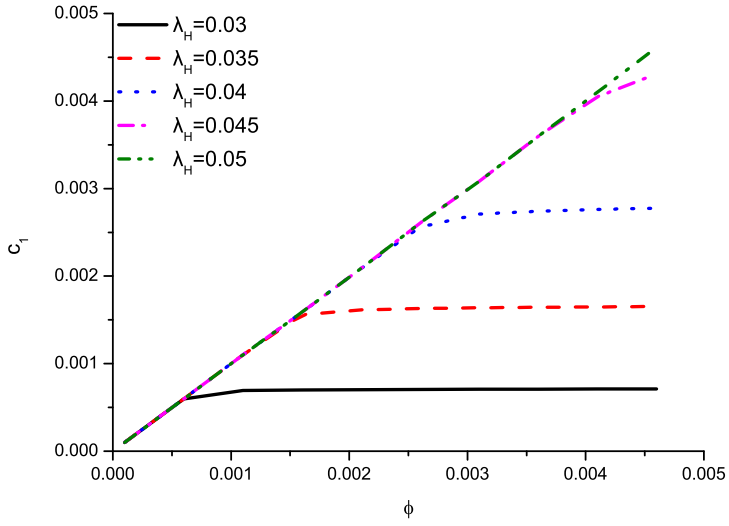

Figure 4.4.: Free surfactant mole fraction (c_1) as a function of the total surfactant concentration ($\phi(c_1)$) for different charge ratio λ_H. The salt density in the solution is fixed by $\kappa l_B = 0.001$.

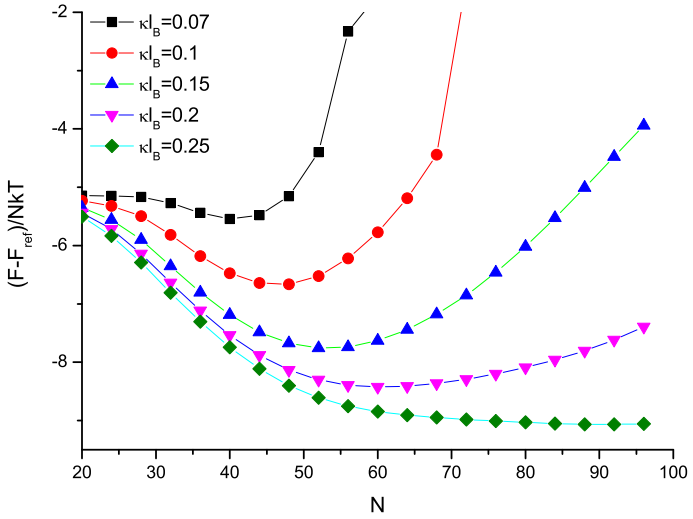

Figure 4.5.: Free energy per surfactant of H_6T_6 in solution with different dimensionless salt density κl_B. With the salt density κl_B increasing, the numbers of aggregating polymers according to the minimum free energy per surfactant increases correspondingly.

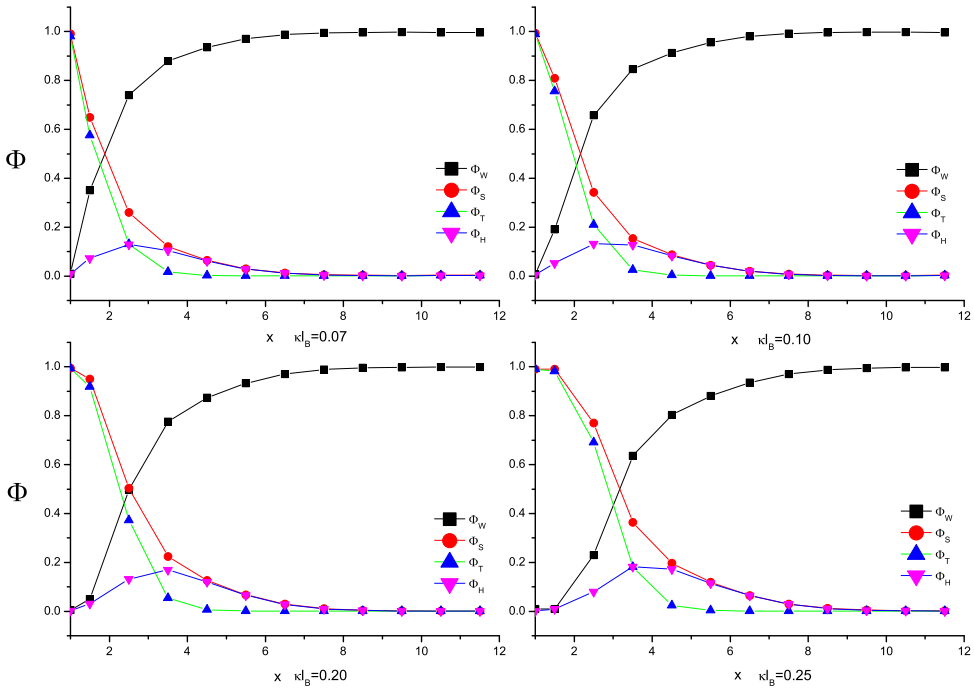

Figure 4.6.: Radial variation of volume fraction profile of tail $\phi_T(x)$, head $\phi_H(x)$, solvent $\phi_W(x)$ and solute $\phi_S(x)$ of the spherical micelle, which are aggregated by the charged surfactants with the fixed charge ratio $\lambda_H = 0.03$ on beads H, and the salt density in the solution varies from 0.07 to 0.25.

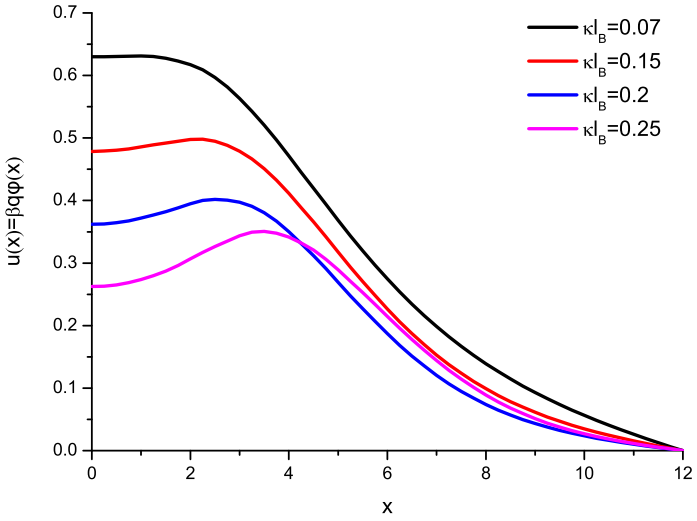

Figure 4.7.: Electrostatic potential (volt) of the spherical micelle with fixed charge ratio $\lambda_H = 0.07$, in solution of different dimensionless salt density κl_B.

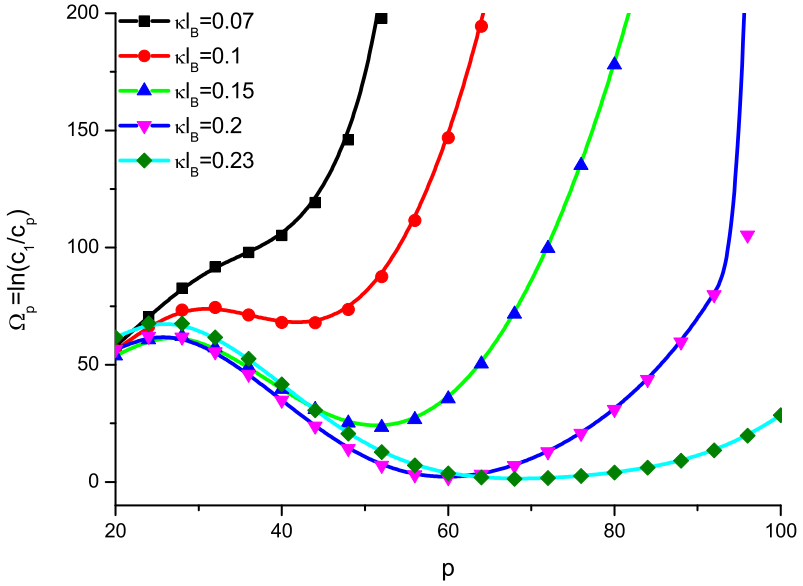

Figure 4.8.: Potential Ω_p as a function of the aggregation number p for inoic micelles in solution with different salt density. The micells are composed by the charged surfactants with fixed charge raio $\lambda_H = 0.07$. The valley value of Ω_p decrease while correspondingly p increase with the salt density κl_B increases.

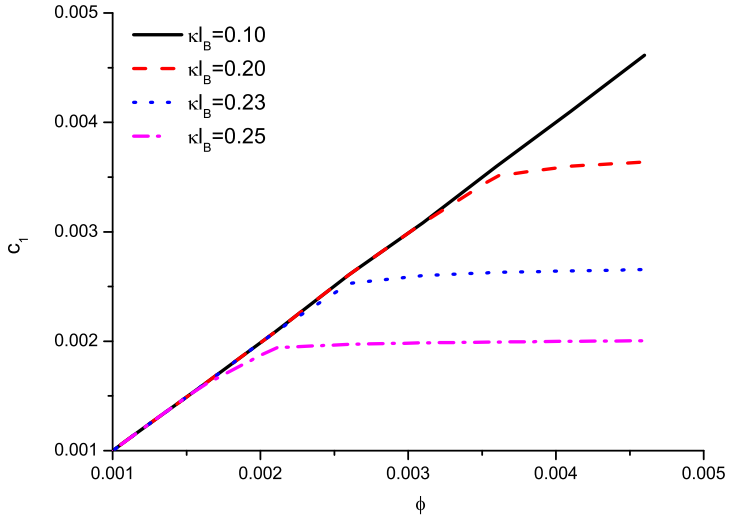

Figure 4.9.: Free surfactant mole fraction (c_1) as a function of the total surfactant concentration ($\phi(c_1)$) in solution with different salt density. The charge raio of the charged surfactant is fixed by $\lambda_H = 0.07$.

5. Electrostatic Effect in Shape Transition of Micelles Aggregated by Charged Surfactants

5.1. Introduction

Amphiphilic molecules, such as lipids and surfactants are an important class of chemicals consisting of two moieties that interact very dfferently with a solvent [35, 32, 2, 26], in which the hydrophobic tail, interacts unfavorably with the solvent while the hydrophilic group interacts favorably with the solvent. In aqueous or organic solvents, these molecules often spontaneously selfassemble into various structures such as micelles, bilayer membranes and bicontinuous structures[8, 36, 26]. In everyday life, these amphiphilic molecules are playing a crucial role in many areas including such diverse fields as detergency, food, paint, pharmaceutical products, cosmetics and industrial as well as biological processes [35, 6, 69, 49, 50], and shape transitions of micelles play an important role in cellular physiology. Earlier, micelles shape transitions in presence of monovalent salt were investigated experimentally[54], and the transitions of micelles in model nonionic surfactantsolutions were theoretically investigated[4]. The sphere to cylinder or disk transitions of surfactant micelles in aqueous solution have recently been investigated by coarse-grained molecular dynamics (MD) simulations [58, 66], and single-chain mean-field theory (SCMF) with Monte Carlo (MC) simulations[17].

The Poisson-Boltzmann equation (PBE) describes electrostatic interactions between molecules in ionic solutions, and it can be used in modeling implicit solvation, an approximation of the effects of solvent on the structures and interactions of amphiphilic molecules and the corresponding micelles or aggregates[7, 5]. Although the generalized PBE has been modified to adapt to many different applications[42], it is still an powerful tool to study the effect on the aggregation into micelles or aggregates. The Single Chain Mean Field (SCMF) theory provide us a tool to study the self-assembly of a mixture of an arbitrary number of types of molecules of an arbitrary structure interacting with each other through mean fields[61, 62, 8]. Moreover this method can be applied to solutions of linear or branched polymers, solutions of low-molecular weight surfactants and various additives, mixtures of various components and structural and shape transitions universally. Recently SCMF has been used to simulate the self-assembly process of surfactants into micelles, and even the equi-

librium structure of phospholipid membranes at the molecular level [23, 56]. Since Single Chain Mean Field (SCMF) theory can be used for numerically modeling the surfactant and polymer systems in a lattice and continuous space [4, 3], we choose the continuous model for SCMF[12, 46].

In this chapter, we explore the process of shape transition in ionic surfactants aggregation with varying electrostatic properties of surfactants and salt density of solution. The analysis is carried out through two-dimensional SCMF together with Rosenbluth method which are used for generating conformations of a single chain. In our model, the amphiphilic molecules are modelled as a chain of freely connected beads, and the amphiphilic molecules as H_xT_y, where x and y represent the number of beads in the head H and tail$T$. We assume heads H in the amphiphilic molecules carry charge, hence the amphiphilic molecules are treated as linear polyelectrolytes on which evenly distributed the charge. In such macromolecular systems, the stability of finite size aggregates results from the balance of the electrostatic repulsion between the positively charged hydrophilic groups and the attraction between hydrophilic groups (HH interaction), as well as the attraction between hydrophobic groups (TT interaction). Besides, as the free ions of salt and counterions in the solution surrounding the micelles increases, the concentration of small ions of opposite charge inside the complex increases inducing stronger screening effect, and such an effect will weaken the repulsion between charged hydrophilic groups hence break the balance between forces[7, 34].

5.2. Single Chain Mean Field

We adopt 2D Single Chain Mean Field (SCMF) theory to coarse-grained model. In this model the space is divided into Z_l slice along $z-axis$ and N_c nested concentric shells of radii r in the $x-y$ plane, hence (r, z) can be treated as the coordinates of the certain cell in layer z and shell r. The condition for the incompressibility can be described by Eq.

$$\langle\phi_H(r,z)\rangle + \langle\phi_T(r,z)\rangle + \phi_S(r,z) = 1 \tag{5.1}$$

where $\phi_S(r,z) = c_S(r,z)v_s$ is the volume fraction of the solvent in cell (r,z), $c_S(r,z)$ denotes the corresponding concentration. v_s denotes the volume of one solvent bead and $\langle\phi_H(r,z)\rangle$ and $\langle\phi_T(r,z)\rangle$ denote the corresponding mean volume fraction of beads H and T respectively. The angular brackets $\langle\ldots\rangle$ denote the average over the probability distribution function $P(\Gamma)$ of the system, hence

$$\langle\phi_H(r,z)\rangle = \int P(\Gamma)\phi_H(\Gamma,r,z)d\Gamma \tag{5.2}$$

$$\langle \phi_T(r,z) \rangle = \int P(\Gamma)\phi_T(\Gamma,r,z)d\Gamma \tag{5.3}$$

We define $c(\Gamma) = \frac{NP(\Gamma)}{V}$ is the distribution function that related to the probability of a single surfactant of conformation $P(\Gamma)$, and V is the volume of the simulation box. The intramolecular attractive contribution to the interaction energy is simplified

$$E_{intro}(\Gamma) = \int dv \varepsilon_{TT} \int c(\Gamma) u_{intro}(\Gamma,r,z)d\Gamma \tag{5.4}$$

where $u_{intro}(\Gamma)$ is the potential generated by the $T-T$ interactions inside conformation Γ, and it is obtained after all conformations are generated. Then the interaction between moleculars can be written into

$$\begin{aligned} E_{inter}(\Gamma) &= d\Gamma c(\Gamma) \Bigg\{ \frac{N-1}{2} \int dv \Bigg[\varepsilon_{HH} \phi^H_{int}(\Gamma,r,z) \langle c_H(r,z) \rangle \\ &\quad + \varepsilon_{TT} \phi^T_{int}(\Gamma,r,z) \langle c_T(r,z) \rangle \Bigg] \Bigg\} \end{aligned} \tag{5.5}$$

The entropies of the polymers and solvent are combined as

$$E_{ps} = V \int c(\Gamma) \ln \frac{c(\Gamma)}{e} \Lambda_p d\Gamma + \int dv c_S(r,z) \ln \frac{c_S(r,z)}{e} \Lambda_s \tag{5.6}$$

where V denotes the volume of the simulation box. Λ_p and Λ_s denote Broglie lengths of the beads of polymers and solvent respectively.

5.3. Poisson Boltzmann Theory

We consider the Coulombic contribution F_{el} of the aggregated complex, and the corresponding entropy F_{idea} arising from free ions is also taken into account. The simulation box is discretized into concentric spherical shells, hence we only need to consider its equilibrium properties in this one dimensional system with the radius r of the shells as the coordinate. Firstly, Poisson Equation is one of the fundamental equations of classical electrostatics, which relates the variation of the potential $\varphi(r,z)$ within the dielectric variable $\varepsilon(r,z)$ to the total charge density $\rho_{total}(\Gamma,r,z)$. If in a medium of uniform dielectric constant ε, the Poisson equation adopts the following form:

$$\nabla^2 \varphi(r,z) = -\frac{4\pi q}{\varepsilon} \rho_{total}(r,z) \tag{5.7}$$

In this homogeneous solution, the total charge density $\rho_{total}(r,z)$ reads

$$\rho_{total}(r,z) = N\int P(\Gamma)d\Gamma\left\{c_H(\Gamma,r,z)\lambda_H + c_T(\Gamma,r,z)\lambda_T\right\} + c_\infty\left(e^{-\beta q\varphi(r,z)} - e^{\beta q\varphi(r,z)}\right) \tag{5.8}$$

where the first term on the right side is the density of fixed charge which is in proportion to the linear combination of the concentrations of polymers, and λ_H and λ_T denotes the charge ratio which is a scale coefficient in proportion to the corresponding beads concentration. It is noted that Eq.5.7 connects the microscopic properties of individual surfactant ($(\Gamma,r)\lambda_H$ and $c_T(\Gamma,r)\lambda_T$) to the macroscopic charge density $\rho_{total}(r)$. The second term is the charge density of the free ions in the solution, c_∞ denotes the bulk concentration of ions.

Then we substitute Eq.5.8 into Eq.5.7. As it can be approximated in 2D $r-z$ coordinates, the differencial Poisson-Boltzmann equation is obtained

$$\begin{aligned}\frac{\partial\varphi(r,z)}{r\partial r} + \frac{\partial^2\varphi(r,z)}{\partial r^2} + \frac{\partial^2\varphi(r,z)}{\partial z^2} &= -\frac{4\pi q}{\varepsilon}\left\{N\int P(\Gamma)d\Gamma\left[c_H(\Gamma,r,z)\lambda_H + c_T(\Gamma,r,z)\lambda_T\right]\right.\\ &\left. + c_\infty\left[e^{-\beta q\varphi(r,z)} - e^{\beta q\varphi(r,z)}\right]\right\}\end{aligned} \tag{5.9}$$

where q denotes the elementary charge and ε is the solvent dielectric constant. In our model, the space of the box is divided into concentric circular shells of radius r and layers of slices with total length z, and the thickness of each cell are δ_h and δ_r respectively, then $x_h = \frac{z}{\delta_h}$, $x_r = \frac{r}{\delta_r}$. For brevity we set $u(x_r,x_h) = \beta q\varphi(x_r,x_h)$, and $\int P(\Gamma)d\Gamma\left[c_H(\Gamma,r,z)\lambda_H + c_T(\Gamma,r,z)\lambda_T\right] = \langle c_H(r,z)\rangle\,\lambda_H + \langle c_T(r,z)\rangle\,\lambda_T$ then the $2D$ differencial Poisson-Boltzmann equation

$$\begin{aligned}\frac{\partial u(x_r,x_h)}{x_r\partial x_r} + \frac{\partial^2 u(x_r,x_h)}{\partial x_r^2} + \frac{\partial^2 u(x_r,x_h)}{\partial x_h^2}\left(\frac{\delta_r}{\delta_h}\right)^2 &= -4\pi\delta_r^3 N\left[\langle c_H(x_r,x_h)\rangle\,\lambda_H + \right.\\ &\left. + \langle c_T(x_r,x_h)\rangle\,\lambda_T\right]/\left(\frac{\delta_r}{l_B}\right) +\\ &+ \frac{(\kappa l_B)^2}{2}\left(\frac{\delta_r}{l_B}\right)^2\left[e^{u(x_r,x_h)} - e^{-u(x_r,x_h)}\right]\end{aligned}$$

where $\left(\frac{\delta_r}{\delta_h}\right)$ and $\left(\frac{\delta_r}{l_B}\right)$ are two ratios determined by the input parameters. N is the number of polymers, and (κl_B) is proportion to the salt density which can be used for tuning the salt density in the solution. Inverse Debye length $\frac{1}{\kappa}$ is defined by $l_B c_\infty = \frac{\kappa^2}{8\pi}$, and $l_B = \frac{\beta q^2}{\varepsilon}$ is the Bjerrum length and ε is the solvent dielectric constant. where $(\kappa l_B)^2$ is a parameter which is proportional to the salt density,

and $\frac{\delta}{l_B}$ is the ratio of the thickness to the Bjerrum length, which is a constant in the numerical test we set it 2.0. Finally, discretisation of the boundary Γ with the Dirichlet boundary condition are

$$u(x_r, x_{h=0}) = 0, u(x_r, x_{h=max}) = 0 \tag{5.10}$$

and

$$u(x_{r=max}, x_h) = 0, u'(0, x_h) = 0 \tag{5.11}$$

where $x_{h=max}$ and $x_{h=0}$ corresponds to the heights of the top layer and bottom layer, and $x_{r=max}$ is the radius of the outermost layer of the nested cylinder.

The electrostatic free energy functional F_{el} in terms of the local co- and counterion densities ρ_{total} which include Coulombic contribution F_{el}, and the ions detached from the polymers consist of the usual ideal F_{id}

$$\frac{F_{el}}{VkT} = \int dv \frac{\rho_{total}(r,z)u(r,z)}{2V} \tag{5.12}$$

Then the contribution to the free energy due to the entropy of free ions can be written as

$$\begin{aligned} \frac{F_{idea}}{VkT} &= \frac{1}{V}\int dv\Big\{\sum_{\varpi=\pm}\rho_{\varpi}(r,z)\left(\ln\left[\frac{\rho_{\varpi}(r,z)}{c_{\infty}}\right]-1\right)\Big\} \\ &= \frac{1}{V}\int dv\Big\{u(r,z)\sinh u(r,z) - \cosh u(r,z)\Big\} \end{aligned}$$

where $\rho_{\pm}(r,z) = c_{\infty}e^{\mp u(r,z)}$, as $u(r,z)$ is independent of $P(\Gamma)$, hence the entropy of free ions $F_{idea-eff}$ makes no effective contribution to the final Hamiltonian. Finally, combined with the contribution of the entropy of free ions

$$\frac{F_{el-eff}+F_{idea-eff}}{kT} = \frac{N}{2}\int dv\left\{u(r,z)c_H(\Gamma,r,z)\lambda_H + u(r,z)c_T(\Gamma,r,z)\lambda_T\right\}$$

then substitute $x_h = \frac{z}{\delta_h}, x_r = \frac{r}{\delta_r}$,

$$\frac{F_{el-eff}+F_{idea-eff}}{kT} \approx \sum_k \delta_h\delta_r^2 V_{x_r,x_h} N\left\{\frac{u(x_r,x_h)c_H(\Gamma,x_r,x_h)\lambda_H + u(k)c_T(\Gamma,x_r,x_h)\lambda_T}{2}\right\}$$

where x_r, x_h denotes the coordinates of the cell in simulation box, V_{x_r,x_h} and $u(x_r,x_h)$ denote the volume and electrostatic potential of the corresponding cell respectively.

5.4. Numerical test and disscussion

We developed the programm in C++ to test the equations. For brevity and clarity, in all numerical tests we fix the fixed charge density represented by the values of coefficients related to the linear combination of the concentrations of polymers $\rho^f(\Gamma, r) = c_H(\Gamma, r)q\lambda_H + c_T(\Gamma, r)q\lambda_T$, and tune the charge density of free ions by changing the values of κl_B. In the first numerical test, the chains consist of 6 beads in type H and 6 beads in type T, and the size of the box is $30 \times 30 \times 30$ (in units of Kuhn length), and $\delta_h = 2.0$ and $\delta_r = 2.0$, ratio of thickness to Bjerrum length $\frac{\delta_r}{l_B} = 4.0$. 1 million of conformations is adopted in the sampling simulation, and the configuration parameters are summarized in Tab. 5.1.

	Parameters
Bead radius	0.5
Interaction range	1.61
Bond length	1.0
T-T contact energy, kT	-6.0
H-H contact energy , kT	-1.0

Table 5.1.: Molecular configuration parameters of block copolymers used in simulations for H_6T_6.

Although solution for the 2D SCMFT is not unique, and it means more than one aggregate could exist in solution, we have always obtained solutions with one single aggregate. Fig. 5.1 shows the free energy per surfactant of the spherical complex aggregated by the fixed charge ratio $\lambda_H = 0.1$ with different dimensionless density of salt ions $\kappa l_B = 0.01, 0.05, 0.07, 0.10$.

Fig. 5.2 illustrates the self-assembly behaviors of H_6T_6, showing salt density changing induces sphere to cylinder transition of the micelle. The variation of volume fraction profile of the complex ϕ_P according to different dimensionless salt density, in which the charge ratio of beads is fixed to $\lambda_H = 0.1$. In particular, the volume fraction of ϕ_H is shown in Fig. 5.3, in which it indicates ϕ_H increase prominently with the salt density κl_B increasing, and the corresponding dimensionless electrostatic potentials are listed in Fig. 5.4, which shows decrease of electrostatic potentials with salt density increasing.

In the second numerical test, the chains consist of 3 beads in type H and 6 beads in type T, and the size of the box is $25 \times 25 \times 25$ (in units of Kuhn length), and $\delta_h = 2.0$ and $\delta_r = 2.0$, ratio of thickness to Bjerrum length $\frac{\delta_r}{l_B} = 4.0$. 1 million of conformations is adopted in the sampling simulation, and the configuration parameters are summarized in Tab. 5.2. Similarly, the charge ratio on beads H of the polymers is fixed $\lambda_H = 0.08$, and the salt density of the solution κl_B is gradually

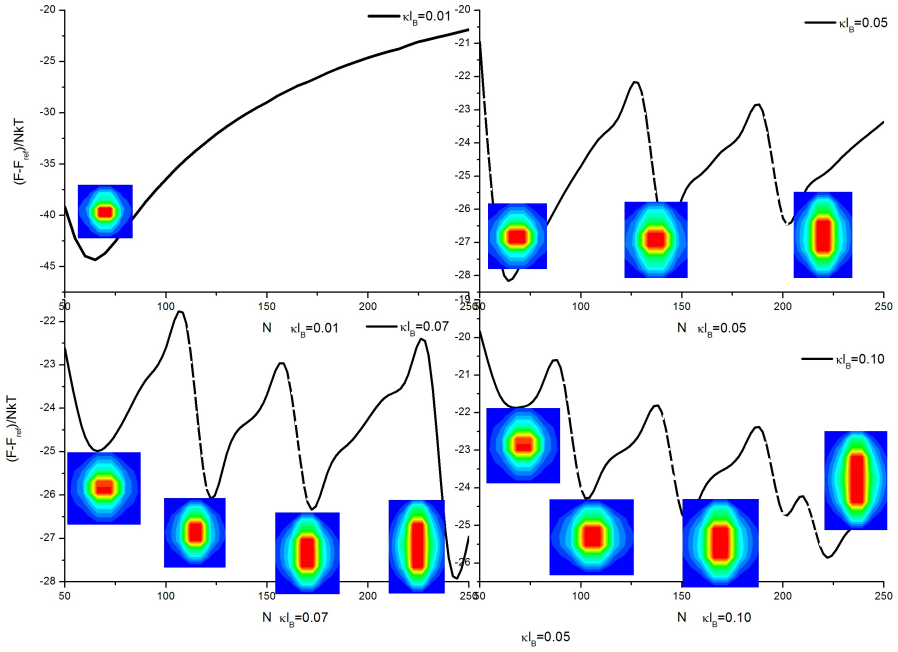

Figure 5.1.: Free energy per surfactant of H_6T_6 in solution with different dimensionless salt density $\kappa l_B = 0.01, 0.05, 0.07, 0.1$

increased. Fig. 5.5 presents the solvent free energy of the complex aggregated by the same number of the polymer chains. Fig. 5.6 and Fig. 5.7 illustrate the variation of volume fraction profile of the micelle $\phi_P = \phi_H + \phi_T$ and charged beads H ϕ_H respectively in the solution with different salt density κl_B, and the corresponding electrostatic potential is shown in Fig. 5.8. It indicates the volume of the micelle that composed by the asymmetrical surfactant H_3T_6 does not change much with salt density of the solution increases, while the shape changes from cylinder to sphere when micelle is large.

	Parameters
Bead radius	0.5
Interaction range	1.61
Bond length	1.0
T-T contact energy, kT	-5.5
H-H contact energy , kT	-2

Table 5.2.: Molecular configuration parameters of block copolymers used in simulations for H_3T_6.

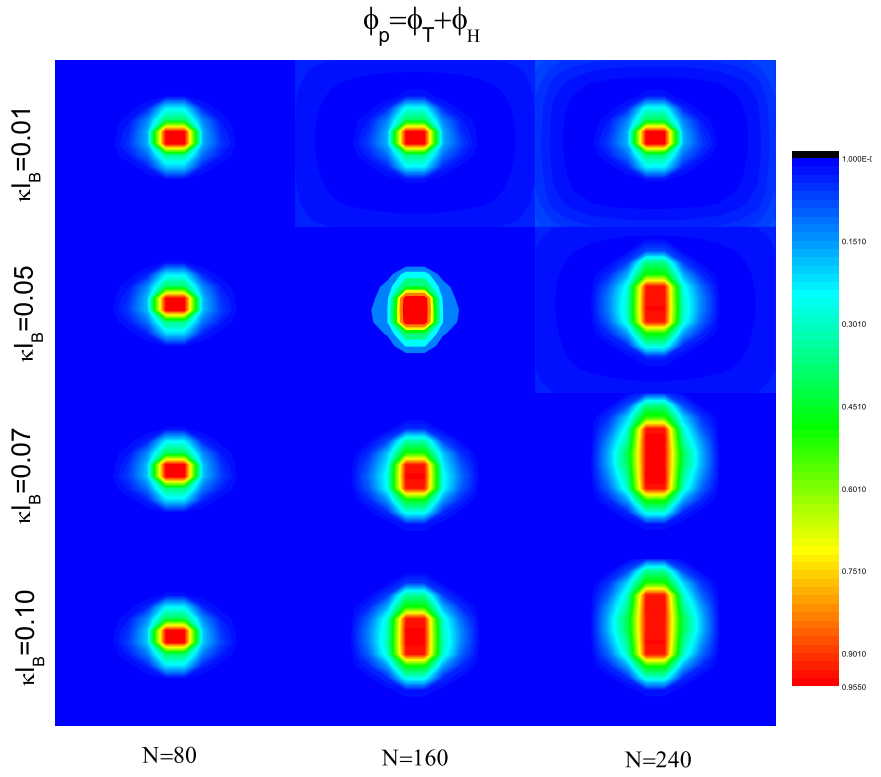

Figure 5.2.: The volume fraction profile of $\phi_P = \phi_T + \phi_H$ of the micelle, which are composed by the charged surfactants with fixed charge ratio $\lambda_H = 0.1$ on beads H, in the solution with different dimensionless salt density $\kappa l_B = 0.01, 0.05, 0.07, 0.1$. It shows the salt density changing induced sphere to cylinder transition of the micelle.

5.5. Conclusions

In this chapter, the 2D single chain mean field (SCMF) theory is incorporated with Poisson Boltzmann theory to explore the electrostatic effect in the shape transition behavior of the micelles composed by ionic surfactant molecules. We adopt coarse grained model to simulate chemical structures of ionic surfactants and their micellization process. Combined with the Poisson Boltzmann theory, the charge-charge repulsions between charged surfactant, and the electrostatic screening effects by free salt ions are both taken into account. By tuning the density of free salt ions we can obtain the possible micelles as predicted in the computer simulation, and it can be used for the structural modeling in experimental techniques that require the specific molecular structure.

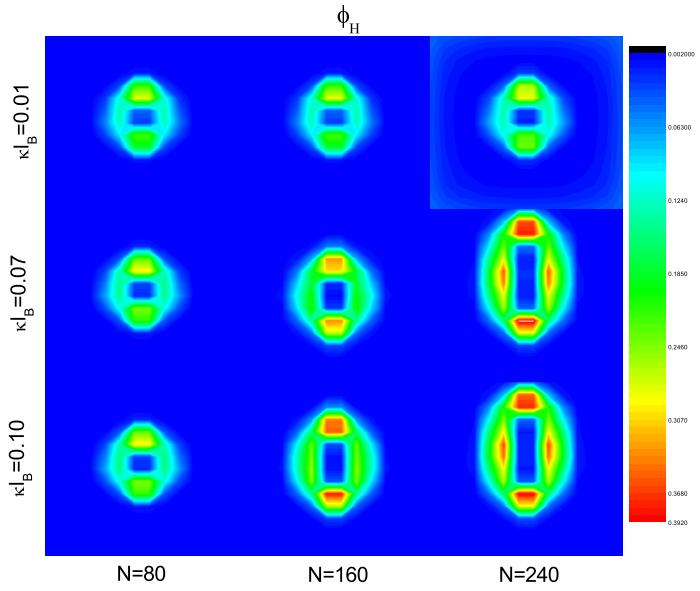

Figure 5.3.: The volume fraction profile of ϕ_H of the micelle composed by the charged surfactants with fixed charge ratio $\lambda_H = 0.1$ on beads H, in the solution with different dimensionless salt density κl_B.

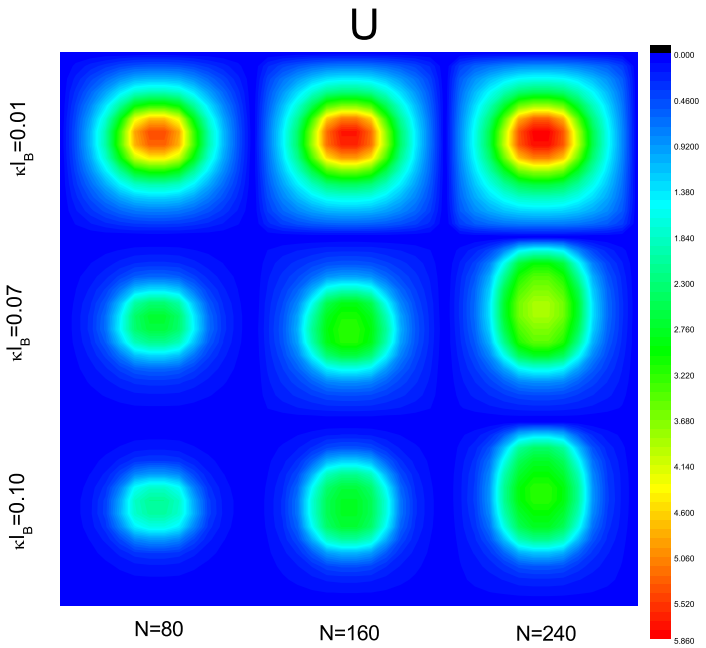

Figure 5.4.: Dimensionless electrostatic potential of the spherical micelle with fixed charge ratio $\lambda_H = 0.1$, in solution of dierent dimensionless salt density κl_B.

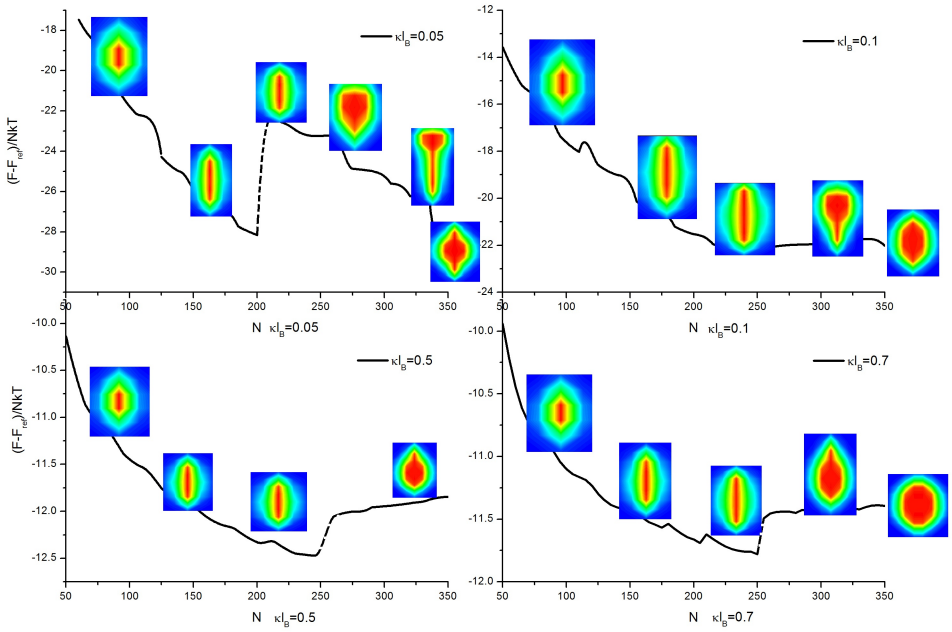

Figure 5.5.: Free energy per surfactant of H_3T_6 in solution with different dimensionless salt density $\kappa l_B = 0.01, 0.05, 0.07, 0.10$.

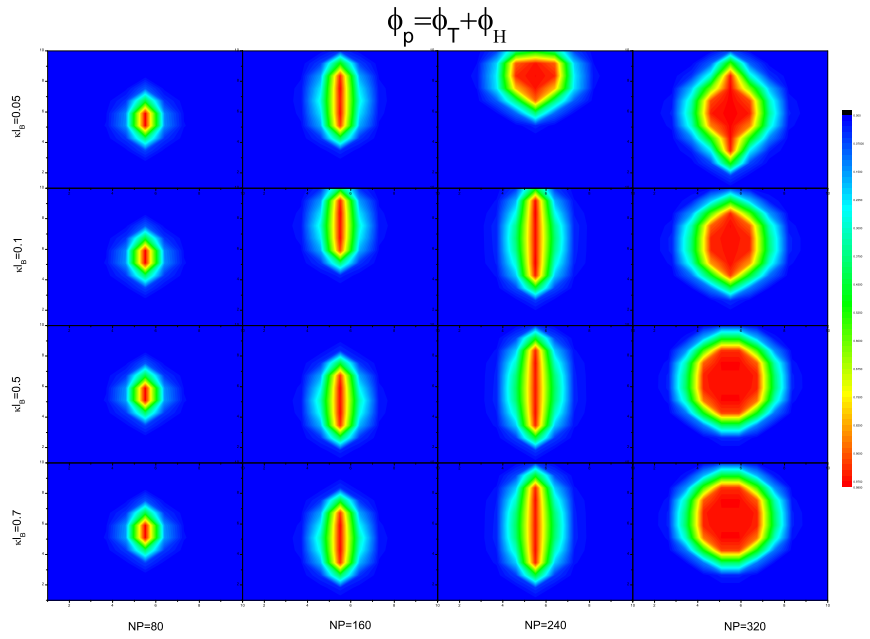

Figure 5.6.: Variation of volume fraction profile of micelles $\phi_P(x) = \phi_T(x) + \phi_H(x)$, which are aggregated by the polymer chains with the fixed charge ratio $\lambda_H = 0.08$ on beads H, and the salt density in the solution varies from 0.05 to 0.7.

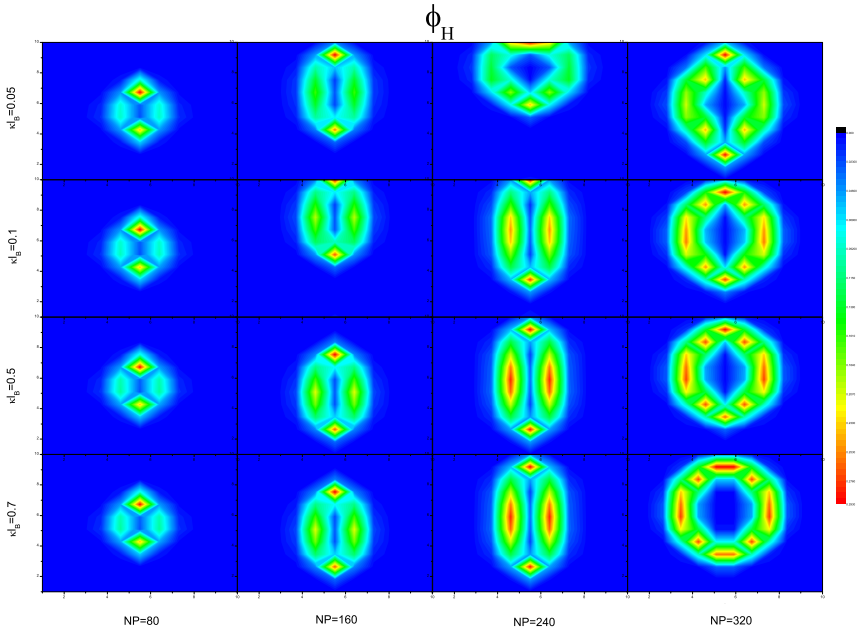

Figure 5.7.: The volume fraction profile of ϕ_H of the micelle composed by the charged surfactants with fixed charge ratio $\lambda_H = 0.08$ on beads H, in the solution with different dimensionless salt density κl_B.

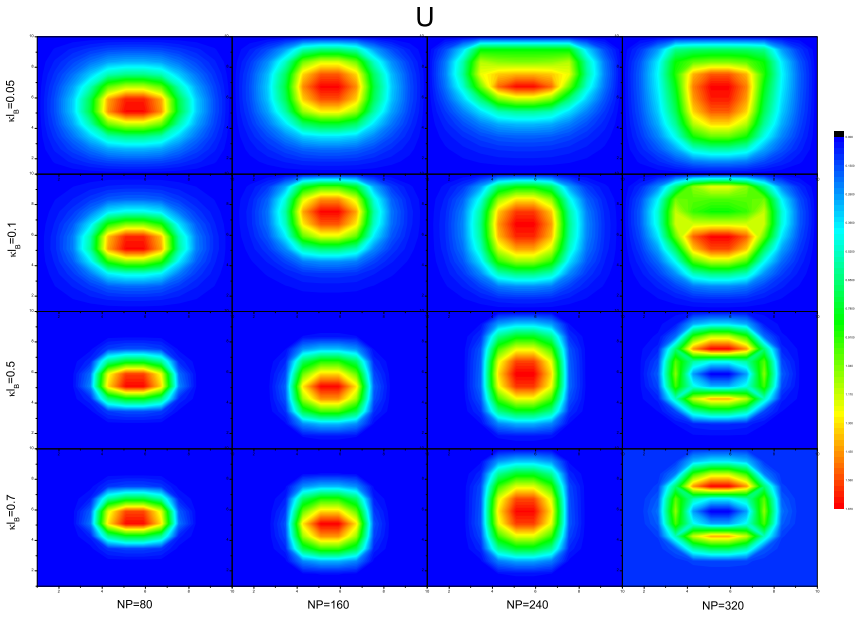

Figure 5.8.: Electrostatic potential of the spherical micelle with fixed charge ratio $\lambda_H = 0.08$, in solution of different salt density .

Bibliography

[1] *Structure-performance relationships in surfactants*. Number v. 112 in Surfactant science series. Marcel Dekker, New York, 2nd ed., rev. and expanded edition, 2003.

[2] Frontmatter. In *Surfactants and Interfacial Phenomena*, pages i–xvi. John Wiley & Sons, Inc., Hoboken, NJ, USA, January 2012.

[3] Zaid A. Al-Anber, Josep Bonet Avalos, and Allan D. Mackie. Prediction of the critical micelle concentration in a lattice model for amphiphiles using a single-chain mean-field theory. *The Journal of Chemical Physics*, 122(10):104910, March 2005.

[4] Zaid A. Al-Anber, Josep Bonet i Avalos, M. Antonio Floriano, and Allan D. Mackie. Sphere-to-rod transitions of micelles in model nonionic surfactant solutions. *The Journal of Chemical Physics*, 118(8):3816, 2003.

[5] B. Z. Lu, Y.C. Zhou, M.J. Holst, and J.A. McCammon. Recent progress in numerical methods for the poisson boltzmann equation in biophysical applications. *CiCP*, 5(3):973—1009, March 2008.

[6] Vladimir A. Baulin, Albert Johner, and Josep Bonet-Avalos. Aggregation of amphiphilic polymers in the presence of adhesive small colloidal particles. *J. Chem. Phys.*, 133:174905, 2010.

[7] Vladimir A. Baulin and Emmanuel Trizac. Self-assembly of spherical inter-polyelectrolyte complexes from oppositely charged polymers. *Soft Matter*, 8(25):6755–6766, 2012.

[8] A. Ben-Shaul, I. Szleifer, and W. M. Gelbart. Chain organization and thermodynamics in micelles and bilayers. i. theory. *The Journal of Chemical Physics*, 83(7):3597, 1985.

[9] Eva Betthausen, Markus Drechsler, Melanie Fortsch, Dmitry V. Pergushov, Felix H. Schacher, and Axel H. E. MÃŒller. Stimuli responsive micellar interpolyelectrolyte complexes control of micelle dynamics via core crosslinking. *Soft Matter*, 2012.

[10] O. V. Borisov and E. B. Zhulina. Effect of salt on self-assembly in charged block copolymer micelles. *Macromolecules*, 35(11):4472–4480, May 2002.

[11] Markus Burkhardt, Markus Ruppel, Sandrine Tea, Markus Drechsler, Ralf Schweins, Dmitry V. Pergushov, Michael Gradzielski, Alexander B. Zezin, and

Axel H. E. Muller. Water soluble interpolyelectrolyte complexes of polyisobutylene block poly(methacrylic acid) micelles: Formation and properties. *Langmuir*, 24:1769–1777, 2008.

[12] Jianwei Che, Joachim Dzubiella, Bo Li, and J. Andrew McCammon. Electrostatic free energy and its variations in implicit solvent models. *The Journal of Physical Chemistry B*, 112(10):3058–3069, March 2008.

[13] Pavel S. Chelushkin, Evgeny A. Lysenko, Tatiana K. Bronich, Adi Eisenberg, Victor A. Kabanov, and Alexander V. Kabanov. Polyion complex nanomaterials from block polyelectrolyte micelles and linear polyelectrolytes of opposite charge. 2. dynamic properties. *J. Phys. Chem. B*, 112:7732–7738, 2008.

[14] Deh Ying Chu and J. K. Thomas. Photophysical studies of a water-soluble copolymer of methacrylic acid and 1-pyreneacrylic acid. *Macromolecules*, 17(10):2142–2147, October 1984.

[15] Deh Ying. Chu and J. K. Thomas. Effect of cationic surfactants on the conformation transition of poly(methacrylic acid). *Journal of the American Chemical Society*, 108(20):6270–6276, October 1986.

[16] Deh Ying Chu and J. K. Thomas. Photophysical characterization of polyelectrolytes in the form of polymerized micelles from an ionic surfactant with a terminal double bond. *Macromolecules*, 24(9):2212–2216, April 1991.

[17] Asfaw Gezae Daful, Josep Bonet Avalos, and Allan D. Mackie. Model Shape Transitions of Micelles: Spheres to Cylinders and Disks. *Langmuir*, 28(8):3730–3743, February 2012.

[18] Thomas Dence. Cubics, chaos, and newton's method. *The Mathematical Gazette*, 3(3):403—408, November 1997.

[19] E. S. Dragan and S. Schwarz. Polyelectrolyte complexes. VI. polycation structure, polyanion molar mass, and polyion concentration effects on complex nanoparticles based on poly(sodium 2-acrylamido-2-methylpropanesulfonate). *J. Polym. Sci. A: Polym. Chem.*, 42:2495–2505, 2004.

[20] Ecaterina Stela Dragan, Marcela Mihai, and Simona Schwarz. Polyelectrolyte complex dispersions with a high colloidal stability controlled by the polyion structure and titrant addition rate. *Coll. and Surf. A: Physicochem. Eng. Aspects*, 290:213–221, 2006.

[21] Tomas Etrych, Laurent Leclercq, Mahfoud Boustta, and Michel Vert. Polyelectrolyte complex formation and stability when mixing polyanions and polycations in salted media: A model study related to the case of body fluids. *Eur. J. Pharm. Sci.*, 25:281–288, 2005.

[22] C. W Gear. *Numerical initial value problems in ordinary differential equations.* Prentice-Hall, Englewood Cliffs,N.J., 1971.

[23] Asfaw Gezae Daful, Vladimir A. Baulin, Josep Bonet Avalos, and Allan D. Mackie. Accurate critical micelle concentrations from a microscopic surfactant model. *The Journal of Physical Chemistry B*, 115(13):3434–3443, April 2011.

[24] Elizabeth R. Gillies and Jean M. J. Frechet. Development of acid-sensitive copolymer micelles for drug delivery. *Pure Appl. Chem.*, 76(7-8):1295–1307, 2004.

[25] M K Gilson and B Honig. Calculation of the total electrostatic energy of a macromolecular system: solvation energies, binding energies, and conformational analysis. *Proteins*, 4(1):7–18, 1988.

[26] Ian W. Hamley. *Introduction to soft matter: synthetic and biological self-assembling materials*. John Wiley & Sons, Chichester, England ; Hoboken, NJ, rev. ed edition, 2007.

[27] A. Harada and Kazunori Kataoka. Chain length recognition: Core-shell supramolecular assembly from oppositely charged block copolymers. *Science*, 283(5398):65—67, January 1999.

[28] Atsushi Harada and Kazunori Kataoka. Novel polyion complex micelles entrapping enzyme molecules in the core: Preparation of narrowly-distributed micelles from lysozyme and poly(ethylene glycol)-poly(aspartic acid) block copolymer in aqueous medium. *Macromolecules*, 31(2):288—294, 1998.

[29] Martin E. H. Heeley, Joseph K. Gallaher, Thanh Luan Nguyen, Han Young Woo, and Justin M. Hodgkiss. Surfactant controlled aggregation of conjugated polyelectrolytes. *Chemical Communications*, 49(39):4235, 2013.

[30] David K. Hoffman and Donald J. Kouri. Distributed approximating function theory: a general, fully quantal approach to wave propagation. *The Journal of Physical Chemistry*, 96(3):1179–1184, February 1992.

[31] David K. Hoffman, Naresh Nayar, Omar A. Sharafeddin, and D. J. Kouri. Analytic banded approximation for the discretized free propagator. *The Journal of Physical Chemistry*, 95(21):8299–8305, October 1991.

[32] Krister Holmberg, Bo JÃ¶nsson, Bengt Kronberg, and BjÃ¶rn Lindman. *Surfactants and Polymers in Aqueous Solution*. John Wiley & Sons, Ltd, Chichester, UK, October 2002.

[33] Michael J. Holst and Faisal Saied. Numerical solution of the nonlinear poisson boltzmann equation: Developing more robust and efficient methods. *Journal of Computational Chemistry*, 16(3):337—364, March 1995.

[34] Beibei Huang and Vladimir A. Baulin. IPEC solver: Numerical simulation tool to study inter-polyelectrolyte complexation. *Computer Physics Communications*, 184(9):2221–2229, September 2013.

[35] International Symposium on Surfactants in Solution. *Adsorption and aggregation of surfactants in solution*. Number v. 109 in Surfactant science series. Marcel Dekker, New York, 2003.

[36] Jacob N. Israelachvili. *Intermolecular and surface forces*. Academic Press, Burlington, MA, 3rd ed edition, 2011.

[37] A. V. Kabanov and V. A. Kabanov. DNA complexes with polycations for the delivery of genetic material into cells. *Bioconjug. Chem.*, 6:7–20, 1995.

[38] Alexander V. Kabanov, Tatiana K. Bronich, Victor A. Kabanov, Kui Yu, and Adi Eisenberg. Soluble stoichiometric complexes from poly(n-ethyl-4-vinylpyridinium) cations and poly(ethylene oxide)-block-polymethacrylate anions. *Macromolecules*, 29:6797–6802, 1996.

[39] Alexander V. Kabanov, Irina R. Nazarova, Irina V. Astafieva, Elena V. Batrakova, Valery Yu. Alakhov, Alexander A. Yaroslavov, and Victor A. Kabanov. Micelle formation and solubilization of fluorescent probes in poly(oxyethylene-b-oxypropylene-b-oxyethylene) solutions. *Macromolecules*, 28(7):2303–2314, March 1995.

[40] Kazuhiko Kakuda and Nobuyoshi Tosaka. The generalized boundary element approach to burgers' equation. *International Journal for Numerical Methods in Engineering*, 29(2):245–261, February 1990.

[41] C. T Kelley. *Solving nonlinear equations with Newton's method*. Society for Industrial and Applied Mathematics, Philadelphia, 2003.

[42] I Klapper, R Hagstrom, R Fine, K Sharp, and B Honig. Focusing of electric fields in the active site of cu-zn superoxide dismutase: effects of ionic strength and amino-acid modification. *Proteins*, 1(1):47–59, September 1986.

[43] L. Leclercq, M. Boustta, and M. Vert. Dynamics of polyelectrolyte complex formation and stability when a polycation is progressively added to a polyanion under physico-chemical conditions modeling blood. *Journal of Bioactive and Compatible Polymers*, 26(1):3–19, December 2010.

[44] Albert S. Lee, Vural Butun, M. Vamvakaki, Steven P. Armes, John A. Pople, and Alice P. Gast. Structure of pH-Dependent block copolymer micelles:Â charge and ionic strength dependence. *Macromolecules*, 35(22):8540—8551, October 2002.

[45] Nathalie Lefevre, Charles-Andre Fustin, and Jean-Francois Gohy. Polymeric micelles induced by interpolymer complexation. *Macromol. Rapid Commun.*, 30:1871–1888, 2009.

[46] Yan Levin. Electrostatic correlations: from plasma to biology. *Rep. Prog. Phys.*, 65:1577, 2002.

[47] B. Z. Lu and Xiaolin Cheng. Order n algorithm for computation of electrostatic interactions in biomolecular systems. *PNAS*, 103(51):19314—19319, December 2006.

[48] Benzhuo Lu and J. Andrew McCammon. Improved boundary element methods for Poisson Boltzmann electrostatic potential and force calculations. *JCTC*, 3(3):1134—1142, May 2007.

[49] Allan D. Mackie, Kaan Onur, and Athanassios Z. Panagiotopoulos. Phase equilibria of a lattice model for an oil water amphiphile mixture. *The Journal of Chemical Physics*, 104(10):3718, 1996.

[50] Allan D. Mackie, Athanassios Z. Panagiotopoulos, and Igal Szleifer. Aggregation behavior of a lattice model for amphiphiles. *Langmuir*, 13(19):5022–5031, September 1997.

[51] Rosenbluth Marshall N. and Rosenbluth Arianna W. Monte carlo calculation of the average extension of molecular chains. *The Journal of Chemical Physics*, 23(2):356, 1955.

[52] Hideharu Mori, Axel H. E. Muller, and Joachim E. Klee. Intelligent colloidal hybrids via reversible pH-Induced complexation of polyelectrolyte and silica nanoparticles. *Journal of the American Chemical Society*, 125(13):3712—3713, April 2003.

[53] K. W Morton and D. F Mayers. *Numerical solution of partial differential equations*. Cambridge University Press, Cambridge; New York, 2005.

[54] F. Muller, P. Guenoun, M. Delsanti, B. Deme, L. Auvray, J. Yang, and J. W. Mays. Spherical polyelectrolyte block copolymer micelles: Structural change in presence of monovalent salt. *EPJ E*, 15(4):465–472, December 2004.

[55] Anthony Nicholls and Barry Honig. A rapid finite difference algorithm, utilizing successive over-relaxation to solve the poisson boltzmann equation. *Journal of Computational Chemistry*, 12(4):435–445, May 1991.

[56] Sergey Pogodin and Vladimir A. Baulin. Coarse-grained models of phospholipid membranes within the single chain mean field theory. *Soft Matter*, 6(10):2216, 2010.

[57] William H Press. *Numerical recipes : the art of scientific computing*. Cambridge University Press, Cambridge, UK; New York, 2007.

[58] Ashish V. Sangwai and Radhakrishna Sureshkumar. Coarse-Grained Molecular Dynamics Simulations of the Sphere to Rod Transition in Surfactant Micelles. *Langmuir*, 27(11):6628–6638, June 2011.

[59] Felix Schacher, Eva Betthausen, Andreas Walther, Holger Schmalz, Dmitry V. Pergushov, and Axel H. E. Muller. Interpolyelectrolyte complexes of dynamic multicompartment micelles. *ACS Nano*, 3(8):2095–2102, 2009.

[60] P. Sens, C. M. Marques, and J.-F. Joanny. Mixed micelles in a bidisperse solution of diblock copolymers. *Macromolecules*, 29:4880–4890, 1996.

[61] I. Szleifer, A. Ben-Shaul, and W. M. Gelbart. Chain organization and thermodynamics in micelles and bilayers. II. model calculations. *The Journal of Chemical Physics*, 83(7):3612, 1985.

[62] I. Szleifer, A. Ben-Shaul, and W. M. Gelbart. Statistical thermodynamics of molecular organization in mixed micelles and bilayers. *The Journal of Chemical Physics*, 86(12):7094, 1987.

[63] Frank C Thames, Joe F Thompson, C Wayne Mastin, and Ray L Walker. Numerical solutions for viscous and potential flow about arbitrary two-dimensional bodies using body-fitted coordinate systems. *Journal of Computational Physics*, 24(3):245–273, July 1977.

[64] Emmanuel Trizac and Gabriel Tellez. Onsager-manning-oosawa condensation phenomenon and the effect of salt. *Physical Review Letters*, 96(3), January 2006.

[65] V. V. Vasilevskaya, L. Leclercq, M. Boustta, M. Vert, and A. R. Khokhlov. Study of interpolymer complexes of oppositely charged macromolecules with different affinity to solvent. *Macromolecules*, 40:5934–5940, 2007.

[66] Maria Velinova, Durba Sengupta, Alia V. Tadjer, and Siewert-Jan Marrink. Sphere-to-Rod Transitions of Nonionic Surfactant Micelles in Aqueous Solution Modeled by Molecular Dynamics Simulations. *Langmuir*, 27(23):14071–14077, December 2011.

[67] Ilja K. Voets, Arie de Keizer, Frans A. M. Leermakers, Antoine Debuigne, Robert Jerome, Christophe Detrembleur, and Martien A. Cohen Stuart. Electrostatic hierarchical co-assembly in aqueous solutions of two oppositely charged double hydrophilic diblock copolymers. *Eur. Pol. J.*, 45(10):2913–2925, 2009.

[68] F. T. Wall and J. Berkowitz. Numerical solution to the poisson boltzmann equation for spherical polyelectrolyte molecules. *J. Chem. Phys.*, 26(1):114–122, 1957.

[69] Jonathan V. M. Weaver, Steven P. Armes, and Shiyong Liu. A holy trinity of micellar aggregates in aqueous solution at ambient temperature: Unprecedented self assembly behavior from a binary mixture of a neutral-cationic diblock copolymer and an anionic polyelectrolyte. *Macromolecules*, 36:9994–9998, 2003.

[70] G.W. Wei, D.S. Zhang, D.J. Kouri, and D.K. Hoffman. Distributed approximating functional approach to burgers' equation in one and two space dimensions. *Computer Physics Communications*, 111(1-3):93–109, June 1998.

[71] G Y Wu and C H Wu. Receptor-mediated in vitro gene transformation by a soluble DNA carrier system. *J. Biol. Chem.*, 262(10):4429–4432, April 1987. PMID: 3558345.

[72] Tjalling J. Ypma. Historical development of the Newton Raphson method. *SIAM Review*, 37(4):531—551, December 1995.

[73] D. S. Zhang, G. W. Wei, D. J. Kouri, and D. K. Hoffman. Burgers equation with high reynolds number. *Physics of Fluids*, 9(6):1853, 1997.

[74] Jingyan Zhang, Yueming Zhou, Zhiyuan Zhu, Zhishen Ge, and Shiyong Liu. Polyion complex micelles possessing thermoresponsive coronas and their covalent core stabilization via 'click' chemistry. *Macromolecules*, 41:1444–1454, 2008.

[75] Zuoquan Zhang, Qiquan Sun, Jinglian Zhong, Qihua Yang, Hao Li, Du Cheng, Biling Liang, and Xintao Shuai. Magnetic resonance imaging-visible and pH-Sensitive polymeric micelles for tumor targeted drug delivery. *Journal of Biomedical Nanotechnology*, 10(2):216–226, February 2014.

[76] E. B. Zhulina and O. V. Borisov. Poisson Boltzmann theory of pH-Sensitive (annealing) polyelectrolyte brush. *Langmuir*, 27(17):10615–10633, September 2011.

A. IPEC Solver: Numerical simulation tool to study inter-polyelectrolyte complexation

Computer Physics Communications 184 (2013) 2221–2229

Contents lists available at SciVerse ScienceDirect

Computer Physics Communications

journal homepage: www.elsevier.com/locate/cpc

IPEC Solver: Numerical simulation tool to study inter-polyelectrolyte complexation☆

Beibei Huang, Vladimir A. Baulin*

Departament d'Enginyeria Quimica, Universitat Rovira i Virgili, 26 Av. dels Paisos Catalans, 43007 Tarragona, Spain

ARTICLE INFO

Article history:
Received 14 November 2012
Received in revised form
25 April 2013
Accepted 1 May 2013
Available online 10 May 2013

Keywords:
Polyelectrolyte
Micelle
IPEC
Block copolymers
Electrostatic interactions
Self-assembly
Poisson–Boltzmann equation

ABSTRACT

IPEC Solver is a Windows program designed to analyze the stability of core–shell inter-polyelectrolyte complexes formed by complexation of oppositely charged block copolymers. The two-dimensional size distribution of the complexes composed by different numbers of positively or negatively charged polyelectrolytes is calculated based on the scaling model of block copolymer aggregation and Poisson–Boltzmann theory for electrostatic interactions [V.A. Baulin, E. Trizac, Self-assembly of spherical inter-polyelectrolyte complexes from oppositely charged polymers, Soft Matter 8 (25) (2012) 6755–6766]. Salt effects, charge distribution and distributions of labile cations and anions around the complexes are calculated numerically as a function of chain composition and solvent properties.

Program summary

Program title: IPEC Solver

Catalogue identifier: AEPM_v1_0

Program summary URL: http://cpc.cs.qub.ac.uk/summaries/AEPM_v1_0.html

Program obtainable from: CPC Program Library, Queen's University, Belfast, N. Ireland

Licensing provisions: Standard CPC licence, http://cpc.cs.qub.ac.uk/licence/licence.html

No. of lines in distributed program, including test data, etc.: 53802

No. of bytes in distributed program, including test data, etc.: 4582576

Distribution format: tar.gz

Programming language: C++ (VS.10)

Computer: PC

Operating system: WinXP, Win7

Has the code been vectorized or parallelized?: Supports parallel computation through OpenMP

RAM: 1 GB

Classification: 16.11

Nature of problem:
This free software is designed to illustrate physical mechanisms of self-assembly of inter-polyelectrolyte complexes in the presence of salt. It can suggest an optimal structure of the aggregates as a function of the structure of block copolymers.

Solution method:
The distribution of the complexes composed by a different number of positively or negatively charged polyelectrolytes is calculated based on a scaling model of block copolymer aggregation and Poisson–Boltzmann theory for electrostatic interactions [V.A. Baulin, E. Trizac, Self-assembly of spherical inter-polyelectrolyte complexes from oppositely charged polymers, Soft Matter, 8 (25) (2012)

☆ This paper and its associated computer program are available via the Computer Physics Communication homepage on ScienceDirect (http://www.sciencedirect.com/science/journal/00104655).

* Corresponding author. Tel.: +34 644448558.
E-mail addresses: va.baulin@gmail.com, vladimir.baulin@urv.cat (V.A. Baulin).
URL: http://vbaulin.softmat.net/ (V.A. Baulin).

0010-4655/$ – see front matter
http://dx.doi.org/10.1016/j.cpc.2013.05.003

6755–6766]. Salt effects, charge distribution and distributions of labile ions around the complexes are provided.

Restrictions:
IPEC complex is assumed to have a core–shell structure: a spherical core containing charged polymers is surrounded by a neutral corona. To insure stability of the solution, salt concentration, $ka > 0.2$

Additional comments:
Solves the Poisson–Boltzmann equation in a broad range of parameters.

Running time:
From seconds to several hours.

1. Introduction

Long range electrostatic interactions provide high stability of the complexes formed by molecules of opposite charge. This insures their potential use in a number of functional devices [1], such as drug delivery carriers [2–4] or molecular recognition devices [5]. Dilute solutions of oppositely charged block-polymers can form thermodynamically stable finite size inter-polyelectrolyte complexes (IPEC) [5–10] or polyion micelles [11,12,1]. Adjusting the structure of the polymer chain as well as the solution properties allows one to control the composition and structure of the resulting IPECs.

The Poisson–Boltzmann (PB) equation describes electrostatic interactions and distribution of ions around charged objects in equilibrium at a mean field level. Numerical approaches to solve the PB equation [13,14] in different practical situations and different geometries are widely available [15]. The common methods to solve the PB equation include finite difference methods and finite element methods [14], where the space is discretized in grids and elements; boundary element [16,17] and boundary integral equation methods [18], where only the surface of a big molecule is discretized while the surrounding distribution of labile ions is treated as a continuous field. Most of these methods are more suitable for 3D geometry models describing a big molecule of arbitrary shape in the electrostatic field. In contrast, IPEC complexes usually have symmetrical shapes with uniform distribution of charges. According to a recent theory of IPEC complexation [19], block copolymers of opposite charge aggregate into a spherical complex comprised of m_+ polycations and m_- polyanions. The total free energy of the solution of IPECs of different compositions (m_+, m_-) is written as

$$\frac{F}{VkT} = \sum_{m_+,m_-=0}^{\infty} c_{m_+,m_-}((\ln[c_{m_+,m_-}v] - 1) + F_{m_+,m_-}) \tag{1}$$

where V is the volume of the system, v is the molecular volume associated with the de Broglie length, and $c_{m+,m-}$ is the concentration of the complexes of a given composition (m_+, m_-). The free energy of the complex $F_{m+,m-}$ consists of an electrostatic contribution $\Omega_{\rm el}$, and a term accounting for the steric repulsion of chains forming a corona around the complex $F_{\rm corona}$. The electrostatic contribution is given by [19]

$$\Omega_{\rm el} = \int dr\left\{\frac{1}{2}\rho(r)\phi(r) + kT\sum_{\alpha}\rho_\alpha(r)\ln\frac{\rho_\alpha(r)}{c_\infty} - kT\sum_{\alpha}\rho_\alpha(r) + 2c_\infty\right\} \tag{2}$$

where r is the distance from the center of the complex, $\phi(r)$ is the electrostatic potential at a distance r, $\rho(r)$ is the charge density, $\alpha = \pm$ corresponds to labile cations and anions, respectively, while c_∞ is the bulk salt concentration. The complexes coexist in the solution with isolated charged copolymers. To calculate the electrostatic potential of isolated copolymers, they are approximated by cylinders placed in a salty media. The corresponding electrostatic contributions to the free energy from positively charged, $F_{1,0}$, and negatively charged polymers, $F_{0,1}$ are given by [19]

$$\frac{\Omega_{\rm el}}{kTN_\pm} = \frac{1}{2}u(0)\xi + \frac{1}{4}\int_{\kappa a}^{\infty}\tilde{r}d\tilde{r}u(\tilde{r})\sinh(u(\tilde{r})) - \frac{1}{2}\int_{\kappa a}^{\infty}\tilde{r}d\tilde{r}u(\tilde{r})[\cosh(u(\tilde{r})) - 1]. \tag{3}$$

Here the chain lengths $N_\pm$ are expressed in units of l_B and ξ is the Manning parameter. Tuning the chain composition, charge and lengths of the blocks, and solvent properties one can obtain the regions of stability of IPEC complexes, the size of the complexes and their size distribution [19]. However, this implies that the stability of the complexes depends on many factors that act simultaneously. Thus, a numerical tool solving efficiently PB equations would allow us to explore various possibilities and the influence of different parameters on the stability of complexes. Fast solution of equations for a large range of parameters may suggest a solution for a reverse problem, when the composition of the polymers and solvent properties that provide stable IPEC complexes can be guessed.

This work describes IPEC Solver (available at http://softmat.net/ipec-solver/), a numerical tool for the analysis of the stability of IPECs, and mostly focuses on the numerical implementation of the program and solution methods for estimating the equilibrium distribution of the electrostatic energy of the complexes. The core of IPEC Solver is the PB equation which is solved in spherical and cylindrical geometries based on the structure of the block copolymer chains and the solvent properties [19].

2. Poisson–Boltzmann equation in spherical geometry

In this section we focus on the methodology of solving the PB equation in spherical geometry with boundary conditions defined in Ref. [19]:

$$\nabla^2\phi(r) = -\frac{4\pi q}{\epsilon}\left\{\frac{Z_1H(R_c - r)}{4\pi R_c^3/3} - 2c_\infty\sinh(\beta q\phi(r))\right\} \tag{4}$$

where $\phi(r)$ denotes the potential at a distance r, q is the elementary charge, $\beta = 1/kT$, $H(R_c - r)$ is a Heaviside step function, and c_∞ is the bulk density of labile cations and anions. The dielectric permittivity ϵ is assumed to be constant inside and outside the complex to reduce the number of parameters of the model. Variable dielectric permittivity can easily be included; however this may not be essential in such a qualitative model. The bare charge of the core (due to polymers and not screened by labile cations and anions) [19] is $Z_1 = z_+m_+ - z_-m_-$, where $z_\pm$ is the charge and $m_\pm$ is the number of polymers of each sign in

the complex. Introducing the dimensionless electrostatic potential $u(r) = \beta q\phi(r)$ and the dimensionless distance $x = r/R_c$, where R_c is the radius of the charged sphere, Eq. (4) is then written as

$$\begin{cases} u''(x) + \dfrac{2}{x}u'(x) = -3\tilde{Z}_1 H(1-x) + (\kappa R_c)^2 \sinh(u(x)) \\ u'(0) = 0 \\ u'(\infty) = 0 \end{cases} \tag{5}$$

where $\tilde{Z}_1 = Z_1 l_b/R_c$ is the dimensionless bare charge of the sphere, $l_b = \beta q^2/\varepsilon$ is the Bjerrum length and $\kappa^2 = 8\pi l_B c_\infty$ is a rescaled labile cations and anions concentration, which includes counterions and salt molecules. In this nonlinear equation $\sinh(u)$ may lead to overflow for large values of $u(x)$. Thus, for convenience we set $w = e^u$, $y = w'$ and get an equivalent system

$$\begin{cases} y' = \dfrac{y^2}{w} - \dfrac{2y}{x} - 3\tilde{Z}_1 w + \dfrac{w^2-1}{2}(\kappa R_c)^2 \\ w' = y \\ y(0) = 0 \\ y(\infty) = 0 \end{cases} \tag{6}$$

where $\tilde{Z}_1$ and κR_c are two control parameters. The solution of this equation can be obtained by the conventional approach based on the finite difference method and the Newton–Raphson method [20–22]. However, this standard approach may not be stable for all sets of parameters.

To analyze the stability of the equation for different sets of parameters, we write this equation in a general form

$$\frac{d\mathbf{y}}{dx} = f(x, \mathbf{y}), \tag{7}$$

If $\tilde{\mathbf{y}}(x)$ is the solution of the equation that satisfies the corresponding boundary condition, we can write a linear approximation function

$$\frac{dZ}{dx} = J(x)(Z - \tilde{\mathbf{y}}(x)) + f(x, \tilde{\mathbf{y}}(x))$$

or

$$\frac{dZ}{dx} = J(x)Z + F(x)$$

hence

$$F(x) = f(x, \tilde{\mathbf{y}}(x)) - J(x)\tilde{\mathbf{y}}(t)$$

where $J(x)$ is the Jacobian matrix. Substituting $\tilde{\mathbf{y}}$ by the vector $[w, y]^T$ in Eq. (6) one obtains the corresponding Jacobian matrix

$$J = \begin{bmatrix} 0 & 1 \\ (kR_c)^2 w - \dfrac{y^2}{w^2} - 3\tilde{Z}_1 & \dfrac{2y}{w} - \dfrac{2}{x} \end{bmatrix}. \tag{8}$$

According to Ref. [23], if the eigenvalues of Jacobian matrix J of dimension k, $\lambda_j = \lambda_j(x), j = 1, 2 \ldots k$ satisfy

1. $\mathrm{Re}(\lambda_j) < 0, j = 1, 2 \ldots k.$
2. $s(x) = \dfrac{\max_{1\le j\le k}(\mathrm{Re}(\lambda_i))}{\min_{1\le j\le k}(\mathrm{Re}(\lambda_j))} \gg 1$

the nonlinear system is considered to be stiff on x, and $s(x)$ is the stiffness ratio at x. This signifies the instability of the solution of the equation.

The stiffness ratio $s(x)$ of the finite-difference method combined with the Newton–Raphson method [20–22] to solve Eq. (6) with values of x in the range from 0.02 to 0.8, and the eigenvalues of the matrix J, Eq. (8), is given in Table 1.

All the values in the table are smaller than or equal to 1, thus the system is not stiff for most $\tilde{Z}_1$ and the solution is stable.

Table 1
Stiffness ratio $s(x)$ of Eq. (6).

x	$\tilde{Z}_1 = 42$	$\tilde{Z}_1 = 60$	$\tilde{Z}_1 = 138$	$\tilde{Z}_1 = 216$	$\tilde{Z}_1 = 294$
0.02	0.01	0.02	0.04	0.07	0.11
0.04	0.06	0.08	0.26	1.00	1.00
0.06	0.15	0.25	1.00	1.00	1.00
0.08	0.38	1.00	1.00	1.00	1.00
0.10	1.00	1.00	1.00	1.00	1.00
0.12	1.00	1.00	1.00	1.00	1.00
0.14	1.00	1.00	1.00	1.00	1.00
0.16	1.00	1.00	1.00	1.00	1.00
0.18	1.00	1.00	1.00	1.00	1.00

3. Poisson–Boltzmann equation in cylindrical geometry

Spherical IPECs coexist in the solution with isolated chains of both signs. To calculate the electrostatic contribution to the free energy of an isolated chain, one can approximate a polymer chain with a linear charge $\lambda_\pm$ with an infinite cylinder surrounded by counterions and salt molecules. In this section we describe the numerical method of solving the PB equation in cylindrical geometry [19]:

$$\begin{cases} \dfrac{1}{\tilde{r}}\dfrac{d}{d\tilde{r}}\left(\tilde{r}\dfrac{d}{d\tilde{r}}\right)u = \sinh u \\ \left.\dfrac{du}{d\tilde{r}}\right|_{\tilde{r}=\kappa a} = \pm\dfrac{2\xi}{\kappa a} \\ u(\tilde{r} \longrightarrow \infty) = 0 \end{cases} \tag{9}$$

where $\xi = \ell_B\lambda_\pm$ is a dimensionless linear charge, the so-called Manning parameter [24], a is the radius of the cylinder, $\kappa^2 = 8\pi l_B c_\infty$ is a rescaled labile cations and anions concentration and $\tilde{r} = \kappa r$ is a dimensionless distance. This equation is controlled by two parameters, κa related to salt concentration, and a dimensionless parameter $\beta = \pm 2\xi/\kappa a$. Both of them appear in the boundary condition, thus the stiffness of the equation will be determined by these parameters.

Similar to the spherical case, a change of variables $w = e^u$, $y = w'$ leads to

$$\begin{cases} y' = \dfrac{y^2}{w} - \dfrac{y}{x} + \dfrac{w^2-1}{2} \\ w' = y \\ \left.\dfrac{y}{w}\right|_{\tilde{r}=\kappa a} = \pm\beta \\ w(\infty) = 1. \end{cases} \tag{10}$$

The corresponding Jacobian matrix J is given by

$$J = \begin{bmatrix} 0 & 1 \\ w - \dfrac{y^2}{w^2} & \dfrac{2y}{w} - \dfrac{1}{x} \end{bmatrix} \tag{11}$$

and the stiffness ratios $s(x)$ are given in Table 2. The values of the stiffness ratio $s(x) > 1$ for certain sets of parameters in this table may indicate that commonly used methods to solve differential equations could be unstable, and no general strategy guarantees [20] the existence or uniqueness of a solution of such nonlinear second-order equations. One of the most commonly used methods to solve such a boundary value problem is the 4th-Order-Runge–Kutta iteration technique [20], and we find that the solution of this equation is very sensitive to the parameter β when it is used together with the shooting method [25]. It becomes unstable for some sets of the parameters and thus is not suitable for the solution of Eq. (10) for all sets of parameters. It is quite difficult to choose an appropriate initial estimate for the shooting method. In addition, slight variations in the boundary values may lead to

Table 2
Stiffness ratio $s(x)$ of nonlinear equations (10).

x	$\xi = 1$				$\xi = 2$			
	$\beta = 1.0$	$\beta = 2.0$	$\beta = 10.0$	$\beta = 20.0$	$\beta = 2.0$	$\beta = 4.0$	$\beta = 20.0$	$\beta = 40.0$
0.02	1.0e+004	1.0e+003	48.22	18.51	1.0e+003	228.85	18.51	17.43
0.04	2.91	1.04	40.92	16.26	1.04	220.85	16.26	15.41
0.06	0.09	4.80	40.94	15.87	4.80	311.77	15.87	15.04
0.08	0.03	0.67	43.52	16.05	0.67	970.65	16.05	15.19
0.10	0.02	0.25	48.30	16.53	0.25	548.75	16.53	15.62
0.12	0.01	0.14	56.07	17.23	0.14	189.83	17.24	16.24
0.14	0.00	0.09	69.02	18.15	0.09	108.06	18.15	17.04
0.16	0.00	0.07	93.20	19.30	0.07	72.78	19.30	18.04
0.18	0.00	0.05	151.38	20.73	0.05	53.50	20.73	19.27
0.20	0.00	0.04	464.77	22.50	0.04	41.55	22.50	20.78

great changes in the solution, thus it is not possible to use a previous solution as an initial guess for the next solution. Such a method can be used to solve the equation only for small values of β.

In order to overcome this problem, we use the finite difference method [26] to discretize the differential equations into a set of nonlinear equations. There are two sources of error in this method: one is the rounding error which may accumulate in a sequence of calculations and another is the discretization error or truncation error, which comes from the difference between the exact solution and the solution of the finite difference equation. Substitution of $y = w'$ into Eq. (10) leads to

$$\begin{cases} w'' = \dfrac{w'^2}{w} - \dfrac{w'}{x} + \dfrac{w^2 - 1}{2} \\ \dfrac{w'}{w}\Big|_{\tilde{r}=\kappa a} = \pm\beta \\ u(\infty) = 1. \end{cases} \tag{12}$$

Using Taylor expansion and the method of undetermined coefficients, we discretize the first and second derivatives into finite differences expressions. The space is divided uniformly into a grid, $x_0, x_1 \ldots x_i$ with step h, which gives

$$w_i = w(x_i) \tag{13}$$

$$w_i' = -\frac{w_{i-1}}{3h} - \frac{w_i}{2h} + \frac{w_{i+1}}{h} - \frac{w_{i+2}}{6h} \tag{14}$$

$$w_i'' = \frac{w_{i-1}}{h^2} - \frac{2w_i}{h^2} + \frac{w_{i+1}}{h^2}. \tag{15}$$

Further we discretize the first derivative of the boundary condition [23],

$$w_i' = \frac{-3w_i + 4w_{i+1} - w_{i+2}}{2h}. \tag{16}$$

The truncation errors for the above three differences expressions are of order $O(h^2)$. This method effectively decreases the discretization error and accelerates the convergence speed.

The resulting system of nonlinear equations is then solved using the Newton–Raphson method [20–22] with values of x from 0.02 to 0.8. A properly chosen initial guess of the solution is an important factor for fast convergence to the solution. It becomes even more important when $\beta > 1$, because the values in the Jacobian determinant (8) also increase leading to the accumulation of small errors. Thus, we first solve a linearized PB equation (Debye–Huckel (DH) equation), which has an analytical expression and use it as an initial guess to solve the PB equation. The solution of linearized Eq. (10) is given by

$$w = \pm\beta \exp\left\{ \frac{K_0(\kappa a) I_0(x)}{I_1(\kappa a) K_0(\kappa a) - K_1(\kappa a) I_0(\infty)} + \frac{I_0(\infty) K_0(x)}{I_0(\infty) K_1(\kappa a) + I_1(\kappa a) K_0(\kappa a)} \right\} \tag{17}$$

where I_α and K_α are modified Bessel functions of the 1st kind and the 3rd kind respectively [27]. For weakly charged chains or large salt concentrations, i.e. when $\beta \ll 1$, the potential $u < 1$ and the DH equation is close to the exact solution of PB. Thus, using its solution as an initial guess provides a good convergence of the PB equation. When $\beta > 1$, the solution of the PB equation can be obtained in the iterative process by a gradual increase of β, when the solution of the PB equation with smaller β is used as the initial guess for larger β.

However, a gradual increase of β slows down the calculation. Thus, we use the adaptive method to approach larger β, starting with the DH solution as the initial guess for small β and using it as an initial guess for larger β. Using an adaptive step in β values, we can approach the solution faster. Such a "relay race strategy" is summarized in Algorithm 1 with grid vector $\mathbf{x}$, step size h, boundary condition value β and relative iteration convergence tolerance *tol* as input parameters, and the vector $\mathbf{w}_0$ as the output solution. An example of the algorithm performance is shown in Table 3.

Input: *vector* $\mathbf{x}$, *float* h, β, *tol*
Output: *vector* $\mathbf{w}$
set $\beta_{step} \ll 1$;
create a vector $\mathbf{w}_0$ which is a solution of the corresponding DH Eq. (17) with $\beta_{init} \ll 1$;
i = 1;
$num = \left\lceil \dfrac{\beta}{\beta_{step}} \right\rceil$;
while $i < num + 1$ **do**
  $\beta = \beta_{step} * i$;
  $\mathbf{w}_1$=Newton–Raphson($\mathbf{x}$, β, $\mathbf{w}_0$, h, *tol*);
  if $\mathbf{w}_1$ *does not converge to a solution* **then**
    num=num*2;
    $\beta_{step} = \beta_{step}/2$;
    i = 1;
    continue;
  end
  $\mathbf{w}_0 = \mathbf{w}_1$;
  i=i+1;
end
$\mathbf{w} = \mathbf{w}_0$

Algorithm 1: Adaptive "relay race" algorithm using combination of finite difference and Newton–Raphson methods.

Such a method provides a stable solution of the PB equation in cylindrical geometry, Eq. (12) for a large range of parameters, although it takes more time than the solution of the PB equation in spherical geometry, Eq. (6). Solution of these equations provides an equilibrium distribution of counterions and salt ions in the solution, distribution of charges, free energy of the chains in the

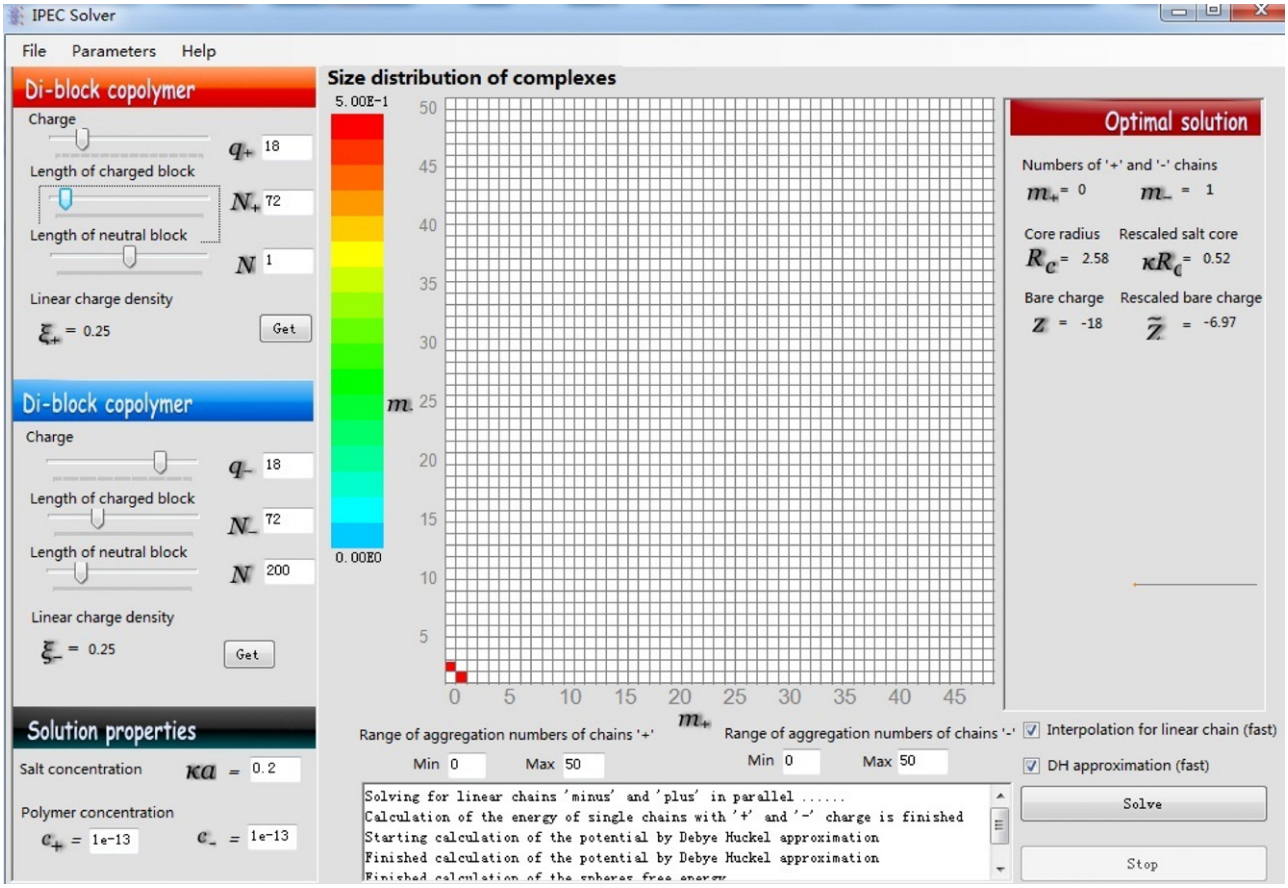

Fig. 1. IPEC: overview of the main window. Left panel: structure of block copolymers and solution properties; Central field: probability of complexes of a given composition of polycations and polyanions; Right panel: optimal solution; Window below: solution process.

Table 3
The number of steps in β and the number of iterations of Newton–Raphson method.

β	$\kappa a = 0.5$		$\kappa a = 1.0$		$\kappa a = 2.0$		$\kappa a = 10.0$	
	β steps	Iter num	β steps	Iter num	β steps	Iter num	β steps	Iter num
0.4	2	6	2	7	2	8	2	8
2.0	2	10	2	10	2	10	2	10
4.0	2	12	2	12	2	12	2	12
8.0	7	35	7	36	7	41	7	34
16.0	7	50	7	42	7	62	7	55
32.0	7	53	7	69	7	71	7	54
64.0	12	88	12	63	12	72	12	134
128.0	12	79	12	76	12	91	12	92
256.0	12	103	12	78	12	84	12	88
512.0	17	111	17	88	17	105	17	90

solution and in the self-assembled complexes and thus allows us to determine the range of stability of IPEC micelles in terms of the numbers of polyanions and polycations in the complex.

4. Implementation of IPEC Solver

In this section we introduce IPEC Solver (available at http://softmat.net/ipec-solver/), which is a Windows program designed to analyze the stability of core–shell polyelectrolyte complexes formed by the complexation of oppositely charged block copolymers. The two-dimensional size distribution (number of polyanions and polycations) of the complexes is calculated based on a scaling model of block copolymer aggregation and PB theory for electrostatic interactions [19]. The program supplies a graphical interface for input parameters, and output probabilities of IPEC sizes, charge and labile cations and anions distributions around the complexes.

4.1. Structure of IPEC Solver

IPEC Solver is designed to provide a rapid estimate of the stability region of polyelectrolyte complexes self-assembled from di-block copolymers, Fig. 1. The left column is reserved for input parameters, such as the structure of block copolymer chains, their charge and the length of charged and neutral blocks. The resulting distribution of the complexes is displayed in the main field in the center. The range of aggregation numbers of the complexes, i.e. numbers of positively and negatively charged chains in the complexes, can be fixed before the solution of the equations and the equations are solved in the indicated region of aggregation numbers. The complexes are shown in the central field with different colors, which represent different probabilities to form a complex with a given composition (the probability of the complex aggregated by certain numbers of oppositely charged copolymers is demonstrated by the corresponding color, as shown in Fig. 1). The optimal solution, i.e. the solution which corresponds to the maximum of the probability is shown in the right column. It contains aggregation numbers, core radius R_c, the bare charge of the core Z_1 and a schematic representation of the complex at the bottom. Double clicking on the grid in the main field opens a new window with the electrostatic details of the complex with the corresponding aggregation numbers.

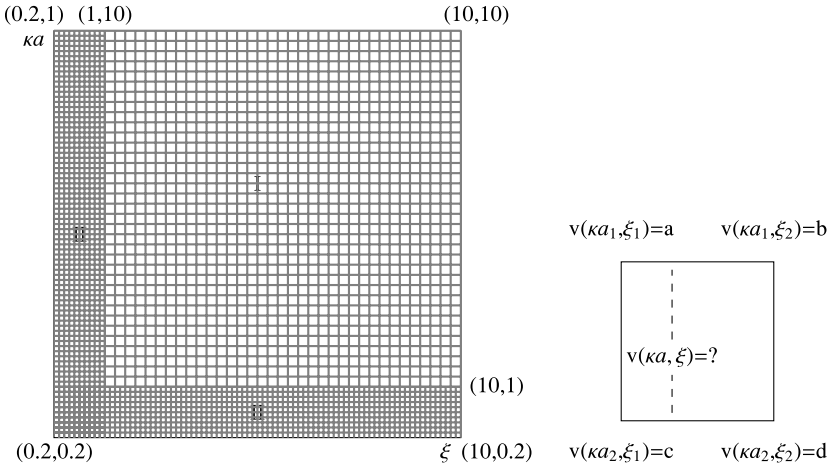

(a) Table of interpolation values for electrostatic energy of a cylinder.

(b) Getting values for given κa and ξ.

Fig. 2. Interpolation of electrostatic energy of a cylinder.

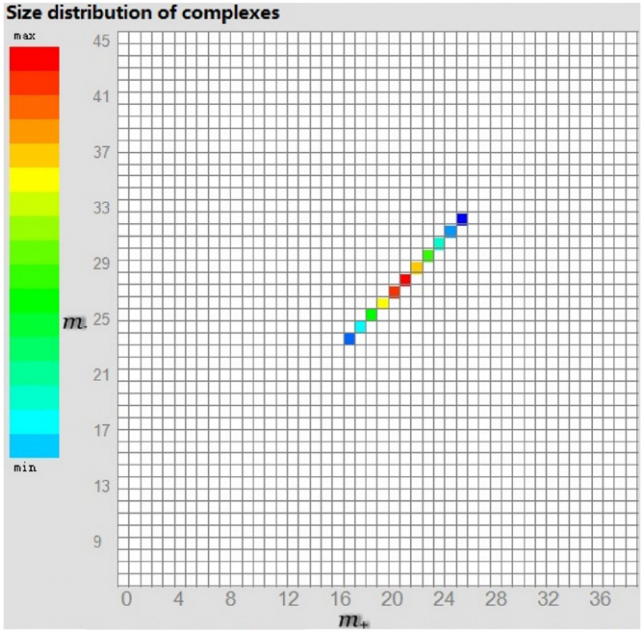

(a) Size distribution for $z_+ = z_- = 44$ and concentrations of individual chains $c_+ = c_- = 10^{-7}$, salt concentration $\kappa a = 0.2$, $\xi = 0.25$.

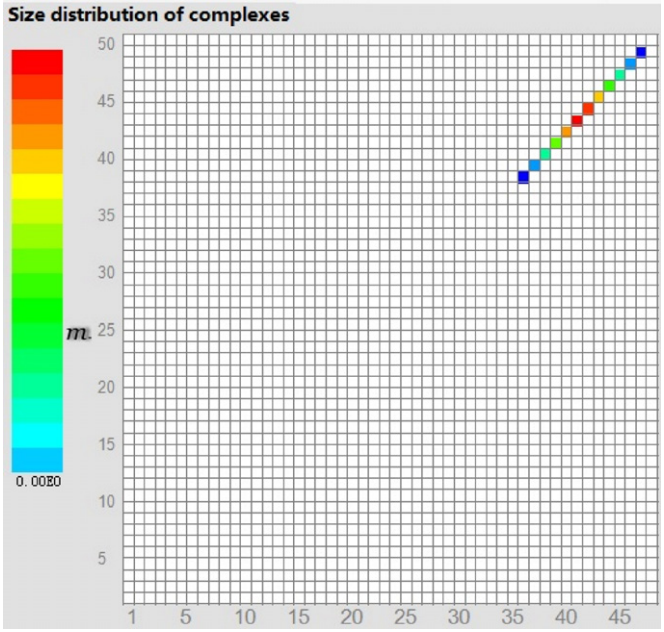

(b) Size distribution for $z_+ = z_- = 78$ and concentrations of individual chains $c_+ = c_- = 10^{-13}$, salt concentration $\kappa a = 0.2$, $\xi = 0.25$.

Fig. 3. Probability distribution function for different lengths of block copolymers of opposite charge for two groups of different input parameters.

The work with the program is summarized in the following steps:

1. Define the structure of the chains (positively and negatively charged) defining the length of charged and neutral blocks and their charge.
2. Define solvent conditions, such as salt concentration and concentrations of block copolymers.
3. Define the aggregation number range in the main field, where the solution needs to be found.
4. Solve equations either choosing the DH approximation for weakly charged objects or the full PB equation.
5. Analyze the resulting distribution of complexes in the main field, the optimal solution in the right column and detailed electrostatic properties of the complexes by double clicking the grids in the main field.

IPEC Solver first solves the PB equation for linear chains, Eq. (10), since this solution is the same for all grids in the main field. Then it solves the PB or DH equations (depending on the choice of the user) for each grid in the main field. Using the solution of the equations, the size distributions of complexes are calculated taking into account non-electrostatic contributions as described in [19]. The complexes are colored according to their probability, while the most probable in the indicated aggregation numbers range is shown in the right column.

4.1.1. Input parameters

Input parameters are divided in two groups: (i) the structure and geometry of the chains: the charge and the lengths of charged and neutral blocks and (ii) solution properties: salt concentration κa and the total concentrations of oppositely charged block copolymers $c_+ = \sum_{m_+=0}^{\infty} m_+ c_{m+,m-}$ and $c_- = \sum_{m_-=0}^{\infty} m_- c_{m+,m-}$.

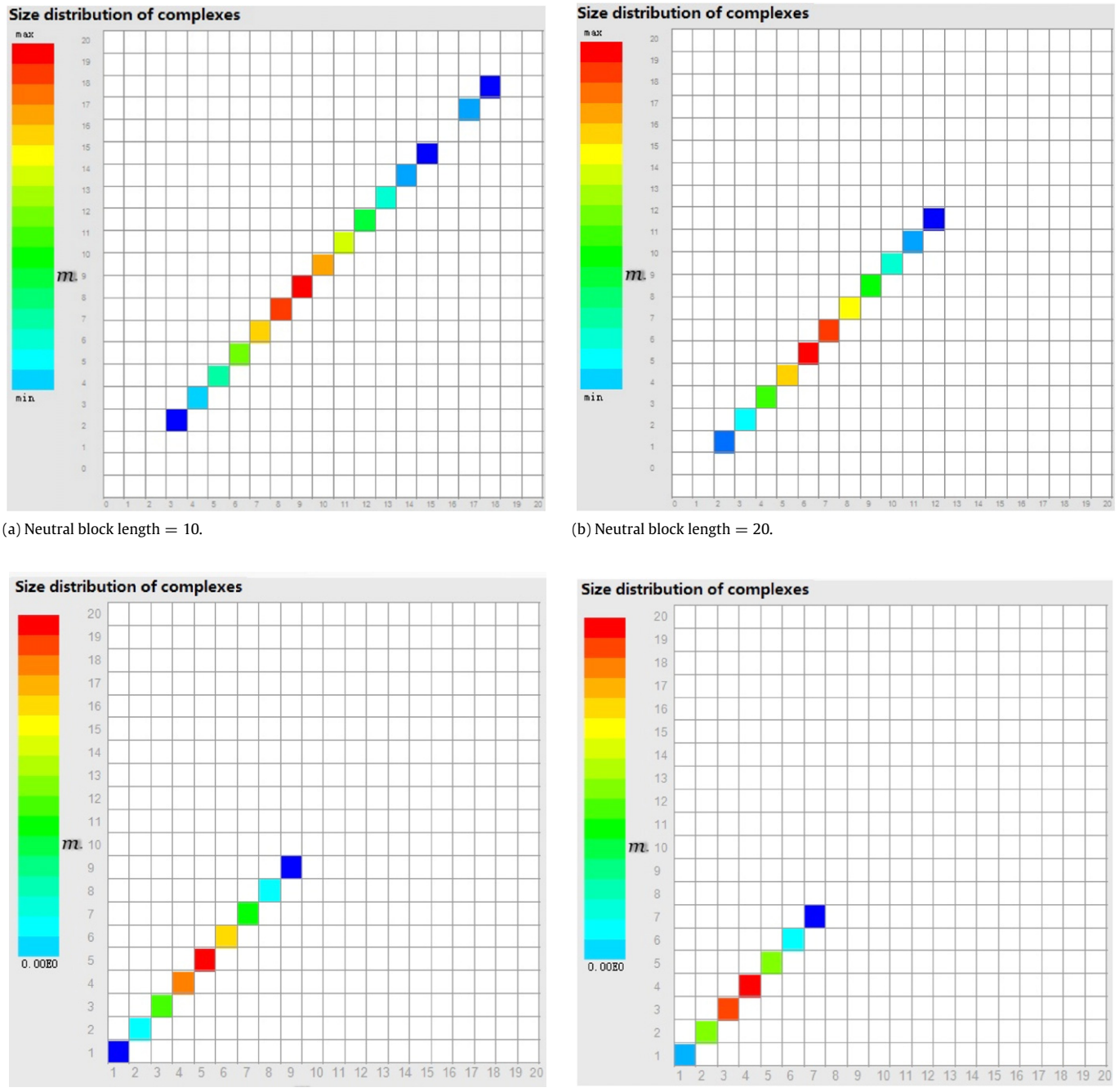

(a) Neutral block length = 10.

(b) Neutral block length = 20.

(c) Neutral block length = 50.

(d) Neutral block length = 200.

Fig. 4. Size distributions of IPECs for different length of neutral block of a negatively charged block copolymer, $z_+ = z_- = 18$, $c_+ = c_- = 10^{-3}$ and $\kappa a = 0.2$, $\xi = 0.25$.

In addition, the range of aggregation numbers of polymer chains of both signs is introduced below the grid, see Fig. 1.

4.1.2. Interpolation for speeding up the calculations

The first step in calculation of the size distributions of complexes is the solution of PB equations for linear chains, Eq. (10). This time consuming step can be optimized by using the interpolation of the stored results. Indeed, Eq. (10) depends only on two parameters, κa and ξ, thus solving the equation for different combinations of κa and ξ in advance and storing the result in a table may save time. If the values of κa and ξ are not in the table, their values are approximated as shown in Fig. 2. We compute the value of the free energy for given κa and ξ for each intersection point and store it in the table. The dependence of electrostatic energy of a cylinder on κa and ξ becomes linear [19] when κa and ξ are sufficiently large. Thus, the interpolation table is divided into two regions: region I with step 0.1 and region II with step 0.2. The electrostatic energy between the table values is obtained using Eq. (18). Here v denotes the required value of the energy, κa_1, κa_2, ξ_1 and ξ_2 are the values in the table with the corresponding values a, b, c, d, as shown in Fig. 2:

$$\begin{cases} v = v_2 + (v_1 - v_2) * (\kappa a - \kappa a_1)/(\kappa a_2 - \kappa a_1) \\ v_1 = b - (b - a) * \dfrac{\xi_2 - \xi}{\xi_2 - \xi_1} \\ v_2 = d - (d - c) * \dfrac{\xi_2 - \xi}{\xi_2 - \xi_1}. \end{cases} \tag{18}$$

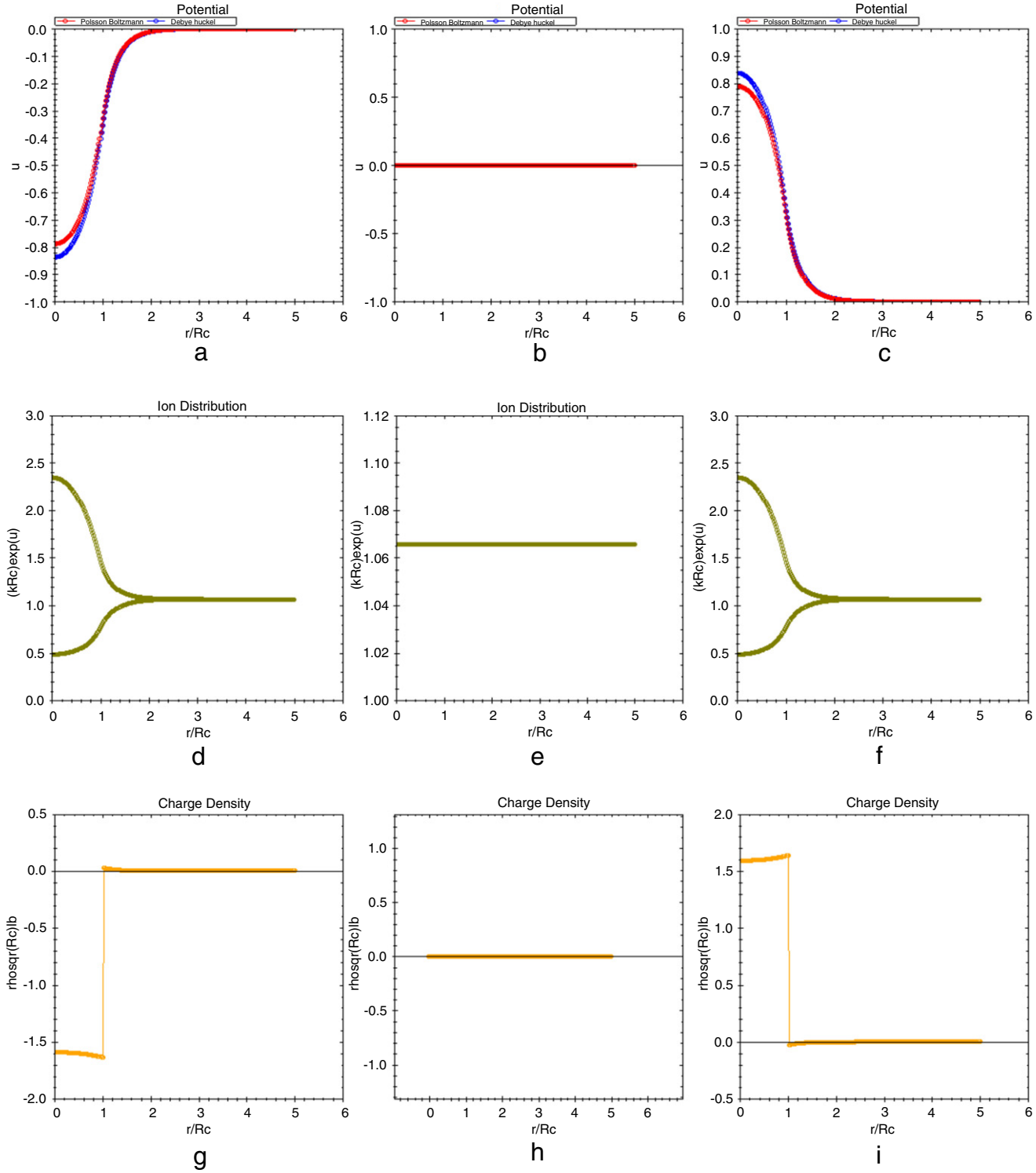

Fig. 5. Dimensionless electrostatic potential (a)–(c), reduced charge density of labile cations and anions around the core $\rho_{\pm} = c_{\infty} e^{\mp u(x)}$ (d)–(f) and charge density $\rho R_c^2 l_B$ as a function of distance from the core for different charges of the core (g)–(i). Three groups of figures correspond to IPECs with aggregation numbers (3, 5), (4, 4), and (5, 3), respectively. Here (m, n) denotes the probability value of the complex composed by m positively charged copolymers and n negatively charged copolymers. Parameters for all figures are $\kappa a = 0.2$, $\xi = 0.25$, $z_- = z_+ = 18$ and $c_- = c_+ = 0.001$.

4.1.3. Numerical example

Fig. 3 shows the probability distribution function for symmetric di-block copolymers of opposite charge. The size distribution of the complexes moves along the electroneutrality line ($m_+ = m_-$).

Fig. 4 illustrates the effect of the length of a neutral block of a negatively charged polymer. Increasing the length of a neutral block increases repulsive excluded volume interactions in the corona and, as a result, a shift of the size distribution to smaller numbers.

Double clicking on the grid in the main field opens a window with detailed electrostatic properties of the selected IPEC similar to Fig. 5. The dimensionless electrostatic potential $u(x)$, Fig. 5(a)–(c), both DH and PB solutions; the reduced charge density of labile cations and anions around the complex, Fig. 5(d)–(f) and the charge

density, Fig. 5(g)–(i), are shown as a function of the distance from the center of the complex [19]. The middle column has zero values, since the (4,4) complex is composed of 4 positively and 4 negatively charged polymers and the complex is neutral.

5. Conclusion

We have described IPEC Solver, a program designed to estimate the regions of stability of inter-polyelectrolyte complexes composed of linear di-block copolymers of arbitrary lengths of the blocks. The simple structure and graphical interface allows for fast solution of PB equations in a large range of aggregation numbers of the complexes and also investigates the influence of numerous parameters and the structure of the block copolymers on the stability of the complexes. This program is available at http://softmat.net/ipec-solver/.

Acknowledgments

B. Huang thanks Prof. Benzhuo Lu from LSEC and the NFS grant no. 11001257 for computer equipment.

References

[1] E.R. Gillies, J.M.J. Frechet, Development of acid-sensitive copolymer micelles for drug delivery, Pure Appl. Chem. 76 (7–8) (2004) 1295–1307.
[2] K.T. Oh, T.K. Bronich, L. Bromberg, T.A. Hatton, A.V. Kabanov, Block ionomer complexes as prospective nanocontainers for drug delivery, J. Control. Release 115 (2006) 9–17.
[3] A.V. Kabanov, V.A. Kabanov, Interpolyelectrolyte and block ionomer complexes for gene delivery: physicochemical aspects, Adv. Drug Delivery Rev. 30 (1998) 49–60.
[4] K. Kataoka, A. Harada, Y. Nagasaki, Block copolymer micelles for drug delivery: design, characterization and biological significance, Adv. Drug Delivery Rev. 47 (2001) 113–131.
[5] A. Harada, K. Kataoka, Chain length recognition: core–shell supramolecular assembly from oppositely charged block copolymers, Science 283 (5398) (1999) 65–67.
[6] E.S. Dragan, S. Schwarz, Polyelectrolyte complexes. VI. Polycation structure, polyanion molar mass, and polyion concentration effects on complex nanoparticles based on poly(sodium 2-acrylamido-2-methylpropanesulfonate), J. Polym. Sci. A: Polym. Chem. 42 (2004) 2495–2505.
[7] E.S. Dragan, M. Mihai, S. Schwarz, Polyelectrolyte complex dispersions with a high colloidal stability controlled by the polyion structure and titrant addition rate, Colloids Surf. A: Physicochem. Eng. Aspects 290 (2006) 213–221.
[8] O.V. Borisov, E.B. Zhulina, F.A.M. Leermakers, A.H.E. Muller, Self-assembled structures of amphiphilic ionic block copolymers: theory, self-consistent field modeling and experiment, in: Self Organized Nanostructures of Amphiphilic Block Copolymers I, Vol. 241, Springer, Berlin, Heidelberg, 2011, pp. 57–129.
[9] F. Schacher, E. Betthausen, A. Walther, H. Schmalz, D.V. Pergushov, A.H.E. Muller, Interpolyelectrolyte complexes of dynamic multicompartment micelles, ACS Nano 3 (8) (2009) 2095–2102.
[10] T. Etrych, L. Leclercq, M. Boustta, M. Vert, Polyelectrolyte complex formation and stability when mixing polyanions and polycations in salted media: a model study related to the case of body fluids, Eur. J. Pharm. Sci. 25 (2005) 281–288.
[11] P.S. Chelushkin, E.A. Lysenko, T.K. Bronich, A. Eisenberg, V.A. Kabanov, A.V. Kabanov, Polyion complex nanomaterials from block polyelectrolyte micelles and linear polyelectrolytes of opposite charge. 2. Dynamic properties, J. Phys. Chem. B 112 (2008) 7732–7738.
[12] F. Muller, P. Guenoun, M. Delsanti, B. Deme, L. Auvray, J. Yang, J.W. Mays, Spherical polyelectrolyte block copolymer micelles: structural change in presence of monovalent salt, Eur. Phys. J. E 15 (4) (2004) 465–472.
[13] F.T. Wall, J. Berkowitz, Numerical solution to the Poisson–Boltzmann equation for spherical polyelectrolyte molecules, J. Chem. Phys. 26 (1) (1957) 114–122.
[14] B.Z. Lu, Y.C. Zhou, M.J. Holst, J.A. McCammon, Recent progress in numerical methods for the Poisson–Boltzmann equation in biophysical applications, Commun. Comput. Phys. 5 (3) (2008) 973–1009.
[15] M.J. Holst, F. Saied, Numerical solution of the nonlinear Poisson–Boltzmann equation: developing more robust and efficient methods, J. Chem. Theory Comput. 16 (3) (1995) 337–364.
[16] B.Z. Lu, J.A. McCammon, Improved boundary element methods for Poisson–Boltzmann electrostatic potential and force calculations, J. Chem. Theory Comput. 3 (3) (2007) 1134–1142.
[17] B.Z. Lu, D. Zhang, J.A. McCammon, Computation of electrostatic forces between solvated molecules determined by the Poisson–Boltzmann equation using a boundary element method, J. Comput. Chem. 122 (21) (2005) 214102.
[18] B.Z. Lu, X. Cheng, Order n algorithm for computation of electrostatic interactions in biomolecular systems, Proc. Natl. Acad. Sci. 103 (51) (2006) 19314–19319.
[19] V.A. Baulin, E. Trizac, Self-assembly of spherical interpolyelectrolyte complexes from oppositely charged polymers, Soft Matter 8 (25) (2012) 6755–6766.
[20] C.T. Kelley, Solving Nonlinear Equations with Newton's Method, Society for Industrial and Applied Mathematics, Philadelphia, 2003.
[21] T.J. Ypma, Historical development of the Newton–Raphson method, SIAM Rev. 37 (4) (1995) 531–551.
[22] T. Dence, Cubics, chaos, and Newton's method, Math. Gaz. 3 (3) (1997) 403–408.
[23] C.W. Gear, Numerical Initial Value Problems in Ordinary Differential Equations, Prentice-Hall, Englewood, Cliffs, NJ, 1971.
[24] E. Trizac, G. Tellez, Onsager-manning-oosawa condensation phenomenon and the effect of salt, Phys. Rev. Lett. 96 (2006) 038302.
[25] W.H. Press, Numerical Recipes: The Art of Scientific Computing, Cambridge University Press, Cambridge, UK, New York, 2007.
[26] K.W. Morton, D.F. Mayers, Numerical Solution of Partial Differential Equations, Cambridge University Press, Cambridge, New York, 2005.
[27] M. Abramowitz, I.A. Stegun, Handbook of Mathematical Functions: With Formulas, Graphs, and Mathematical Tables, Dover, 1972.

A. Efficient and stable method to solve Poisson-Boltzmann equation with steep gradients

Efficient and stable method to solve Poisson-Boltzmann equation with steep gradients

Beibei Huang and Vladimir A. Baulin

Abstract This work describes a method to solve Poisson-Boltzmann Equation (PBE) with steep gradients when common methods of solving nonlinear equations do not converge or work inefficiently. This is particularly the case for relatively large boundary conditions leading to rapid changes of the solution in a narrow interval. The method uses adaptive step in the region of abrupt change of the solution and adopts invertible mapping algorithm to transform the original PBE into a form with a smooth profile which insures convergency and stability of the solution. The numerical tests demonstrate the advantages of the method compared to usual successive itteration methods, in which the solution is gradually approached by iterations from small values.

1 Introduction

Poisson-Boltzmann Equation (PBE) describes equilibrium distribution of charged objects surrounded by counterions and salt molecules in a mean field approximation, which neglects fluctuations and correlations. Popular methods to solve PBE include Newton methods, finite difference methods, adaptive methods [1, 2]. These methods can successfully solve nonlinear PBE in different geometries and shapes of charged objects such that universal solvers can be used for different practical applications. For example, a package DelPhi [3, 4, 5] is a 3D nonlinear solver of PBE. It is successfully used for modeling of electrostatic interactions of biomolecules. However, universal solvers may not always converge or be always efficient, especially if the solution exhibits abrupt changes. This is the case, for example, for electrostatic potential around highly charged objects in low salt solutions. Thus, such par-

Departament d'Enginyeria Quimica, Universitat Rovira i Virgili, 26 Av. dels Paisos Catalans, 43007 Tarragona, Spain, e-mail: hbb21st@urv.cat, vladimir.baulin@urv.cat

ticular cases need a special treatment, that may improve the convergence of the approximation scheme to the exact solution of the nonlinear system.

In this work we show that a method using adaptive step in the region of abrupt change of the solution may greatly improve the convergence and the stability of the approximation scheme. This method uses invertible mapping algorithm to transform PBE into a form with a smooth profile. This is similar in spirit to successive relaxation strategy described in Ref. [5] or similar invertible mappings strategies used for accurate description of the solution close to boundaries [7], solution of Burgers' equation with high Reynolds numbers [9]. Such a strategy applied to solution of different equations [8, 10, 11, 12] electively reduce the number of grid points and thus decreasing the degrees of freedom of the corresponding matrices in the computation process.

The method is implemented for solution of PBE in cylindrical geometry of infinite charged rod with large charge fixed in the boundary condition. Although the method is implemented in 1D, it can be generalized, in principle, for other dimensions.

2 Poisson-Boltzmann Equation

Poisson-Boltzmann equation describes electrostatic potential of charged objects in implicit ionic solutions, and its general form is written as

$$\nabla \cdot \big[\epsilon(\mathbf{r})\nabla\psi(\mathbf{r})\big] = -4\pi\rho^f(\mathbf{r}) - 4\pi\sum_i c_i^\infty z_i q \exp\big[\frac{-z_i q\psi(\mathbf{r})}{\kappa_B T}\big] \qquad (1)$$

where $\epsilon(\mathbf{r})$ is the position dependent dielectric constant, $\Psi(\mathbf{r})$ is the electrostatic potential, $\rho^f(\mathbf{r})$ is the charge density of fixed charges, c_i^∞ represents the concentration of the ion i in the bulk, z_i is the charge of the ion i, q is the elementary charge, k_B is the Boltzmann constant and T is the temperature.

We solve this equation in cylindrical geometry for infinitely long rod with arbitrary charge and surrounded by small ions and counterions providing electroneutrality of the system. Charged rod is represented by a cylinder with homogeneously distributed linear charge λ.

Aqueous solution outside the rod is homogeneous and thus $\epsilon(\mathbf{r})$ can be treated as a constant ϵ. For simplicity we consider monovalent ions only. Since we calculate the electrostatic potential outside the rod, all fixed charges are on the rod, and thus $\rho^f = 0$. Using $\nabla^2 = \frac{1}{r}\frac{\partial}{\partial r}\big(r\frac{\partial}{\partial r}\big)$ in cylindrical coordinates and introducing dimensionless distance $\widetilde{r} = \kappa r$, where $\kappa^2 = 8\pi l_B c_\infty$ is a rescaled ion concentration, PBE of infinitely charged rod takes the form [6, 13]

$$\begin{cases} \frac{1}{\widetilde{r}}\frac{d}{d\widetilde{r}}\left(\widetilde{r}\frac{d}{d\widetilde{r}}\right)u = \sinh u \\ \left.\frac{du}{d\widetilde{r}}\right|_{\widetilde{r}=\kappa a} = -\frac{2\xi}{\kappa a} \\ u(\widetilde{r}\longrightarrow\infty) = 0 \end{cases} \tag{2}$$

where $\xi = l_B\lambda$ is a dimensionless linear charge, the so-called Manning parameter [14], a is the radius of the cylinder. This equation is controlled by two parameters: κa related to salt concentration, and a dimensionless parameter $\beta = 2\xi/\kappa a$ which reflects the effective charge of a cylinder screened by salt solution.

The difficulty in solving this equation may arise from two terms: (i) $\sinh(u)$ may lead to overflow for large values of $u(\widetilde{r})$, and (ii) high charges and low ion concentration, i.e. when $\beta \gg 1$, produce steep gradients in the potential. To overcome first problem we set $w = e^u$, $y = w'$ and get an equivalent system

$$\begin{cases} y' = \frac{y^2}{w} - \frac{y}{\widetilde{r}} + \frac{w^2-1}{2} \\ w' = y \\ \frac{y}{w}\,|_{\widetilde{r}=\kappa a} = -\beta \\ w(\infty) = 1 \end{cases} \tag{3}$$

To analyze the stability of the equation for different sets of parameters, we use the same procedure as in [6] and derive the corresponding Jacobian matrix arising from the above Eq. (3)

$$J(\widetilde{r}) = \begin{bmatrix} 0 & 1 \\ w - \frac{y^2}{w^2} & \frac{2y}{w} - \frac{1}{\widetilde{r}} \end{bmatrix} \tag{4}$$

According to [15], if the eigenvalues λ_i of Jacobian matrix J satisfy

- $Re(\lambda_i) < 0$, $i = 1, 2, 3 \ldots k$
- $S(\widetilde{r}) = \frac{\max_{1\le i\le k}(Re(\lambda_i))}{\min_{1\le i\le k}(Re(\lambda_i))} \gg 1$

the nonlinear system is considered to be stiff on $\widetilde{r}$, and $S(\widetilde{r})$ is the stiffness ratio at $\widetilde{r}$. The stiffness ratios $S(\widetilde{r})$ arising from Eq. (4) are given in [6], and they indicate that commonly used methods to solve differential equations could be unstable, and no general methods guarantee the existence or uniqueness of a solution of such nonlinear second-order equations [16]. Furthermore, the 4th-Order-Runge-Kutta iteration technique was used and incorporated it with shooting method [17]. It turns out that the solution is very sensitive to the initial guess when the boundary value β is large. Thus, to address this issue [6], we adopted a method that successively increases β from small values, using previous solution in each iteration as the initial guess for solving the PBE with larger β. As a result, the number of iterations greatly increases making this method slow and unstable for $\beta \gg 1$. Thus a more efficient method is required to solve PBE for $\beta \gg 1$.

3 Invertible Mappings for PBE

The idea behind invertible mappings methods [10] is to replace a uniform discretization of space in a common finite-difference technique by adaptive discretization resulting in sufficiently higher density of points in the region of large variations of the solution and lower density outside this range.

To implement this strategy for Eq. (2) we introduce mapping of the coordinate $\widetilde{r}$ with the function f to a new coordinate $t = f(\widetilde{r})$, or $\widetilde{r} = f^{-1}(t)$. Function f should satisfy the condition that large but finite gradient of the solution in the large variation region is effectively reduced in t-space. The inverse function

$$f(\widetilde{r}) = \frac{\arctan\left[\widetilde{r}\tan(A)\right]}{A} \tag{5}$$

satisfies these conditions. Here a smoothing parameter A is used to adjust the number of grid points in the large variation region. With the help of such function f, one can find a uniform distribution of grid points in coordinates t that map non-uniform distribution in original coordinates $\widetilde{r}$, as shown in Ref. [10]. Thus, we substitute first and second derivatives

$$\frac{dw}{d\widetilde{r}} = \frac{dw}{dt} f(t) \tag{6}$$

$$\frac{d^2w}{d\widetilde{r}^2} = \frac{d^2w}{dt^2} f^2(t) + \frac{dw}{dt} f(t) f'(t) \tag{7}$$

into Eq. (3), and obtain PBE in coordinates t

$$\frac{d^2w}{dt^2} f^2(t) - \left(\frac{dw}{dt}\right)^2 \frac{f^2(t)}{w} + \frac{dw}{dt}\left\{\frac{1}{\tan(At)} - \sin(2At)\right\}\tan(A) f(t) = \frac{w^2-1}{2} \tag{8}$$

where $f(t) = \frac{\tan(A)\cos^2(At)}{A}$ and $f'(t) = \frac{\tan(At)}{A}$. Substituting Eq. (6) into Eq. (3), we get the first boundary condition in the form

$$\left.\frac{\tan(A)\cos^2(At)}{wA}\frac{dw}{dt}\right|_{t=(\arctan[\kappa a\tan(A)])/A} = -\beta \tag{9}$$

To obtin the second boundary condition, we cut off ∞ up to a constant r_{cut}, and get $t = \frac{\tan(r_{cut}A)}{\tan A}$, hence

$$w\left(\frac{\arctan\left[r_{cut}\tan(A)\right]}{A}\right) = 1 \tag{10}$$

To evaluate the stability of Eq. (8), we transform it into equations

$$\begin{cases} W' = \frac{W^2}{w} - \frac{W}{f(t)}\left\{\frac{\tan(A)}{\tan(At)} - \tan(A)\sin(2At)\right\} + \frac{\left(w^2-1\right)}{2f^2(t)} \\ w' = W \\ w'\big|_{t=(\arctan[\kappa a \tan(A)])/A} = -\frac{\beta w A}{\tan(A)\cos^2(At)} \end{cases} \tag{11}$$

and the corresponding Jacobian matrix reads

$$J(t) = \begin{bmatrix} \frac{2W}{w} - \frac{1}{f(t)}\left\{\frac{\tan(A)}{\tan(At)} - \tan(A)\sin(2At)\right\} & -\frac{W^2}{w^2} + \frac{w}{f^2(t)} \\ M & N \end{bmatrix} \tag{12}$$

where $M = 1$, $N = 0$ when $t \neq \frac{\arctan[\kappa a \tan(A)]}{A}$, $M = 0$, $N = -\frac{\beta A}{\tan(A)\cos^2(At)}$ when $t = \frac{\arctan[\kappa a \tan(A)]}{A}$.

The best convergence of the equation is obtained for $A = 1.45$. The corresponding stiffness ratios for $A = 1.45$ are shown in Table 1. Comparing the stability of the two equations, we consider the stiffness ratios of the grid points in the same interval through mapping $t = \frac{\arctan[\widetilde{r}\tan(A)]}{A}$, but reduce the number of grid points to 100.

Table 1: Stiffness ratios S($\widetilde{r}$) of nonlinear PBE, Eq. (8)

$\widetilde{r}(t)$	$\xi = 0.02$				$\xi = 0.2$			
	$\beta = 1.0$	$\beta = 2.0$	$\beta = 10.0$	$\beta = 20.0$	$\beta = 10.0$	$\beta = 20.0$	$\beta = 30.0$	$\beta = 60.0$
0.04	22.10	2180.64	6230.57	1603.52	4.01	14.23	14.27	13.88
0.06	183.20	198.54	185.68	277.00	10.98	11.12	10.73	10.70
0.08	39.46	40.53	44.18	46.96	7.64	7.68	7.53	7.49
0.10	9.37	9.51	8.78	11.12	4.96	4.98	4.74	4.69
0.12	2.01	2.06	2.05	2.01	2.71	2.74	2.76	2.69
0.14	1.50	1.59	1.47	1.24	1.00	1.00	1.00	1.00
0.16	3.00	3.11	2.75	2.79	1.00	1.00	1.00	1.00
0.18	4.50	4.66	4.14	4.16	1.00	1.00	1.00	1.00
0.20	5.53	5.43	5.55	5.29	1.00	1.00	1.00	1.00

The values of S in Table 1 suggest that the solver may be unstable in some isolated grid points, that does not affect the overall stability, while in most cases it is stable in all grid points. Further more, it reduces the number of grid points and hence greatly speeding up the solving process. The value of A in Eq. (5) can be used to tune the distribution of the grid points. If we set A close to 0, the grid points are distributed more or less evenly both in $\widetilde{r}$- and t-spaces. When A is close to $\pi/2$ the grid points are densely distributed in the vicinity of κa in $\widetilde{r}$-space. Such high distribution density leads to high values of derivatives close to 0 (Figure 1). This situation corresponds to Eq. (9) when value of β in boundary condition is large.

Note that when A is close to $\pi/2$, the convergence may decrease as shown in Figure 2. This can be attributed to the fact that fixed number of grid points crowd around limited area in the vicinity of κa, which prevents the convergence. To overcome it, we can treat A as adaptive variable, i.e. gradually increasing A from an initial value $S(A_0)$ (for example $A_0 = 1.0$) until $S(A_0 + h)$ such that $\|S(A_0) - S(A_0 + h)\| < C$, where C is a certain threshold.

4 Numerical Test

We ran a series of tests to check the performance of the method using invertible mapping and solving Eq. (8) in t-space compared to the solver of PBE with fixed step and solving directly Eq. (3) in $\widetilde{r}$-space. Such solver was implemented in IPEC-solver (http://softmat.net/ipec-solver/) for electrostatic potential of a linear chain in salt solution, which serves as a reference state for equilibrium structures of self-assembled inter-polyelectrolyte complexes [13, 6]. The solver corresponding to Eq. (3) corresponds to the version IPEC V1.0, while the solver corresponding to Eq. (8) corresponds to IPEC V1.2.

The performance of two methods is illustrated in Figure 3 for large β. It allows to conclude that (i) invertible mappings method implemented in IPEC V1.2 can converge to the solution with the same precision with smaller number of grid points; (ii) for sufficiently high values of β invertible mappings method converge to a solution when the direct method fails (blue dashed line for $\beta = 300$).

However, invertible mappings method slightly decrease the accuracy of the solution, since the inverse function transmits the original error $O(h_{\widetilde{r}})$ to the solver with the error $O(h_t)$ when the number of grid points is fixed. Here $h_{\widetilde{r}}$ and h_t are two steps in corresponding solvers respectively and satisfy $h_t = \frac{\arctan[h_{\widetilde{r}} \tan(A)]}{A}$.

5 Conclusion

We have demonstrated that invertible mapping can be efficient and stable method for solution of PBE for highly charged objects in low salt solutions. The method is implemented in 1D for the solution of PBE of a charged infinite rod in cylindrical coordinates for arbitrary charge of the rod. Numerical tests confirm the efficiency and stability of the method. The method can further be generalized for other systems and geometries.

Acknowledgements Authors thanks Prof G. Wei from Department of Mathematics, Michigan State University. BH thanks NFS grant No.11001257 for computer equipment.

References

1. F. T. Wall, J. Berkowitz, Numerical solution to the Poisson-Boltzmann equation for spherical polyelectrolyte molecules, The Journal of Chemical Physics 26 (1) (1957) 114–122.
2. B. Z. Lu, Y. C. Zhou, M. J. Holst, J. A. McCammon, Recent progress in numerical methods for the Poisson-Boltzmann equation in biophysical applications, Communications in Comptational Physics 5 (3) (2008) 973–1009.
3. I. Klapper, R. Hagstrom, R. Fine, K. Sharp, B. Honig, Focusing of electric fields in the active site of cu-zn superoxide dismutase: effects of ionic strength and amino-acid modification, Proteins 1 (1) (1986) 47–59.
4. M. K. Gilson, B. Honig, Calculation of the total electrostatic energy of a macromolecular system: solvation energies, binding energies, and conformational analysis, Proteins 4 (1) (1988) 7–18.
5. A. Nicholls, B. Honig, A rapid finite difference algorithm, utilizing successive over-relaxation to solve the Poisson-Boltzmann equation, Journal of Computational Chemistry 12 (4) (1991) 435–445.
6. B. Huang, V. A. Baulin, IPEC solver: Numerical simulation tool to study interpolyelectrolyte complexation, Computer Physics Communications 184 (9) (2013) 2221–2229.
7. F. C. Thames, J. F. Thompson, C. Wayne Mastin, R. L. Walker, Numerical solutions for viscous and potential flow about arbitrary two-dimensional bodies using body-fitted coordinate systems, Journal of Computational Physics 24 (3) (1977) 245–273.
8. D. S. Zhang, G. W. Wei, D. J. Kouri, D. K. Hoffman, Burgers equation with high Reynolds number, Physics of Fluids 9 (6) (1997) 1853.
9. K. Kakuda, N. Tosaka, The generalized boundary element approach to Burgers' equation, International Journal for Numerical Methods in Engineering 29 (2) (1990) 245–261.
10. G. Wei, D. Zhang, D. Kouri, D. Hoffman, Distributed approximating functional approach to Burgers' equation in one and two space dimensions, Computer Physics Communications 111 (1-3) (1998) 93109.
11. D. K. Hoffman, N. Nayar, O. A. Sharafeddin, D. J. Kouri, Analytic banded approximation for the discretized free propagator, The Journal of Physical Chemistry 95 (21) (1991) 8299–8305.
12. D. K. Hoffman, D. J. Kouri, Distributed approximating function theory: a general, fully quantal approach to wave propagation, The Journal of Physical Chemistry 96 (3) (1992) 1179–1184.
13. V. A. Baulin, E. Trizac, Self-assembly of spherical interpolyelectrolyte complexes from oppositely charged polymers, Soft Matter 8 (25) (2012) 6755–6766.
14. E. Trizac, G. Tellez, Onsager-manning-oosawa condensation phenomenon and the effect of salt, Physical Review Letters 96 (3).
15. C. W. Gear, Numerical initial value problems in ordinary differential equations., Prentice-Hall, Englewood Cliffs,N.J., 1971.
16. C. T. Kelley, Solving nonlinear equations with Newton's method, Society for Industrial and Applied Mathematics, Philadelphia, 2003.
17. W. H. Press, Numerical recipes : the art of scientific computing, Cambridge University Press, Cambridge, UK; New York, 2007.

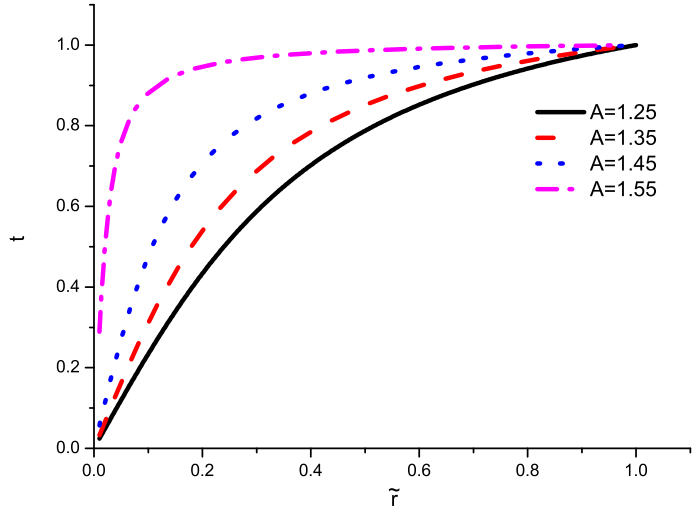

Fig. 1 Distribution of grid points in t- and $\widetilde{r}$- spaces with different values of tuning parameter A.

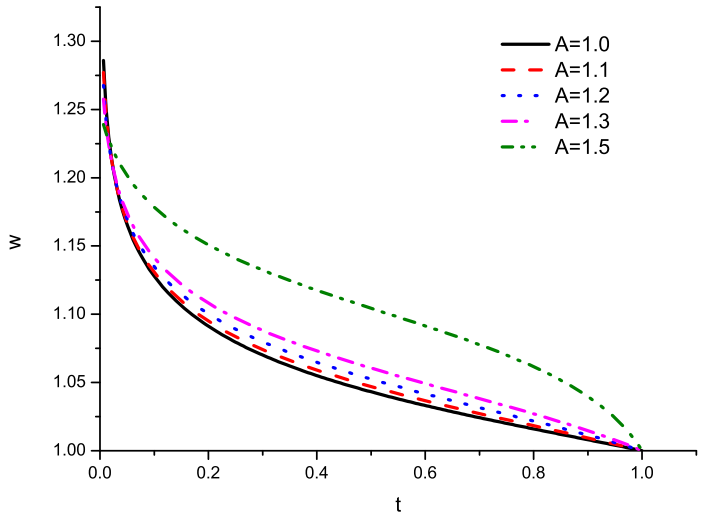

Fig. 2 The solution of Eq. (3), $w = \exp(u)$ for different values of A obtained with 200 grid points, and $\beta = 10$, $\xi = 0.02$. The curve $A = 1.5$ is distorted due to lack of gird points in numerical test interval (0.0,1.0).

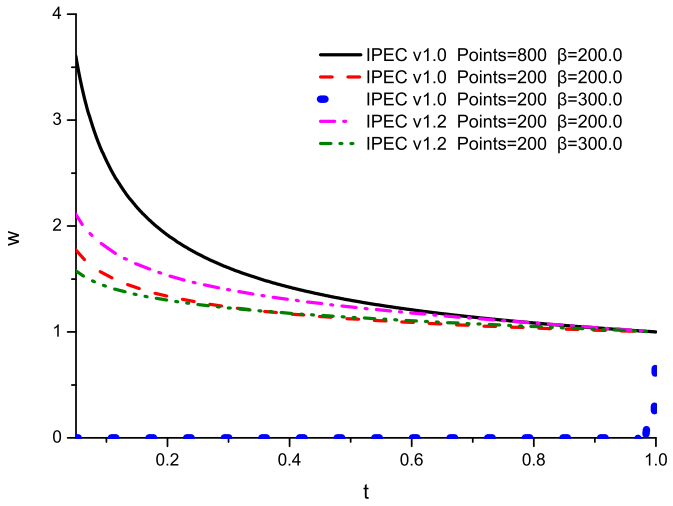

Fig. 3 The solution of Eq. (3), $w = \exp(u)$ for large values of β and fixed $A = 1.05$. The value of A is obtained by starting from an initial value $A_0 = 1.0$, and set $S(A)$ denote the corresponding solution, $h = 0.05$,$C = 0.1$ then $\|S(A_0 + h) - S(A_0)\| < C$. Invertible mapping method (IPEC V1.2) needs less grid points and converges readily when the direct method (IPEC V1.0) fails (blue dashed line).